A scalable method for the production of pH responsive polyamide microcapsules for drug delivery

A thesis submitted in partial fulfilment of the requirements for the degree of Master of Engineering in Chemical and Process Engineering

William Kelton

University of Canterbury

2008

Abstract

A scalable method for the synthesis of polyethylene terephthalamide microcapsules grafted with polyacrylic acid to enable pH responsiveness has been developed. Microcapsules were produced by interfacial polymerisation of an oil-in-water emulsion in a 2 L batch reactor and subsequently circulated through an external loop reactor for UV irradiative surface grafting. Ungrafted microcapsule samples yielded 1.0 – 1.2 g desiccated capsules per experiment. Initial production trials were subject to severe agglomeration, observed during dialysis of the microcapsules with 30 % (v/v) ethanol solution. Lowering of the terephthaloyl dichloride monomer concentration, to 0.2 mol L^{-1} in the chloroform / cyclohexane (3 : 1) organic solution, alleviated this unwanted agglomeration. Laser diffraction particle size analysis revealed microcapsules were produced with a 51 μm average diameter.

A purpose built external loop irradiation reactor was used to facilitate graft polymerisation of acrylic acid on the microcapsules, using 254 nm UV light at 19 mW cm^{-2}. Characterisation of the external loop flow regime showed a mild deviation from ideal plug flow, with a vessel dispersion number of 0.014 and a Reynolds number of 1310. Confirmation of monomer polymerisation was ascertained by back titration and Fourier transform infrared spectroscopy. No distinction between homopolymer and grafted polyacrylic acid could be made by these characterisation methods. A Taguchi analysis on variables influencing grafting revealed high temperature to contribute most significantly to graft yield, followed by a long irradiation period. The development of a packed column pulse response method for testing pH response showed a high repeatability. However, release profile testing of a microcapsule slurry with an observed graft yield of 1.13 mmol g^{-1} did not provide a definitive pH-based release of mPEG 5000 or PEGylated TAMRA dye. Determination of acrylic acid polymerisation kinetics following UV irradiation of the microcapsules is required for future optimisation of a functional graft yield.

Acknowledgements

I would like to thank Professor Conan Fee for his excellent and supportive supervision over the course of this project. His expertise and guidance have been much appreciated since my undergraduate study at the University of Canterbury and have greatly influenced my future career plans.

In addition, I would like to thank the sponsors involved in this project. The Foundation for Research Science and Technology (FoRST) for providing project funding and a year of scholarship (project no. UOC X0506), the Dick and Mary Earl Scholarship trust for support in the final six months and Ballance Agri-nutrients for financial support over the past three years.

Many thanks go to the technicians and postgraduate students who have provided technical advice over the course of this project. In particular, Mr Peter Jones, Mr Tim Moore, Mr Trevor Berry, Mrs Rayleen Fredericks-Short, Mr Yuewen Lin, Mr Vinod Babu Damodaran and Mr Jagan Billakanti. I would also like to gratefully acknowledge the support of Dr David Collings from the Department of Biological Sciences and Dr Marie Squire from the Department of Chemistry.

Finally, thanks to my family; Mum, Dad, Iz, Gamp and of course Snee, as well as extended family including; Nicole and Bronny, for their continuous support and personal sacrifice made while I have been studying here in Christchurch.

Table of contents

Abbreviations

AAc	Acrylic acid
AAm	Acrylic acid monomer
ANOVA	Analysis of variance
BSA	Bovine serum albumin
CSTR	Continuously stirred tank reactor
CV	Column volumes
DCC	Dicyclocarboxydiimide
DCM	Dichloromethane
DEE	Diethyl ether
DMF	Dimethyl formaldehyde
EDTA	Ethylene diamine triacetic acid
FRAP	Fluorescence recovery after photobleaching
FT/IR-ATR	Fourier transform infrared with attenuated total reflectance
GOD	Glucose oxidase
LD	Lethal dose
LDPE	Low density polyethylene
NHS	N – hydroxysuccinimide
NMR	Nuclear magnetic resonance
PAA	Polyacrylic acid
PBS	Phosphate buffered saline
PCD	Pitch circle diameter
PEG	Polyethylene glycol
PET	Polyethylene terephthalate
pI	Isoelectric point
PNIPAM	Poly(N-isopropylacrylamide)
PTFE	Polytetrafluroethylene
PVA	Polyvinyl alcohol
PVDF	Polyvinylidene fluoride
RBF	Round bottomed flask
RI	Refractive index
RRD	Rumino-reticulum device

SDS	Sodium dodecyl sulfate
SEM	Scanning electron microscope
SG	Specific gravity
SoS	Sum of Squares
SPG	Shirasu porous glass
TAMRA	6 – carboxytetramethylrhodamine
TDC	Terephthaloyl dichloride
TEA	Triethylamine
TsCl	Tosyl chloride
UV	Ultraviolet
XPS	X-ray photoelectron spectra

List of Figures

List of Tables

Chapter 1 Introduction

The delivery of drugs and other bioactive compounds to domestic farm animals is an important aspect of the modern agricultural industry. The simplest and most cost-effective method of delivery has traditionally been unprotected oral delivery of the supplement, except in ruminant animals where protection is required as harsh digestive conditions may inactivate or degrade the compound. A proposed solution to this problem is the use of polymer microcapsules to encapsulate a formulation, shielding the contents from ruminal fluids. A pH difference within the ruminant digestive tract may be exploited by functional gates grafted to microcapsule surfaces, enabling targeted release of the contents to highly absorbent areas of the gut. For this technology to become commercially viable, a scaled-up method of production needs to be developed to ensure the product is cost-competitive with existing techniques for ruminant drug delivery. To this end, the objective of this study was to scale-up microcapsule production, a step towards future commercial manufacture.

1.1. Post-ruminal drug delivery technology

The concept of using polymer microcapsules for post-ruminal drug delivery is a recent development. In the past, supplements have been protected for post-ruminal drug delivery by heat treatment, chemical treatment or coating with a protective lipid layer (Wu & Papas, 1997). Heat and chemical treatments reduce protein solubility within the rumen, slowing the rate of degradation. These solutions, while inexpensive, suffer from a lack of predictability and often a reduced bioactivity. In addition, the use of chemical additives, such as formaldehyde, introduces significant health risks to personnel during manufacture. The solubility of a compound may also be reduced by coating with a lipid layer, as lipids have an increased resistance to degradation by ruminal enzymes. The cost of producing lipid formulations is usually low but offset by the reduced drug bearing capacity of the method. Common to all these traditional delivery methods is the rate of delivery of the active compound, which is frequently inversely proportional to the degree of protection in the rumen.

A modern alternative is to coat the formulation with a reverse-enteric compound, which dissolves at low pH once past the rumen (Wu & Papas, 1997). As the degradation of the coating is a non-reversible process, the product cannot be exposed to acidic feed materials during ingestion. Shear forces also need to be avoided during dosing to prevent breakage of the micro-particles. Despite these limitations, reverse-enteric compounds can achieve higher delivery efficiencies than solubility reduction techniques. This approach has been successfully used to coat proteins, peptides and antibiotics, highlighting the versatility of the technology.

The flexibility of any new post-ruminal drug delivery system will be a key factor in determining commercial success. The modern farming industry requires a variety of formulations to be administered to livestock including, but not limited to, pharmaceutical antibiotics and drugs, lipids, amino acids, supplementary vitamins and anthelmintics to combat parasites (Vandamme & Ellis, 2004). In addition, a variety of minerals are dosed due to feedstock deficiencies of trace elements, such as cobalt, selenium, zinc, copper and iodine. These formulations are essential for promoting animal growth and health, resulting in more profitable farming practices.

1.2. Ruminant physiology

The direct oral delivery of formulations cannot be achieved without protection from the ruminal environment. This is due to the unique physiology of the ruminant digestive system. Ruminant animals, such as dairy cows, sheep and deer, have a balanced symbiotic relationship with anaerobic bacteria and protozoa in their gut (Wu & Papas, 1997). The structure of the digestive system consists of four main areas; the rumen, the omasum, the reticulum and the abomasum (Figure 1-1). The primary function of the ruminal compartment is fermentation and breakdown of ingested cellulose from plant feed. This section of the digestive tract is the largest at around 80 – 200 L in cattle. The rumen is maintained at a temperature between 38 and 42 $^{\circ}$C. Fermentation reactions in the rumen include hydrolysis of carbohydrates, hydrogenation of unsaturated fatty acids to saturated forms and hydrolysis of proteins and peptides (Cardinal, 1997). Acetic, propanoic and butyric acids are most commonly evolved from these reactions. The microbes themselves are an important source of protein for the animal in addition to

producing amino acids and utilising non-protein nitrogen. It is this microbial action in the rumen that renders many directly ingested formulations inactive.

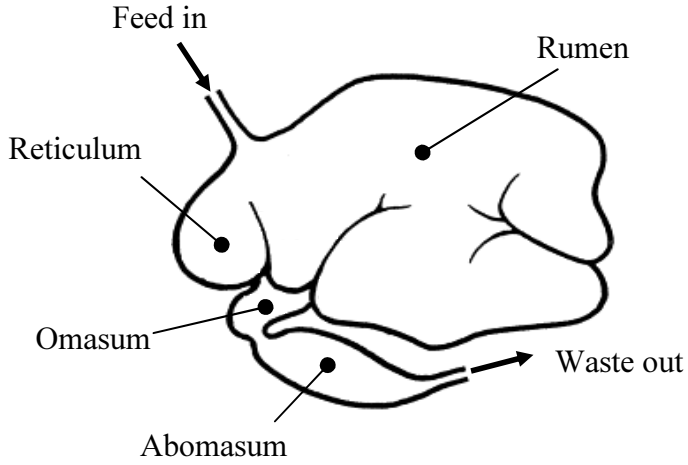

Figure 1-1: Diagram of a typical ruminant digestive system showing the four main compartments; the rumen, reticulum, omasum and abomasum (adapted from Wu & Papas, 1997)

Ruminant digestive tracts are characterised by a distinctive pH profile (Figure 1-2). The rumen has a neutral to slightly acidic pH of approximately 7, in comparison to the abomasum which is acidic and maintained at a lower pH of 3 (Vandamme & Ellis, 2004). These pH differences may be exploited to allow for a controlled release of active compounds to absorbent areas of the gut, such as the abomasum.

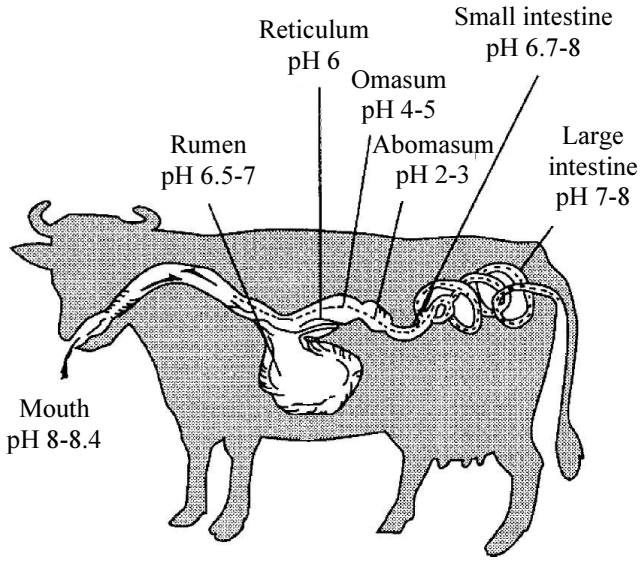

Figure 1-2: pH profile through the bovine digestive tract (adapted from Vandamme & Ellis, 2004)

The average residence time for particulate feed in the rumen is two days (Hobson & Stewart, 1997). Solids are mixed by muscular contractions of the stomach wall and regurgitated periodically, as a bolus, where further mastication occurs in a process termed 'rumination'. Particles cannot leave the rumen until reduced to less than a millimetre in size through both rumination and microbial action. This digested material then passes through the remainder of the digestive tract in approximately 8 – 12 hours (Hobson & Stewart, 1997). Protection of bioactive compounds is required until post-ruminal release can occur in these latter absorptive sections of the digestive tract.

1.3. Microcapsules for controlled release drug delivery

A few key requirements must be met in the development of any new controlled release system; delivery must be targeted to the most appropriate site of action, an appropriate dosage must be delivered at the appropriate time and release must occur over an optimal time period. The vector used must be physiologically inert, not absorbed into the organism influencing quality of meat or milk, non – mutagenic and thermally stable at temperatures encountered during processing and delivery. Polymer microcapsules present novel opportunities for drug delivery by satisfying these requirements. Hollow microcapsules provide a membrane for protection against adverse external environmental conditions, encapsulating a formulation for delivery. Pores within the membrane allow diffusion of compounds into and out of the microcapsules. However, any emerging delivery solution needs to remain cost-effective. This can be achieved through significant improvements in dosing efficiency, thereby reducing the amount of drug required for treatment. Control over the rate of diffusion is critical in ensuring an efficient, targeted release, at the appropriate site within the digestive tract.

The approach is to target drug delivery post-ruminally to the abomasum, a highly absorbent area in ruminant digestive systems. The mechanism of release exploits the pH difference between the fluids in the rumen and the abomasum (Figure 1-2). Responsiveness to pH is effected by utilising the unique swelling behaviour of polyacrylic acid (PAA), also known as polymethacrylate. At high pH, carboxylic groups in the acid chains dissociate, increasing the number of negatively charged COO^- groups. Electrostatic repulsion between these groups increases the length of the molecule and

the distance between adjacent chains, resulting in a swelling of the PAA polymer gel (Jin *et al.*, 2006). Conversely, when the pH is lowered below the pKa value of 4.8, the carboxylic groups lose their negative charge and the polymer chains decrease in size (Lee *et al.*, 1995). As a consequence the PAA gel has a significantly reduced size at pH 3 when compared to the pH 7 state. This swelling phenomenon can be used to significantly reduce the effective membrane pore size at high pH when PAA is grafted onto the surfaces of microcapsules. The reversibility of the chain lengthening and shortening allows the microcapsules to be loaded at low pH. The contents are trapped at elevated pH, then, once the pH is lowered below the pKa, release is enabled at the targeted site (Figure 1-3).

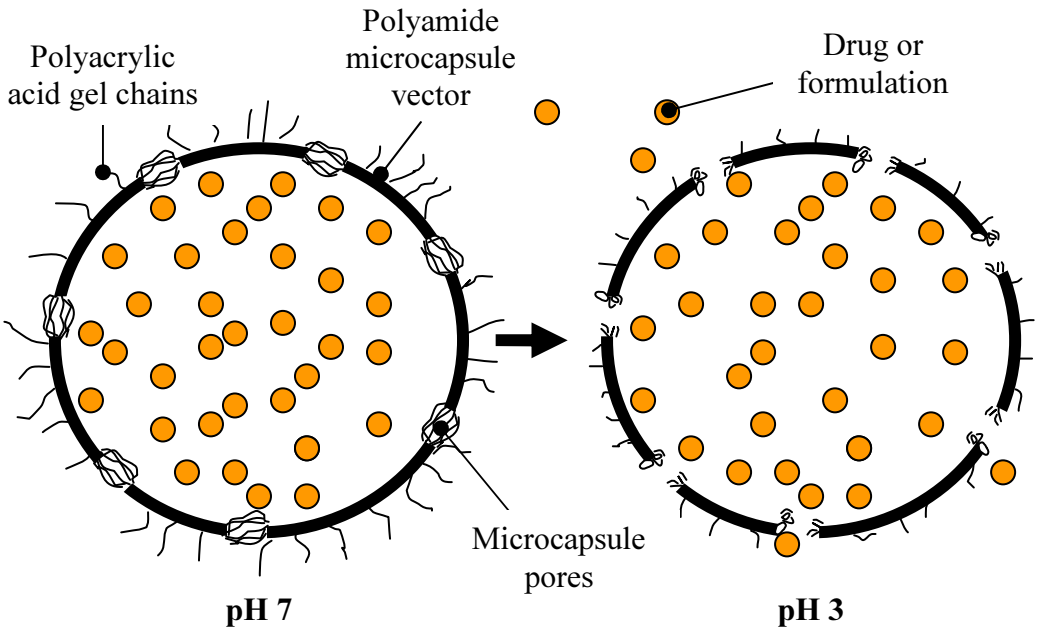

Figure 1-3: Schematic representation of pH responsive release process for polyamide microcapsules grafted with polyacrylic acid

The efficiency of the delivery may be further improved by use of a rumino-reticulum device (RRD), retained in the rumen. Established controlled release devices cannot be held in the abomasum. Therefore, the formulation must be protected from the release point in the rumen. A previously developed electronically controlled syringe device may be loaded with pH responsive microcapsules, allowing for a metered release over an extended time period (McLellan, 2007). The microcapsules are excreted by the animal after the release of the formulation, whereupon they degrade in the environment.

This level of controlled release has several distinct advantages over traditional uncontrolled drug delivery methods. A targeted animal may be supplied with a formulation over an extended period of time with a single application, without the need for multiple human handlings. If delivery of an antibiotic or other therapeutic drug is involved, the blood plasma concentrations are kept at a more constant level without the need for high initial concentration spikes (Cardinal, 1997). This aids in the prevention of side-effect related complications following delivery.

1.4. Polyamide microcapsule formation and grafting of acrylic acid

Polyamide microcapsules were selected in this study as drug-carrying vectors due to their inert porous structure. In the first step of manufacture, a thin polymer shell of polyethylene terephthalamide is formed, by interfacial polymerisation, around oil-in-water emulsion droplets. The polymerisation reaction advances along two simultaneous pathways. Initially, secondary amine groups, as found in the monomer diethylene triamine, react with terephthaloyl dichloride (TDC) dissolved in an organic phase (Figure 1-4). Once the immediately available secondary amine groups are consumed, primary amine groups, such as those in the second amine monomer, ethylene diamine, react with the polyethylene terephthalamide (Figure 1-5). These form yet more secondary amine structures which subsequently react by the same mechanisms, creating a highly cross-linked membrane matrix.

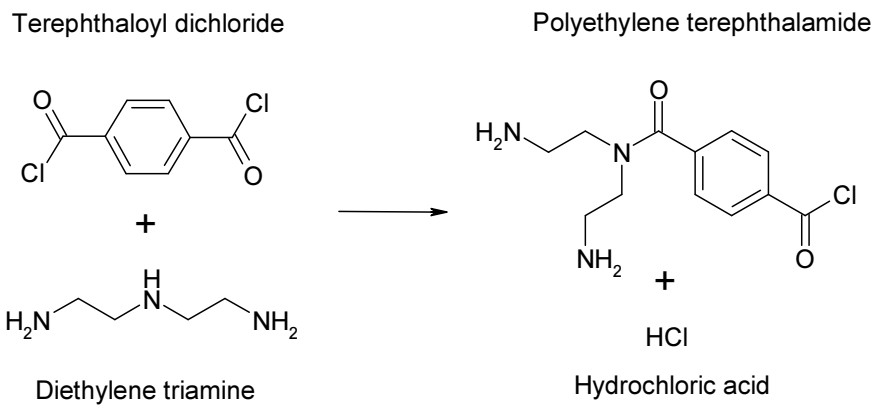

Figure 1-4: Cross-linking reaction of diethylene triamine with terephthaloyl dichloride during microcapsule formation by interfacial polymerisation

Cross-linking reactions between the forming polymer chains increase the mechanical strength of the microcapsules. As polycondensation proceeds, the reaction rate slows due to the polymer membrane hindering diffusion across the liquid phase interface. Following polymerisation the organic phase may be removed in a later production step, allowing the unpartitioned internal cavity to be loaded, encapsulating a drug or formulation.

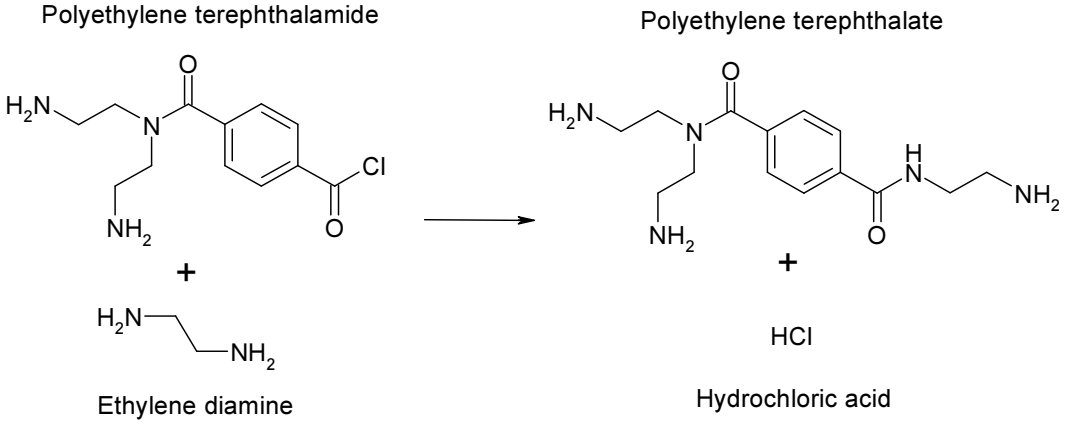

Figure 1-5: Simultaneous polymerisation step of ethylene diamine with polyethylene terephthalamide in microcapsule formation

Microcapsules produced by this method have diameters in the order of tens of microns (Lin *et al.*, 2006). The large surface area-to-volume ratio allows for rapid release of encapsulated formulations through the membrane pores. This makes polyamide microcapsule technology ideally suited for use in controlled delivery applications.

The covalent attachment of functional PAA gates to the external microcapsule surfaces is required following production. This may be achieved by use of a thermal, chemical or irradiative initiator to generate reactive free radical surface sites, allowing for the coupling of the acrylic acid monomer by a chain polymerisation reaction. Previous studies have used a plasma-assisted grafting technique (Lin *et al.*, 2006), but this presents significant challenges for scale-up and was abandoned in this project in favour of an ultraviolet (UV) irradiative approach. Methods already exist for the small scale production of polyamide microcapsules (Chu *et al.*, 2001; Chu *et al.*, 2002b; Chu *et al.*, 2004; Lin *et al.*, 2006). However, the UV grafting technique, adopted in the current work, is a new approach to attachment of polyacrylic acid to microcapsule surfaces. This requires further exploration to enable production of larger quantities than obtained

by plasma-assisted grafting. In particular, a better understanding was sought of the influence of monomer concentration, UV irradiation and temperature on the graft yield and the consequent drug release characteristics.

1.5. Project objectives

There is a need for a cost-effective, versatile, drug delivery system for the dispensing of formulations to ruminant animals over an extended period of time. Microcapsules provide a platform to prolong *in-vivo* drug life and administer the drug directly to targeted absorptive sites, superior to traditional delivery technologies. The challenge now lies in the effective scale-up of production methods to make sufficient quantities for practical application in agricultural and biomedical fields. The primary objective of this project was the development of a scaled-up method for the production of polyamide microcapsules grafted with PAA. This fulfils the requirement for a formulation protection method for controlled drug delivery. The long-term project objective was to prepare a sample for potential *in-vivo* trials to assess the suitability of the microcapsules for commercial use as a post-ruminal drug delivery vector.

This research is being conducted with support from the New Enterprise Research Fund, awarded by the Foundation for Research, Science and Technology, in collaboration with InterAg (Hamilton, New Zealand), DairyNZ formerly known as Dexcel (Hamilton, New Zealand) and the University of Waikato (Hamilton, New Zealand). There are three components to the overall project; development of a controlled release device for ruminal delivery (a RRD), development of a formulation protection method for targeted absorption in the abomasum and clinical studies into the efficacy of the delivery system. If a superior delivery system can be engineered which doses compounds with an associated cost similar to, or less than, existing methods, the technology may become a commercial enterprise.

1.6. Scope and organisation of thesis

A summary of current literature on microcapsule controlled release drug delivery technology and irradiative reactor design is presented in Chapter 2. Due to the broad nature of this field, the focus is on grafting procedures for coupling acrylic acid monomers to polymer substrates and the subsequent grafting yields obtained. Process variable settings during production and methods of release characterisation are also considered. Following the literature review, Chapter 3 provides a brief description of the coupled emulsification and graft reactor design. Equations and design variables relevant to scale-up are provided. A description of the methodology used and adapted for larger-scale production, grafting and testing of microcapsules is contained in Chapter 4. The results of experiments are summarised in Chapter 5, followed by a discussion in Chapter 6. The core conclusions drawn from this project have been detailed in Chapter 7, followed by recommendations for future work in Chapter 8. Finally, the appendices contain derivations of key scale-up equations, dimensioned engineering drawings and key calculations for use in further scaling of the method.

Chapter 2 Literature review

A literature review was undertaken to establish current knowledge on polyamide microcapsule formation techniques and methods of coupling polyacrylic acid to effect pH responsiveness of various polymer substrates. Particular attention was given to process variable settings, the effect of process variables on the polyacrylic acid graft yield and release characteristics of drug substitutes. In conjunction with this, an assessment was made of the biocompatibility of the polymer materials used for microcapsule production, and possible trial compounds for *in-vivo* release characterisation. The final section focuses on confocal microscopy techniques for visualisation of drug release from polymer microcapsules.

2.1. Development of microcapsule technology

Interfacial polymerisation methods have been employed for formation of polyterephthalamide polymers for many years. Copolymers were prepared by this method as early as 1959 (Manfred, 1959) with work by Koishi *et al.* (1969) continuing to develop hollow microcapsules. The latter authors noted the importance of surfactant concentration in controlling the monodispersivity of the microcapsules produced, with a minimum concentration required for stability. Later experiments by other researchers using microcapsules produced from terephthaloyl dichloride and ethylene diamine showed that the mean size of capsules decreased, with a narrower size distribution, for increased stirring speeds during the emulsification process (Yan *et al.*, 1992). These authors also noted a greater uniformity in particle diameter with an increase in stabilising surfactant.

The influence of surfactant concentration on emulsion droplet size has been studied further by Chatzi *et al.* (1991b). It was found agitation of immiscible liquids in a stirred reactor form a dispersion in which the rate of coalescence of droplets is in dynamic equilibrium with the rate of formation of droplets. The authors used a system containing 1 % styrene solvent dispersed in water to study the variables affecting the dynamic equilibrium. A partially hydrolysed poly(vinyl acetate) stabiliser was added in varied

amounts to act as a stabiliser. The primary action of the stabilising surfactant is to adsorb to the water / monomer interface, increasing the strength of the liquid film to reduce coalescence. Interfacial tension is a measure of the ability of a system to resist droplet formation. In general, it was found interfacial tension decreases with an increase in temperature as the surface tension of the stabiliser decreases. This resulted in the formation of smaller emulsion droplets. The same researchers, in separate work, concluded that higher mixing speeds result in smaller droplets as a greater amount of kinetic energy can be transferred from the impeller to the emulsion (Chatzi *et al.*, 1991a). It was shown the time taken to reach the dynamic equilibrium point could be reduced by increasing the turbulence intensity in the reactor, through faster agitation, or increasing the emulsification temperature. Adjustment of these variables was limited by the stability of the emulsion formed.

Chu *et al.* (2001) developed the basis of an interfacial polymerisation method for production of polyethylene terephthalamide microcapsules. Several combinations of solvents containing dissolved TDC monomer were emulsified, using a high-shear impeller, including chloroform / cyclohexane in volume ratios of (1 : 4), (1 : 3), (3 : 1) and benzene / xylene in the ratio of (2 : 1). It was found the average diameter of the capsules prepared in all cases lay in the range of 36.7 – 43.1 μm. Microcapsules produced using chloroform / cyclohexane (3 : 1) had a slightly smaller mean diameter than other combinations of solvent. Increasing the ratio of chloroform to cyclohexane was found to increase the thickness of the membrane shell. The benzene / xylene solvent combination produced microcapsules with a greater porosity, which led them to the conclusion that porosity was determined by the solubility of the solvent in water and to a lesser extent the solubility of water in the organic phase. As expected, an increase in the interfacial polymerisation time resulted in a thicker shell with an increased density of the membrane on the water-based side. Scanning electron microscope (SEM) use revealed an unsymmetrical membrane; smooth on the water phase side and rough on the internal surface in contact with the organic phase (Figure 2-1). This indicated that polymerisation occurred as the amines in the aqueous phase diffused across the phase boundary to the organic phase. The microcapsule membrane in Figure 2-1 was created using a chloroform to cyclohexane solvent ratio of 3 : 1 and a total reaction time of 1 hour.

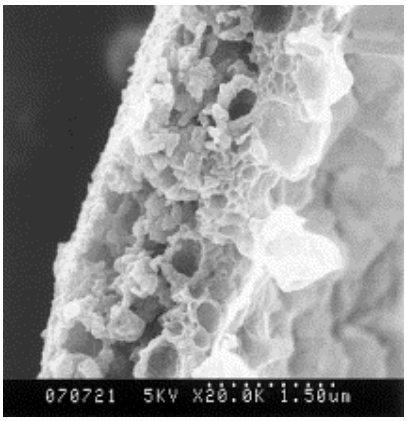

Figure 2-1: SEM micrograph of microcapsule membrane section showing smooth external surface (top) and rough internal surface (bottom) (Chu *et al.*, 2001)

Following production, polyamide microcapsules were dialysed against demineralised water to remove excess monomer and solvent.

The solvent exchange process in microcapsule washing has been investigated in greater detail for poly(β-amino ester) microcapsules by Lynn *et al.* (2001). Residual solvent traces were found to affect the stability of the capsules. Extended drying and dynamic vacuum treatment of the microspheres did not reduce the agglomeration or tackiness. The authors were able to facilitate a better solvent exchange when the ethanol and water washing steps, as well as centrifugation, were performed at 4 °C.

Chu *et al.* (2002), continued work on polyamide microcapsule preparation using a Shirasu porous glass (SPG) filter as depicted in Figure 2-2. Compressed nitrogen gas was used to force the organic phase through a glass filter with a highly uniform pore size.

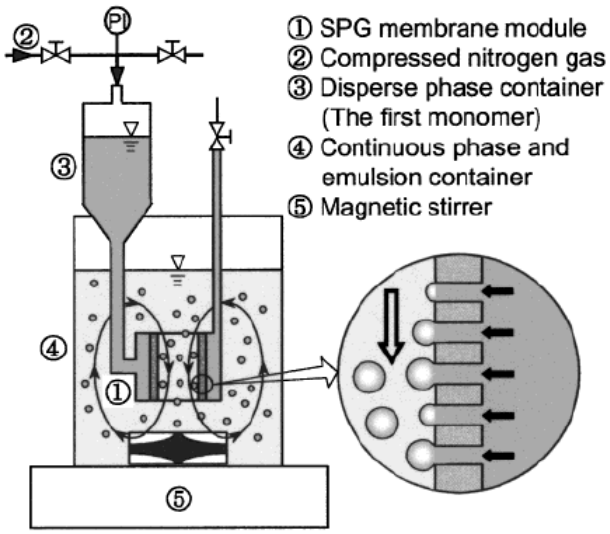

Figure 2-2: Schematic of Shirasu porous glass (SPG) filter membrane equipment for the formation of an emulsion (Chu *et al.*, 2002b)

This method has the advantage that it provides a narrower microcapsule size distribution than produced via mechanical emulsion methods. Microcapsules with an average diameter of 4 μm were prepared and addition of polyvinyl alcohol (PVA) was found to improve emulsion stability. PVA polymer chains increase steric repulsion between the droplets and increase the viscosity of the aqueous phase, which limits the diffusion and solvation of the organic phase. Despite this observation, it was established the emulsion required addition of a non-ionic surfactant, Tween 80, when PVA was added to prevent microcapsule agglomeration during the subsequent polymerisation step.

2.2. Development of a method for production of PAA grafted polyamide microcapsules

Lin, in current PhD work at the University of Waikato, New Zealand, has refined a method for polyterephthalamide microcapsule production based on that of Chu *et al.* (2001). Interfacial polymerisation was used to react TDC dissolved in an emulsified chloroform phase with a solution containing ethylene diamine and diethylene triamine monomers (Lin *et al.*, 2006). A detailed experimental procedure of Lin's method for the small-scale production of these microcapsules is provided in section 4.2.1. During optimisation of the method the authors found brittle microcapsules were produced using

solely ethylene diamine monomer in the organic phase, similar to results published by Mathiowitz & Cohen (1989). The addition of diethylene triamine was required to promote cross-linking in the polymeric structure, resulting in improved membrane strength. Microcapsules manufactured by this method were characterised using an SEM (Figure 2-3) and laser diffraction particle size analysis.

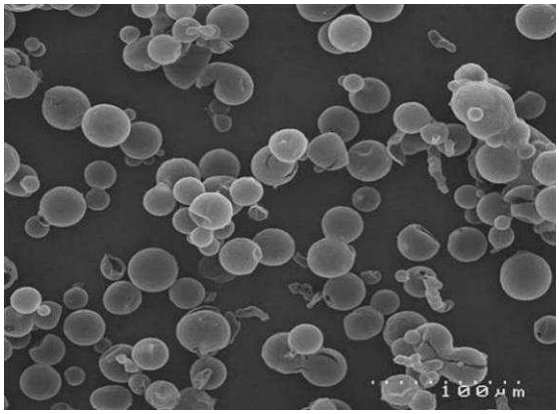

Figure 2-3: SEM micrograph of polyamide microcapsules using interfacial polymerisation method (Lin *et al.*, 2006)

An average microcapsule diameter of 28 µm was reported with a specific surface area of 135 m^2 g^{-1}. The microcapsules were stable across a pH range of 1-14 and when immersed in some solvents such as ethanol, acetone, benzene and chloroform. In addition, it was found washing of the microcapsules with ethanol at low temperatures (around 4 ^oC) after production minimised residual solvent and prevented agglomeration during the lyophilisation step. The yield of dry microcapsules produced using this method was in the range of 100-140 mg per batch.

Lin and his colleagues utilised direct current discharge, plasma-assisted grafting, to bond PAA to the microcapsule surfaces. This process involved excitation, ionisation and dissociation of electrons from the carbon atoms of the polymeric chains, resulting in free radical formation. The free radicals produced were highly reactive and were found to initiate a chain transfer polymerisation reaction with the acrylic acid monomer when in the absence of oxygen. Plasma exposure times were varied from 30 to 90 seconds, which resulted in similar grafting yields, dependant on the polymerisation time (Figure 2-4). A maximum grafting yield of approximately 0.58 mmol g^{-1} was reached after 8 hours of reaction time with acrylic acid monomer (AAm). The number of carboxylic

groups bound was determined through back titration after neutralisation of the microcapsules with dilute sodium hydroxide.

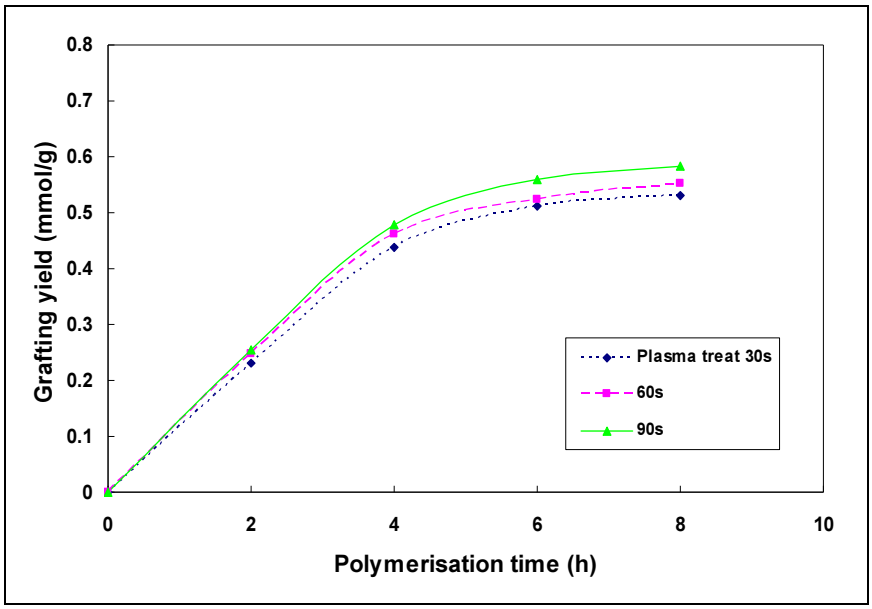

Figure 2-4: Effect of plasma activation time on grafting yield of polymerisation (Lin *et al.*, 2006)

Release profiles were determined for trial proteins cytochrome C and vitamin B_{12} with a maximum of 70 % of the material released after three changes in pH between 7 and 2 (Figure 2-5).

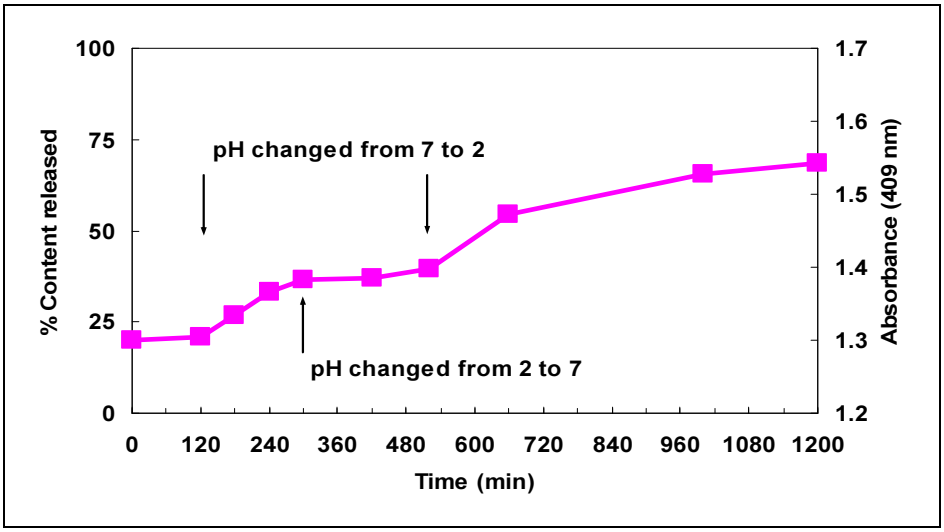

Figure 2-5: Effect of changing pH on the release of Cytochrome C from PAA-grafted polyamide microcapsules (Lin *et al.*, 2006)

Polystyrene, polysulfone and polycaprolatone polymers have also been investigated by Lin for suitability in production of porous microcapsules. In each case spherical porous structures were produced, but grafting by plasma initiation was only successful with polystyrene capsules. Of the polymers tested, polyamide was determined to be most promising for scale-up as the method tended to produce higher proportions of hollow microcapsules rather than microspheres with internal partitioning. Less promising was the plasma-assisted grafting method for attachment of PAA chains to the microcapsules. The small quantities of capsules produced by this grafting method are insufficient for robust release profile testing in future field trials. The method has little scope for process scaling as highly specialised equipment is required with a considerable capital cost.

2.2.1. Effecting polymer response to environmental stimuli

Gupta *et al.* (2002), summarised the range of current polymers used for controlling release of compounds from hydrogels in response to external stimuli. Hydrogels are cross-linked polymers used for tissue scaffolds or drug delivery. The gel matrix is reported to have the ability to swell by more than 20 %, allowing retention of aqueous phase compounds for later release. Table 2-1 below summarises the variety of polymers grafted to hydrogels to enable response to environmental stimuli.

Table 2-1: Stimuli responsive polymers for controlled release in drug delivery applications (Gupta *et al.*, 2002)

Stimuli	Polymer
Magnetic field	Ethylene-co-vinyl acetate
Ultrasonic radiation	Ethylene-co-vinyl alcohol
Electric field	Poly(2-hydroxyethyl methacrylate)
Glucose	Ethylene-co-vinyl acetate
Urea	Methyl vinyl ether-co-maleic anhydride
Morphine	Methyl vinyl ether-co-maleic anhydride
Antibody	Poly(ethylene-co-vinyl acetate)
pH	Chitosan-poly (ethylene oxide) Polyacrylic acid Gelatin : Chitosan-poly (ethylene oxide) Poly(2-hydroxyethyl methacrylate) Poly (acrylamide-co-maleic acid) N-vinyl pyrrolidone, polyethylene glycol diacrylate, chitosan
Temperature	Poly(N-isopropyl acrylamide)
pH and Temperature	Poly(N-isopropyl acrylamide-co-butyl methacrylate-co-acrylic acid)

2.3. Grafting methods of acrylic acid monomer on polyamide substrates

Various methods have been used to induce graft co-polymerisation of acrylic acid to polymer substrates. The most common are irradiative methods or thermal degradation methods using a chemical initiator. Methods involving chemical initiators are less favourable in this instance as contaminants have to be removed before dosing of the microcapsules. This section of the literature review is focused primarily on irradiative grafting methods. The mechanism of formation for free radicals is analogous in each case; sufficient energy is provided at the polymer surface to abstract a hydrogen atom and generate a free radical. At this point chain transfer polymerisation creates the polymer chains that elicit the response to environmental stimuli.

2.3.1. Grafting mechanisms of acrylic acid onto polymer surfaces

The grafting of acrylic acid to the polymer surfaces is reported as a chain transfer free radical polymerisation, which follows the main reaction steps as specified in Equations 2-1 - 2-7 (Fogler, 1999; Dotson *et al.*, 1996). The reaction is initiated by radiation forming a surface free radical on the polymer (*P*) through abstraction of a hydrogen atom (*H*) as detailed in Equation 2-1.

$$PH \xrightarrow{UV} \dot{P} + H^{+} \qquad \textbf{(2-1)}$$

The polymer free radical group is highly reactive with acrylic acid monomer units (*M*) when in a de-oxygenated environment (Equation 2-2).

$$\dot{P} + M \longrightarrow P\dot{M}_1 \qquad \textbf{(2-2)}$$

The reaction is continued through chain transfer polymerisation in which the free radical is propagated along the monomer units as they adhere to the chain terminus (Equation 2-3). Subscript *j* denotes the number of the monomer unit.

$$P\dot{M}_j + M \longrightarrow P\dot{M}_{j+1} \qquad \textbf{(2-3)}$$

This process continues until the chain is terminated in one of three primary ways. The first is chain transfer where the free radical is transferred to a free monomer unit leaving a ‘dead’ polymer chain shown by Equation 2-4.

$$P\dot{M}_j + M \longrightarrow PM_j + \dot{M} \qquad \textbf{(2-4)}$$

There are two other predominant methods of termination. First, addition links two polymer chains forming a ‘dead’ bridge molecule as in Equation 2-5.

$$P\dot{M}_j + P\dot{M}_i \longrightarrow PM_{j+i}P \qquad \textbf{(2-5)}$$

Second, the chain may end by disproportionation in which a proton is exchanged forming two 'dead' chains, one saturated and the other with a terminal double bond (Equation 2-6).

$$P\dot{M}_j + P\dot{M}_i \longrightarrow PM_j + PM_i \qquad \textbf{(2-6)}$$

Aside from these primary reaction steps, some homopolymerisation of the monomer may occur (Equation 2-7).

$$\dot{M}_j + M_i \longrightarrow M_j\dot{M}_i \qquad \textbf{(2-7)}$$

In addition, a number of less dominant side reactions have been described such as; transfer of the free radical to contaminants in free solution and free radical transfer to the suspension solvent.

2.3.2. Low frequency plasma

Low frequency plasma irradiation is a well-established grafting technology allowing for the modification of polymer surface properties. Lee & Shim (1997), used a 30 W plasma grafting method to initiate the formation of highly reactive peroxide groups on the surface of a porous polyamide filtration membrane. The membrane was placed in a monomer solution containing both acrylic acid and N-isopropylacrylamide at 20 % (w/w) with an acrylic acid concentration of less than 10 % (w/w) for a period of 2 hours at 60 ^{o}C. Reduction in the permeability of riboflavin was observed at elevated pH and with lower membrane temperatures. Characterisation of the grafted surface was achieved by Fourier transform infrared spectroscopy, using attenuated total reflectance (FT/IR-ATR), and X-ray photoelectron spectra (XPS). The presence of acrylic acid was confirmed by FT/IR detection of the carbonyl bond at 1730 cm^{-1}.

A corona discharge method has also been exploited to graft acrylic acid monomer onto a low density polyethylene polymer (LDPE) film (Lei & Liao, 2001). The grafting was carried out under an inert nitrogen atmosphere at 70 ^{o}C over 1.5 hours. Increasing the

reaction time was found to increase the grafting degree up until 2 hours of exposure, whereupon the grafting amount levelled (Figure 2-6).

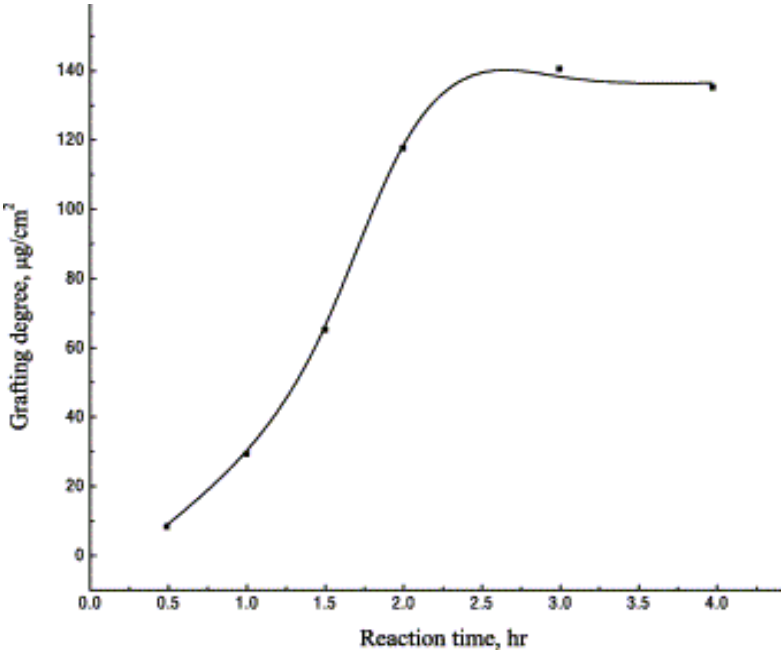

Figure 2-6: Effect of reaction time on the plasma initiated grafting degree of acrylic acid monomer on LDPE film (Lei & Liao, 2001)

Increasing the reaction temperature was also noted to directly increase the grafting yield for a constant period of graft time (Figure 2-7). Likewise, an increase in the concentration of acrylic acid monomer solution increased the grafting degree as shown by Figure 2-8.

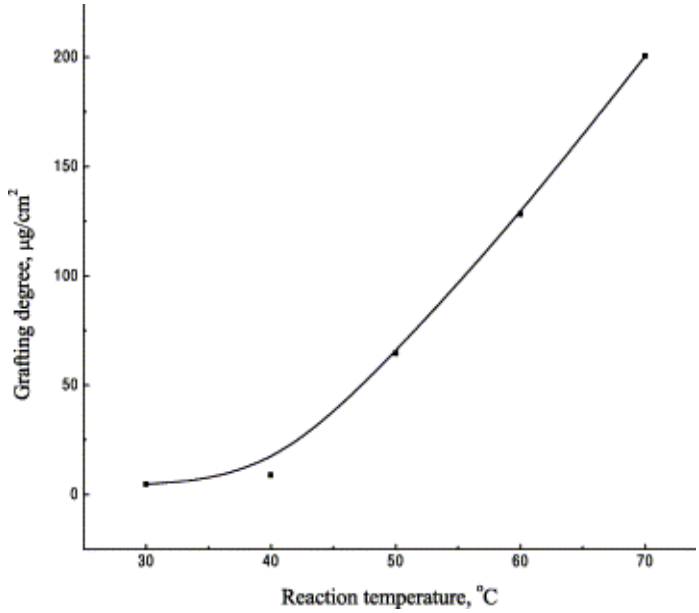

Figure 2-7: Effect of temperature on the plasma initiated grafting yield for acrylic acid monomer on LDPE film (Lei & Liao, 2001)

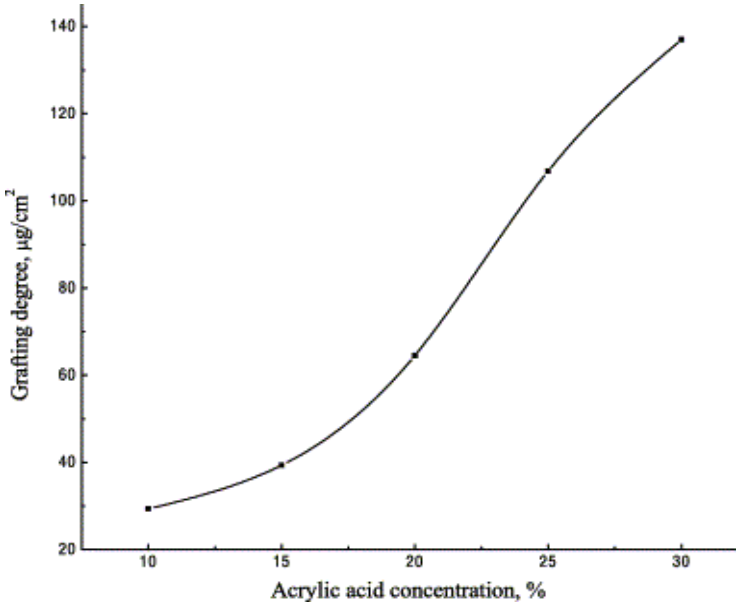

Figure 2-8: Effect of acrylic acid monomer concentration on the plasma initiated grafting yield for acrylic acid on LDPE film (Lei & Liao, 2001)

Of particular note are the membrane characterisation methods used by the authors. The grafting degree was calculated using a back titration method which involved the neutralisation of the film in sodium hydroxide (NaOH) / ethanol (EtOH) solution of known volume and concentration. Dilute hydrochloric acid (HCl) was titrated to neutralise the remaining base using phenolphthalein as an indicator. From this, the grafting degree was determined using Equation 2-8.

$$X = \frac{\left(V_{NaOH} C_{NaOH} - V_{HCl} C_{HCl}\right)}{S} \qquad \textbf{(2-8)}$$

V_{NaOH} and V_{HCl} represent the volume of NaOH and HCl solutions respectively, C_{NaOH} and C_{HCl} the concentration and S the surface area of the film in cm^2. FT/IR-ATR was used to confirm the presence of grafting on the film surface. Both ungrafted and neutralised grafted films were compared. A strong response was obtained at 1574 cm^{-1} due to the stretching motion of the C=O group in the COONa functional group, indicating grafted polyacrylic acid. This method of analysis enables confirmation of grafting after the back titration has determined the number of carboxylic acid groups.

More recently, Choi *et al.* (2004) used a 100 W plasma to graft methacrylate groups onto a polyurethane surface. Similar to the findings of Lee & Shim (1997), contact with oxygen following plasma exposure introduced reactive peroxide groups for grafting of the acrylic acid monomer. The membrane was incubated with the monomer solution for 1.5 hours at a temperature of 70 ^{o}C. Acrylic acid monomer concentrations were tested over a broad range, with the grafting yields peaking at an acrylic acid concentration of 60 % (v/v) (Figure 2-9).

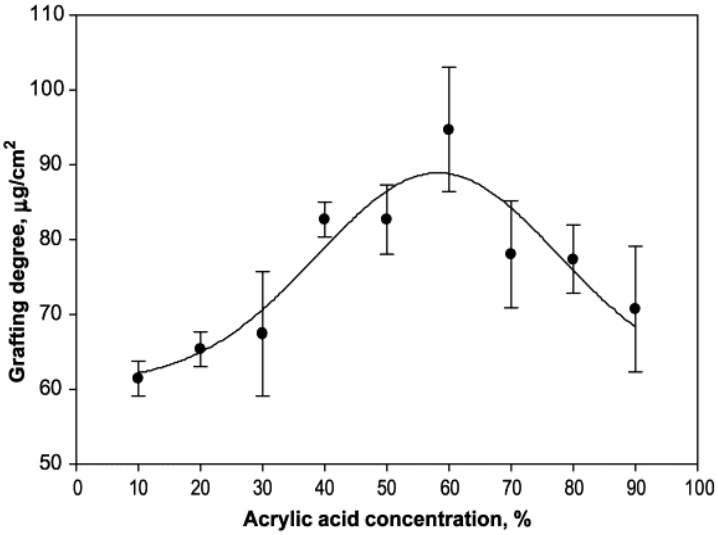

Figure 2-9: Effect of AAc concentration on the grafting of AAc onto polyurethane membranes (Choi *et al.*, 2004)

A maximum grafting degree value of 90 μg cm^{-2} was attained at this concentration corresponding to 0.00125 mmol cm^{-2}. The grafting degree levelled as reaction time was increased above 3 hours as indicated in Figure 2-10, similar to trends identified by Lei & Liao (2001).

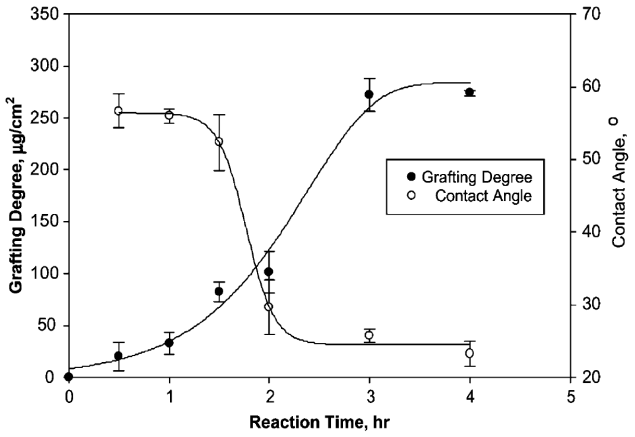

Figure 2-10: Effect of reaction time on the plasma initiated grafting degree of acrylic acid monomer on a polyurethane surface (Choi *et al.*, 2004)

FT/IR-ATR, contact angle measurement and XPS were employed to characterise the membranes. A sharp decrease in the pure water flux was noted at a pH of 5, which continued to decrease gradually as the pH was raised from 3 to 7.

Chu *et al.* (2004) prepared glucose sensitive microcapsules using PAA chains as gate molecules and a glucose oxidase (GOD) enzyme covalently bonded to the polymer shell. An oxidation reaction was catalysed by GOD in which gluconic acid is formed from glucose. The formation of acidic ions lowers the pH of the local environment causing a contraction of the PAA chains. Chain length reduction enables the release of the microcapsule contents as the effective pore size increases. The authors prepared polyamide microcapsules by a similar method to that used by Lin *et al.* (2006), differing only in the absence of the diethylene triamine cross-linking monomer. Desiccated microcapsules were exposed to a 30 W radio-frequency plasma. Following activation, the microcapsules were submerged in acrylic acid monomer and the mixture vibrated at 30 ^{o}C. Potassium bromide pellet FT/IR spectroscopy was used to analyse the grafted capsules, with new peaks occurring at 1715 cm^{-1} and 1453 cm^{-1} when grafted and ungrafted samples were compared. The peak at 1715 cm^{-1} was determined to be the

response from the carboxyl groups in the polyacrylic acid chains. Both sodium chloride (NaCl) and vitamin B_{12} were used to test the glucose sensitive release in a 0.2 mol L^{-1} sugar solution (Figure 2-11). The concentration of NaCl was measured by conductivity readings and vitamin B_{12} concentration by UV absorbance at 361 nm.

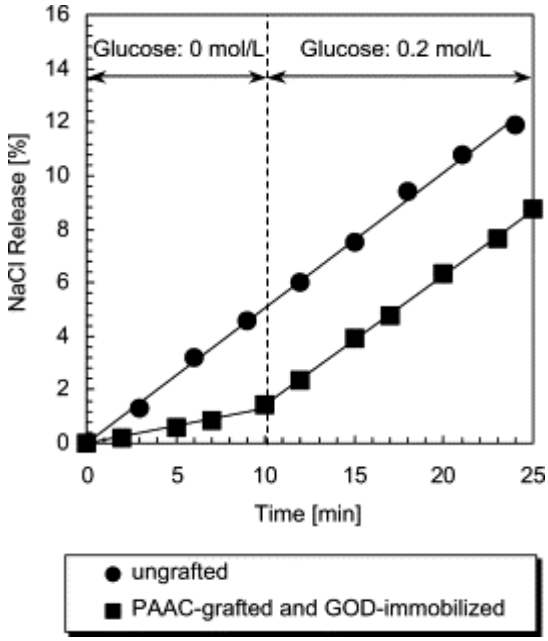

Figure 2-11: Glucose sensitive release of NaCl from polyamide microcapsules with and without grafting (Chu *et al.*, 2004)

The release profile for vitamin B_{12} was reported to follow a similar trend to that of NaCl, except the diffusional permeability, a measure of the rate of the contents leaving the capsule, did not increase as significantly as for NaCl. The authors suggested a possible application of this technology could be the dosing of insulin in the body for treatment of diabetes. It was contested a more consistent insulin concentration in the body, with a reduced dosing frequency, could be achieved than by current injection methods.

Multiple publications detail methods for plasma-activated grafting of poly(N-isopropylacrylamide) (PNIPAM) functional gates to polyamide based microcapsules. Chu and co-workers (2001; 2002b; 2002a; 2003) all prepared porous polyamide microcapsules with PNIPAM gates using a 30 W plasma discharge apparatus. At elevated temperatures, above the lower critical solution temperature, the PNIPAM gates

were observed to be hydrophobic and shrunken, allowing release of the drug into the surroundings.

2.3.3. Ultraviolet light assisted grafting to polymers

The required wavelength of UV radiation for creation of free radicals on the surface of low density polyethylene (LDPE) was studied by Yang & Rånby (1996). Benzophenone, used as photo-initiator, was exposed to UV light emitted from a 2 kW high pressure mercury lamp. They concluded far UV radiation with a wavelength range of 200 – 300 nm was required to overcome the bond energy of the C–H bonds on the polymer surface. Longer wavelength radiation significantly reduced the rate of acrylic acid surface polymerisation. The bond energy of the C–H bond was reported to have approximately the same energy as 300 nm UV light.

UV grafting of AAc monomer to polyethylene terephthalate (PET) plastic film surfaces was performed without the addition of a photosensitiser (Uchida *et al.*, 1990). Instead, the authors added sodium periodate, with an optimal concentration of 1×10^{-3} mol L^{-1}, to the reaction mixture to remove all traces of oxygen prior to grafting. As an alternative, it was suggested oxygen could be removed in a degassing procedure using an inert gas or freeze thaw cycle. However, this was deemed excessively costly if the process was to be scaled. A 400 W high pressure mercury UV lamp was set to a distance of 7.5 cm from the film surface prior to irradiation in a 10 % (w/w) acrylic acid solution. The temperature was maintained at 35 ^{o}C for 90 minutes during the graft operation. Under these conditions a maximum grafting yield of 10 μg cm^{-2} was attained.

The method was repeated by the same authors, Uchida *et al.* (1993), under the same process conditions for grafting of AAc, 2-acrylamide-2-methylpropane sulfonic acid, N,N-dimethyl aminopropyl acrylamide and dimethyl aminoethyl methacrylate monomers. Maximum grafting yields in the order of 5 – 20 μg cm^{-2} were observed for each monomer. This was intended to demonstrate the versatility of the method for grafting a variety of monomers to PET films.

The sole instance of grafting acrylic acid to commercial polyamide membranes by UV radiation in the literature was found in a study comparing the differences between UV and plasma grafting methods (Lee *et al.*, 1995). The UV method used benzophenone as a photo initiator to facilitate the free radical polymerisation. A 20 % AAm solution was used to immerse the membranes at 60 ^{o}C following exposure to either a 450 W UV lamp for 30 minutes or 50 W argon plasma for up to 7 minutes. FT/IR-ATR spectra confirmed the presence of the carboxyl group at an absorption peak value of 1730 cm^{-1}. It was found the plasma discharge technique limited grafting to the external surfaces of the membrane, contrary to UV treatment, which had a greater penetration of the matrix. As a result, the plasma grafted membranes were more sensitive to environmental pH changes when riboflavin permeation was tested. It was asserted the excess monomer polymerised under UV light conditions, subsequently reducing the effectiveness of the polymer gates. Despite this, the UV modified membranes were observed to exhibit response to pH which improved with higher concentrations of AAc monomer (≈ 30 % w/w). The authors suggested higher monomer concentrations were responsible for the creation of higher graft densities on the polyamide membranes.

Richey *et al.* (2000), explored surface modification techniques of polyethylene balloon catheters for use in localised drug delivery. The intention was to improve the efficiency of drug delivery to diseased vessels without causing further tissue damage. Acrylic acid monomer was grafted to the catheters using a 1000 W mercury UV lamp with a wavelength range of 253.7 - 579.1 nm. Modified samples were analysed using XPS, which confirmed a successful surface modification. It was noted that the grafting efficiency was limited by the viscosity of the monomer solution, hence grafting of viscous AA monomer required a longer exposure time in comparison to less viscous solutions.

Wei *et al.* (2006) developed a unique method to modify the surface of an ultrafiltration membrane with charged moieties. In this research polyethersulfone membranes were prepared using UV-C light (254 nm) at an intensity of 2 - 4 mW cm^{-2} to graft AAm to the surfaces. In combination, electrophoresis was employed to generate an electric field surrounding the membrane. This formed a homogenous distribution of PAA chains on the polymer surfaces. Nitrogen gas was used as an inert blanket to prevent oxidation of

the free radical macromolecules generated through irradiation. Characterisation of grafting was achieved by SEM and determination of the membrane pure water flux.

2.3.4. Gamma radiation assisted grafting to polymers

Turmanova *et al.* (1997) grafted acrylic acid onto a polytetrafluoroethylene (PTFE) film for use as a membrane biosensor. The procedure was successful at grafting AAm when gamma radiation was released at a dose rate of 5 kGy h^{-1}. Higher yields were observed with multiple irradiations.

The behaviour of acrylic acid hydrogels synthesised using gamma-induced grafting was investigated in papers by Jabbari & Nozari (2000) and Rosiak & Ulanski (1999). Evidence was presented showing the high intensity of the radiation led to the cross-linking of either homo or co-polymers, forming a networked structure. Jabbari and Nozari used Cobalt 60 isotope to generate 5 kGy h^{-1} radiation with various exposure times to alter the total radiation energy delivered dose. The mechanisms of free radical macromolecule formation by gamma radiation exposure were explored by Rosiak and Ulanski. They concluded the presence of oxygen increases the rate of PAA chain scission through formation of mid-chain peroxides. Despite this, oxygen did not completely prevent the formation of a hydrogel, as cross-linking occurred once the oxygen in free solution was consumed. As long as the consumption rate of oxygen exceeded the rate of diffusion into the medium, the cross-linking mechanism proceeded. These findings indicated a more efficient polymerisation is achieved in a deoxygenated environment.

2.3.5. Alternative methods of grafting acrylic acid to polymer

Alternative and often unconventional methods of delivering energy to the polymer surface to promote electron excitation and free radical formation were explored. Massa *et al.* (2005) published a technique using Argon ion irradiation. Acrylic acid was successfully grafted at monomer concentrations greater than 40 % (v/v) when a 100 keV ion beam was directed at a polypropylene film. Argon ions produced superficial

changes to the polymer surface with penetration depths not exceeding a few millimetres. This was found to prevent an alteration in the mechanical strength and bulk polymer properties. A maximum graft degree of 125 % weight increase of the film was achieved with film submerged in a 79 % (v/v) acrylic acid solution at 62 ^{o}C.

Timus *et al.* (2000) and Clochard *et al.* (2004) both experimented with electron beam irradiative methods on polyamide and polyvinylidene fluoride (PVDF) films respectively. Characterisation of the acrylic acid grafted polyamide film by Timus and colleagues using FT/IR revealed peaks in the wavelength interval 1720 – 1760 cm^{-1} (Figure 2-12).

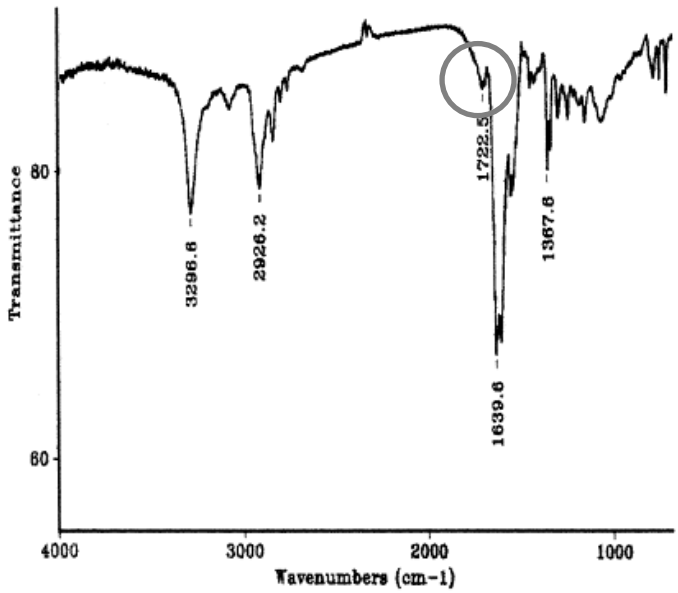

Figure 2-12: FT/IR spectrum of acrylic acid grafted polyamide film showing carbonyl bond circled at 1722.5 cm^{-1} (Timus *et al.*, 2000)

Quantification of the number of acrylic acid monomer units in the PVDF study was possible, with detectability limits approaching the micromole level, using a Cu^{2+} - EDTA complex analysed by UV spectroscopy at 740 nm.

The effect of proton beam radiation on polymer surfaces for graft polymerisation was studied by Mazzei *et al.* (2003). Free radical groups were reportedly generated by irradiation before exposure to oxygen, creating reactive peroxide groups. Subsequent deposition in acrylic acid monomer solution attained a graft yield of 11 % by weight after 22 hours of reaction. Mazzei concluded the post-graft polymerisation approach

was more advantageous than methods where direct monomer exposure to radiation can lead to homopolymerisation of the monomer. Homopolymerisation was found to be further lessened through addition of 0.1 % Mohr salt.

Research undertaken at McMaster University, Canada was aimed specifically at developing a pH responsive membrane for post-ruminal controlled release drug delivery (Hu & Dickson, 2005). Polyacrylic acid was targeted as a gateway mechanism for pores within a PVDF film. The authors used a thermally initiated mechanism to instigate grafting as other methods may have affected the structural integrity of the membrane. A maximum mass gain of 90 % was seen in membranes after the grafting procedure. Membrane pure water flux performance was characterised as a function of pH in the range 2 to 7. A drastic reduction in flux was detected and found to level after the pH reaches 5.

2.4. External irradiation reactor designs

Following the investigation into irradiative methods, design of scalable reactor systems was researched. Summarised below are a few reactor designs which influenced the final graft reactor design as implemented in this work.

A simple design for effluent degradation was employed by Tokumura *et al.* (2006). A UV transmittable column photoreactor was surrounded by three UV tubes outputting 252 nm wavelength light. This conformation allowed for effluent slurries to be treated in a batch operation process. Agitation was provided by a flat bladed impellor.

To reduce the shear stress caused by mechanical agitation, a fluidised bed reactor may be used (Lee *et al.*, 2003). These authors designed a compressed air reactor to fluidise methyl orange in order to study photo-initiated reaction mechanisms. As an alternative to gaseous fluidisation of a dry powder, a bubble column may be used to mix an aqueous solution. This technology is exemplified in a reactor design published by Agustina *et al.* (2008) for use in treatment of waste generated during the winemaking process (Figure 2-13).

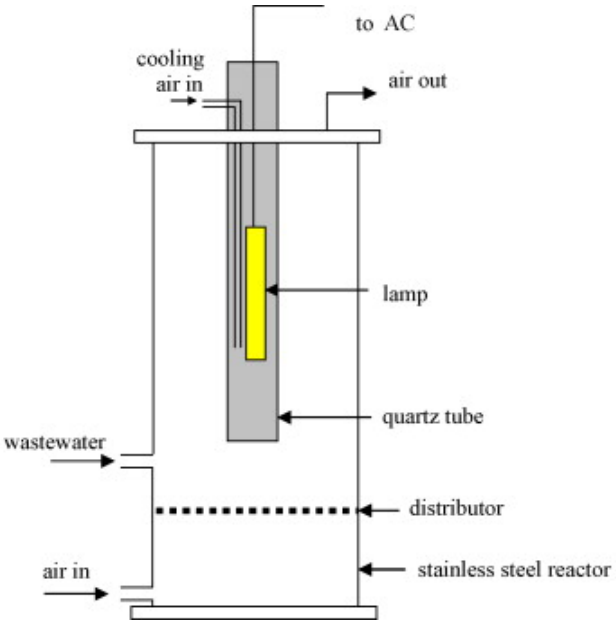

Figure 2-13: Bubble column reactor as used for the treatment of wastewater from the wine industry (Agustina *et al.*, 2008)

An interesting variation on mixed flow reactor design termed the Taylor – Couette reactor was investigated and reported to be easily scaled by Forney *et al.* (2003), Forney & Pierson (2003) and Forney & Pierson (2004). The proposed application was for use in a variety of sterilisation applications such as waste water or orange juice treatment. Plug flow reactor designs yield characteristics such as large surface-to-volume ratios favourable for high UV transmission rates. The major disadvantage to this approach is non-uniform radiation intensity and stagnant boundary wall areas. These unfavourable effects can be substantially reduced with an increase in flow, limited principally by the resulting reduction in the residence time. The Taylor – Couette design incorporated the low holdup volume of a plug flow system with the hydrodynamics of a mixed reactor as demonstrated by the generation of localised vortices (Figure 2-14).

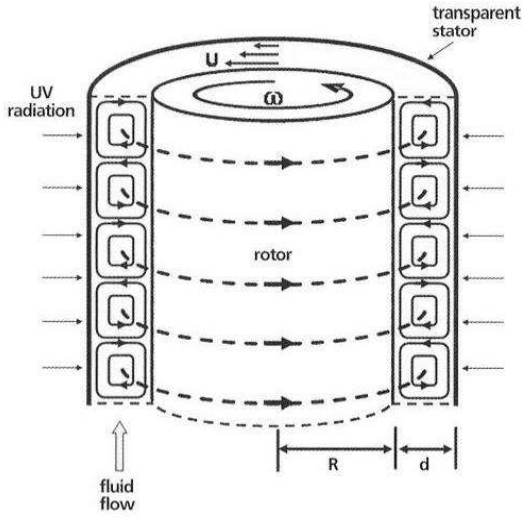

Figure 2-14: Taylor – Couette reactor for low volume high turbulence mixing in photolytic applications (Forney & Pierson, 2004)

A novel approach to increase the surface-to-volume ratio in a photolytic reactor system was published by Ray & Beenackers (1998). The system used quartz rods to internally reflect UV rays delivering a higher intensity of light to a greater proportion of the medium. To prevent total internal reflection, the quartz glass rods were coated in titanium dioxide, a photocatalyst for the removal of pollutants from wastewater.

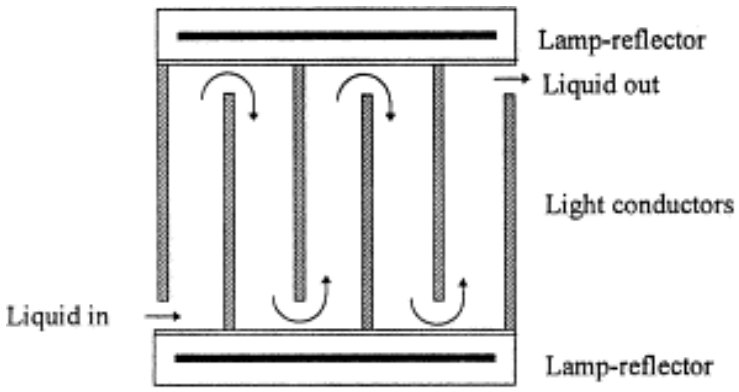

Figure 2-15: Distributive photo-catalytic reactor with increased emission surface area (Ray & Beenackers, 1998)

The paper illustrated that a higher surface area of glass tube exposed to UV will aid in reactor performance.

2.5. Biocompatibility of polyamide, polyacrylic acid and methylene blue dye

A literature search revealed little in the way of toxicity, biocompatibility or cytotoxicity studies on the particular combination of compounds used in this project, namely polyacrylic acid grafted polyethylene terephthalamide. However, a cytotoxicity study on polyurethane membranes UV grafted with polyacrylic acid was performed by Yang & Yeh (1999), to determine the adverse health effects of chemical leaching from the structures. Madin-Darby kidney cells were grown in solutions containing polymer samples for up to 72 hours. Cell counts revealed very low or no growth reduction in samples containing membranes when compared to control samples. A segment of membrane was then introduced to the colon of a female rabbit and implanted for one month to further study the toxicity. Good regeneration was observed around the site of the implant, suggesting a high suitability for in-vivo use of this polymer.

An *in-vitro* study of cross-linked polyacrylic acid hydrogels revealed an excellent biocompatibility with mouse fibroblast cells (Rosa *et al.*, 2004). Propagation of cell growth was observed up to concentrations of 120 mg ml^{-1} of polyacrylic acid. The results of these studies suggested polyacrylic acid, once grafted to a polymer substrate, posed little toxicity threat.

Several sources specifically report the use of Nylon polyamide bags for modelling feed distribution and consumption rates of nutrients in ruminant animals (Reeves *et al.*, 1991; Taghizadeh *et al.*, 2005; Cone & van Gelder, 2006). While no report was made on toxicity evaluations, polyamide was selected by the authors as a bag material due to its inert nature and resistance to ruminal conditions.

Methylene blue was proposed for *in-vivo* use for testing the release profile of the polyamide microcapsules in ruminant animals (Burrows, 1984). Burrows undertook an ovine toxicology study to determine the lethal dose for 50 % of test animals (LD 50) for intravenously delivered methylene blue. The LD 50 over a 24-hour period administering a 3 % solution was determined to be 42.3 mg kg^{-1} with a 95 % confidence limit interval of 37.3 to 47.9 mg kg^{-1}. Based on these figures a safe dosage was recommended to be

15 mg kg^{-1} day^{-1}. After a total combined dose of 50 mg kg^{-1} over 4 weeks no change in haematological composition was observed.

2.6. Confocal microscopy in microcapsule release characterisation

Alternative analysis techniques for characterisation of microcapsule release profiles were investigated in conjunction with the methods reported in section 2.3. The advantages of using confocal techniques for microcapsule characterisation were outlined in work by Lamprecht *et al.* (2000) and a review by Pygall *et al.* (2007). Confocal microscopy is a non-invasive, non-destructive technique, allowing for a qualitative analysis of the optical properties of a sample. The method is most distinguished for the ability to filter out unfocused sources to give a clear image of the sample at a given cross-section below the surface.

Polyanhydride and polylactic acid microspheres were characterised using a fluorescent polyethylene glycol (PEG) marker previously coupled with fluorescein dye by Lacasse *et al.* (1998). A uniform PEG distribution was observed within the microspheres, with no detectable binding to the microspheres following addition of bovine serum albumin blocker protein to the slurry. PEG fluorescein dye was used in this study for several reasons; the PEG molecule is uncharged, exhibits little interaction with other molecules and is available in a variety of molecular weights.

Determan *et al.* (2004) used confocal microscopy with a fluorescein isothiocyanate labelled bovine serum albumin (BSA) protein to study the release profiles from polyanhydride microspheres. Microcapsules loaded with the BSA marker were added to an aqueous solution, whereupon polymer degradation allowed release to the surroundings. This enabled the drug distribution within the microcapsules to be established and the release profile determined. Gel electrophoresis was used to quantify the amount of released protein.

Using the fluorescent dyes Rhodamine B, p-nitroalanine and piroxicam Berkland *et al.* (2004) studied the influence of hydrophobicity on drug retention characteristics and

release rates using poly(sebacic) anhydride microcapsules. The most hydrophilic of the dyes, rhodamine, had a strong affinity for the microcapsule surfaces while piroxicam, the most hydrophobic, showed an even internal distribution. Rhodamine dye was observed to release very quickly from the microcapsules and tended to be independent of microcapsule size. Release of piroxicam showed a more sustained release which, interestingly, was lengthened with a decreasing microcapsule size.

Singer & Johnson (1997) have reported a strong pH sensitivity for fluorescein dyes. As shown in Figure 2-16 fluorescein exhibits very little fluorescent intensity at low pH when compared to a neutral pH. Rhodamine green dye was suggested for studies involving low pH due to a highly stable pH emission intensity profile.

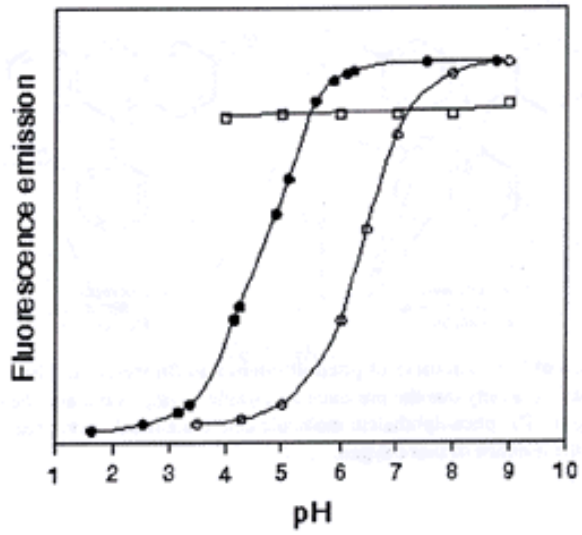

Figure 2-16: Comparison of the fluorescent intensity of several dyes over a range of pH; Oregon Green 488 dye (solid circles), fluorescein (open circles) and Rhodamine Green (open squares) (Singer & Johnson, 1997)

As an alternative, 6 – carboxytetramethylrhodamine (TAMRA) has been identified as a suitable candidate for pH independent fluorescent studies (Brunner *et al.*, 1998). When coupled to atrial natriuretic peptide, a 16708 Da molecule, the fluorescence was reduced at lower pH but was still readily detected over the pH range 2.2 – 8 (Figure 2-17).

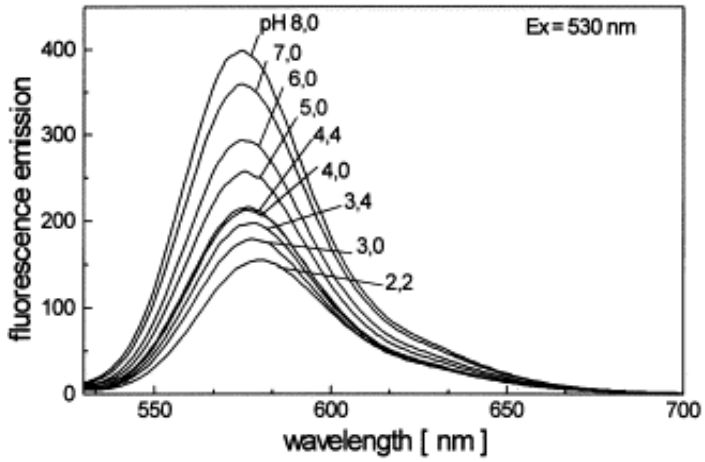

Figure 2-17: Fluorescent emission of ANP coupled TAMRA over a range of varied pH citric acid buffers (Brunner *et al.*, 1998)

It was speculated that conformational changes in the peptide structure or alteration of the dye structure during the reaction produced this sensitivity.

Chapter 3 Reactor design

Several pieces of equipment were specially designed and constructed for both microcapsule fabrication and ultraviolet grafting during the course of the project. The following subsections give details of the design outcomes and calculations performed; particularly those pertaining to scale-up of the apparatus which will be useful for future development of the process.

3.1. Guidelines for reactor design

The design of reactors in this project, both for microcapsule formation and UV grafting, was guided by the following criteria. First, the process should be of low energy requirement. Removal of energy intensive operations from the original production method defined by Lin *et al.* (2006), such as freeze-drying and centrifugation, were targeted. Second, process time was to be kept to a minimum to increase the rate of production of microcapsules. Third, minimisation of the overall cost of the equipment was deemed essential to ensure a greater probability of commercial viability following scale-up. Fourth, robust materials for chemical resistance and durability should be selected to reduce operation time loss due to equipment failure. Materials were often tested in process solvents before implementation to ensure compatibility. Finally, maximisation of the microcapsule yield was pursued by maintaining a closed system without need for extraneous material transfer between process steps. An advantage of this is a much simpler process leading to an easier operation following scale-up.

The design was centred about four main process steps as outlined below. A detailed experimental methodology can be found in section 4.4.1.

- Production of polyamide microcapsules using an oil-in-water emulsion method.
- Washing of ungrafted microcapsules to remove residual solvent and reactants.
- Grafting of acrylic acid functional gates to microcapsule surfaces to provide pH responsiveness through UV irradiative grafting.

- Washing and separation of grafted microcapsules to remove excess acrylic acid monomer and graft reaction by-products such as homopolymer.

The above process operations were achieved by splitting the production into two components; an emulsification reactor for microcapsule formation and an external closed loop UV reactor for grafting. These systems were coupled to provide a continuous 2 L circulation system for production and subsequent grafting of microcapsules. Figure 3-1 below presents a line diagram of this final design solution.

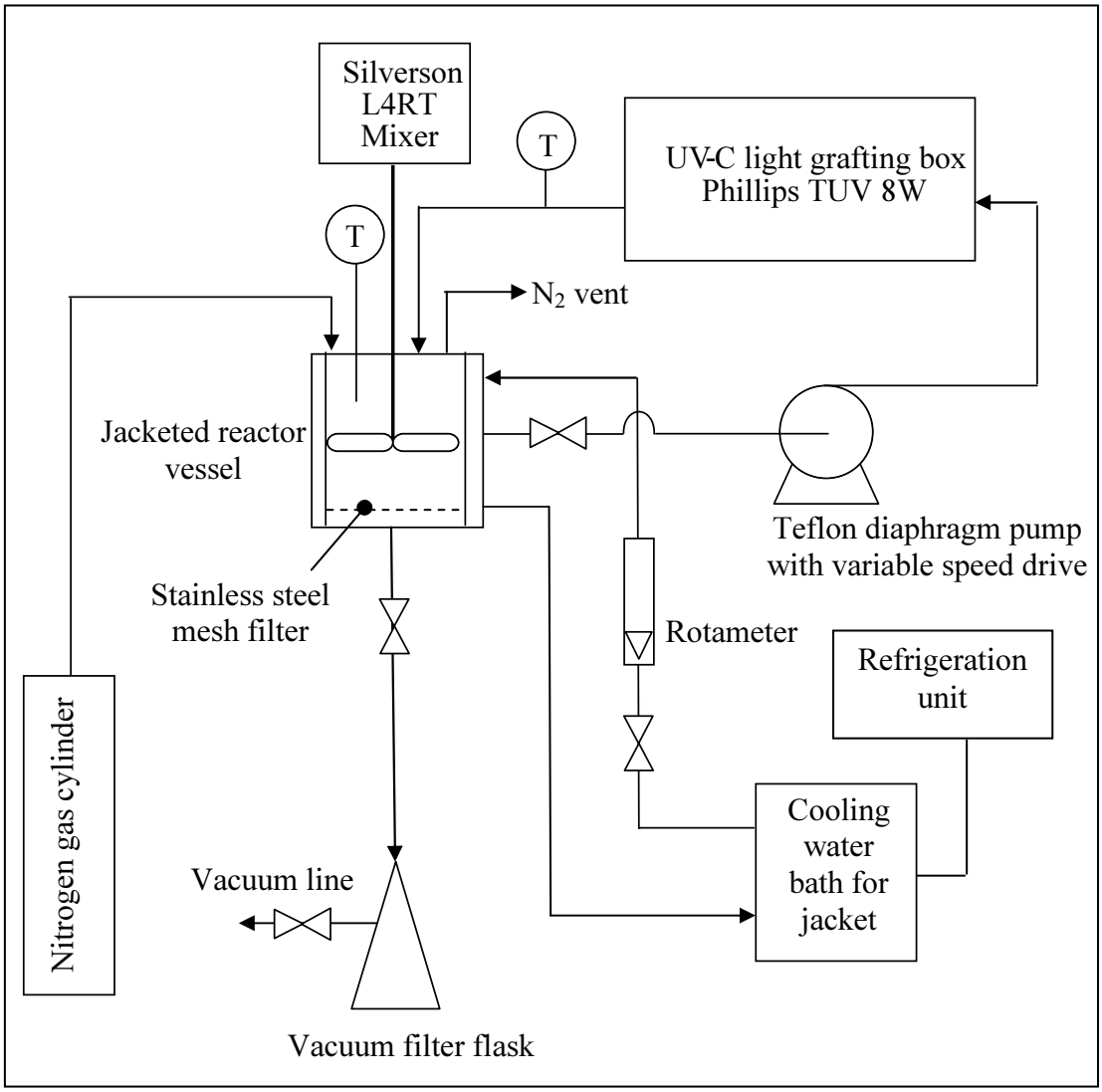

Figure 3-1: Equipment layout for 2 L scale production and grafting of microcapsules

Thermocouple probes were used to obtain temperature measurements at the reactor outlet and in the jacketed reactor vessel. A vacuum filter flask was used to drain microcapsule wash water with an applied vacuum to speed the process. Rationale for

design choices and specific design details surrounding both components are presented in the following sections.

3.2. Rationale for selection of UV for irradiative grafting

Ultraviolet irradiation was found to be a lesser utilised technique for grafting acrylic acid to polymer substrates. Despite this, it has significant advantages over other irradiative treatments as it is much cheaper, safer, simpler and more robust. UV methods do not require expensive equipment (electron beam exposure), high temperatures (chemical grafting), low pressure (plasma grafting), nor is it as inherently dangerous to personnel as gamma radiation exposure (Lei & Liao, 2001). However, a detrimental effect of using UV is a decrease in the mechanical strength of the polymer, which could render the method unsuitable for membrane production where strength is of greater importance. Owing to the small size and proposed application of the microcapsules, small changes in the physical properties are likely to be less important. As a result, UV grafting was pursued as a scalable alternative to the existing plasma grafting procedure.

The limited depth of penetration of UV radiation reduces exposure risk and avoids expensive, bulky containment apparatus. The principle behind the free radical formation is much the same as the plasma-induced method. However, longer exposure times may be required. While there is abundant literature on UV grafting methods to various polymer bases, there was little to be found specifically on UV grafting of acrylic acid to polyamide films. However, as most irradiation processes abstract hydrogen atoms from the carbon backbone of the polymer, methods should be relatively translatable so long as the base polymer structure is similar to that of polyamide.

3.3. UV light box design for proof of concept

The UV grafting concept for attachment of polyacrylic acid chains to polyterephthalamide microcapsules required testing before a pilot grafting reactor could

be constructed. Based on the study by Pieracci *et al.* (1999), a simple reactor design was conceived for grafting polyamide samples, as illustrated in Figure 3-2.

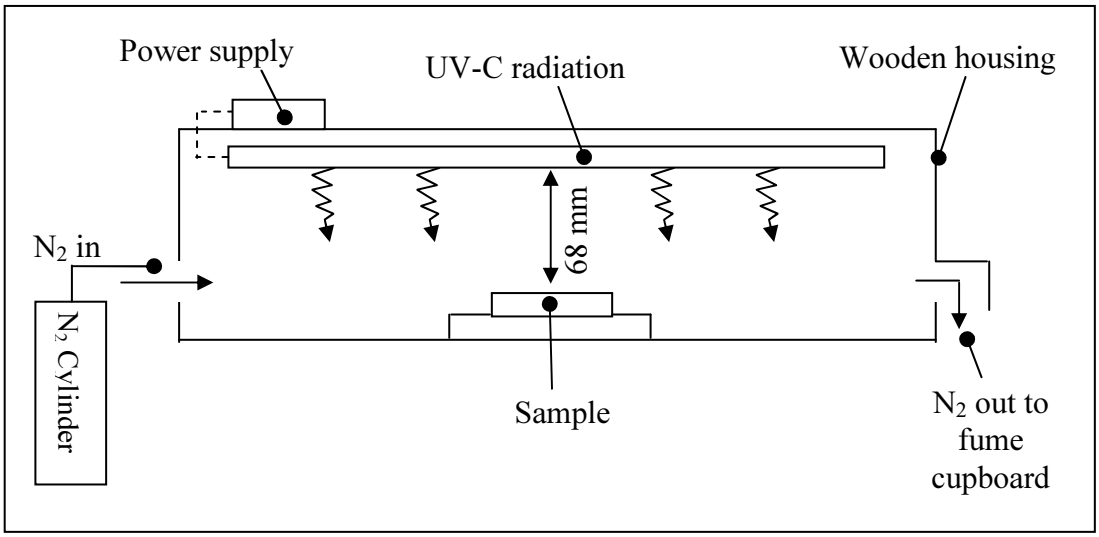

Figure 3-2: Ultraviolet grafting equipment set-up for initial trials using Phillips TUV 8 W UV-C tube

The reactor was constructed of medium density fibreboard with black paint on the interior surfaces to absorb UV and reduce degradation of the walls. A Phillips TUV 8 W disinfection lamp supplied the UV-C radiation at 254 nm wavelength as recommended by Yang & Rånby (1996). Mixing of the microcapsules during grafting was achieved by placing the graft reactor on a Ratek platform mixer. Nitrogen was supplied to provide an inert blanket for the grafting reaction. A conservative target of 1 mW cm^{-2} was determined for initial grafting trials, requiring a distance of 68 mm between the sample and UV tube. The theoretical calculated maximum intensity for the centre of the dish was determined as follows in Equation 3-1;

$$I = \frac{\varepsilon}{4\pi\left(D + 0.5d\right)^2 + 2\pi L\left(D + 0.5d\right)} \qquad \textbf{(3-1)}$$

Where I is the intensity in mW cm^{-2}, ε the total amount of ultraviolet light emitted from the tube (mW), D is the distance from the sample to the UV tube (cm), d the diameter of the UV tube (cm) and L the length of the UV tube (cm). Equation 3-1 is based on the assumption that the total emitted UV intensity is distributed evenly at distance D plus half of the tube diameter, d (mm) from the central UV tube (Figure 3-3).

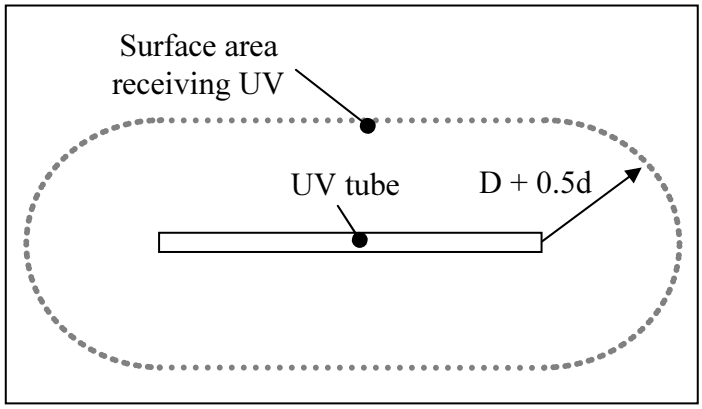

Figure 3-3: Diagrammatic representation of the even distribution of UV intensity assumption at a set distance from the UV tube

The design was later improved for use in a continuous flow operation. The intensity, first trialled at 1 mW cm^{-2} was increased to a final calculated intensity of 19 mW cm^{-2} in order to improve the grafting yield. Details of this modified design are discussed in section 3.5.

3.4. Jacketed glass reactor system

A jacketed glass reactor system was designed for production of polyamide microcapsules by interfacial polymerisation of an emulsion. Temperature control was required to maintain a consistent temperature of 10 ^{o}C during microcapsule formation. To remove the centrifuge step and ensure a consistent size distribution of microcapsules, a filtering procedure through a stainless steel mesh was implemented. This required a simple disassembly procedure as access to the mesh was necessary for cleaning and removal of product. Figure 3-4 shows the final setup constructed. This set-up was the result of several design iterations. Detailed dimensions can be found in Appendix A.3.

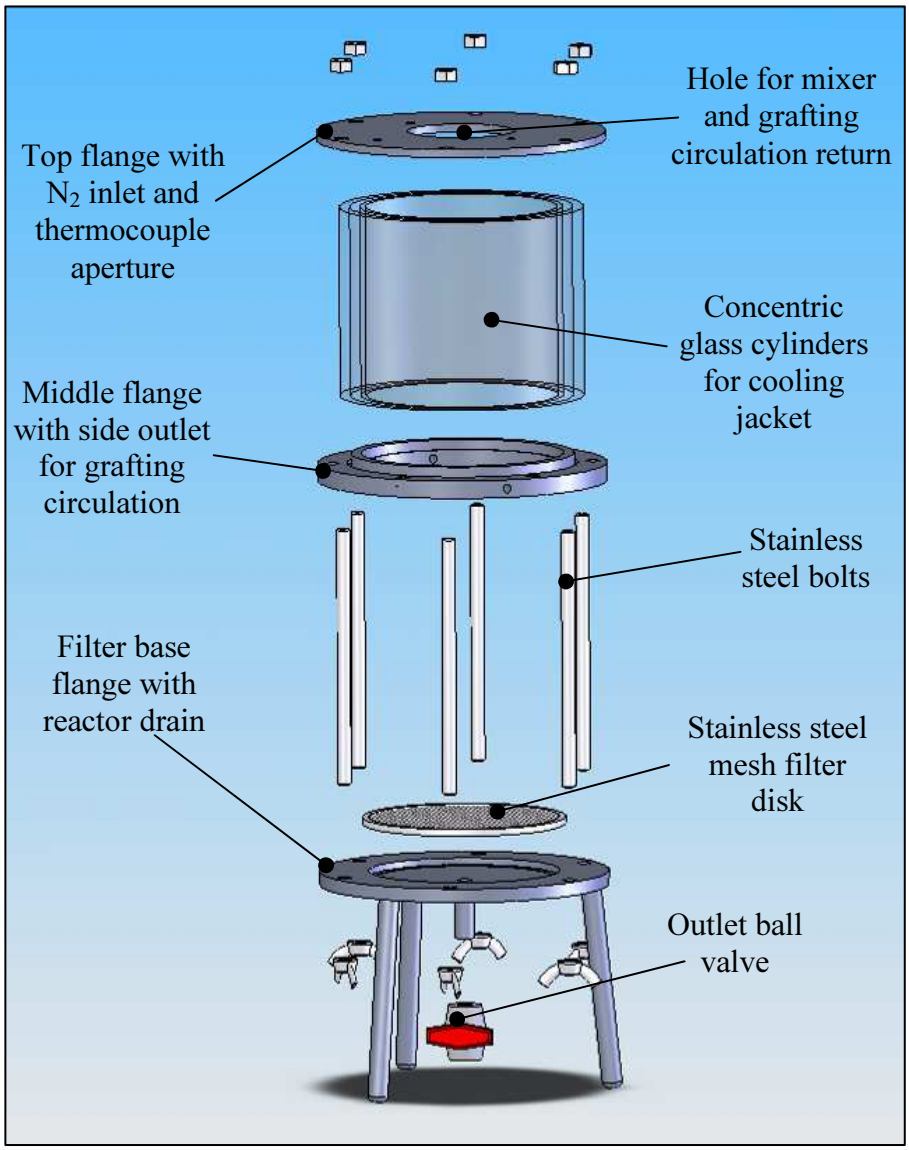

Figure 3-4: Jacketed glass reactor system used for microcapsule production; internal reactor dimensions 143 mm in diameter, 158 mm tall

The reactor system was constructed using 316 grade stainless steel with PTFE coated seals to ensure maximum corrosion resistance towards both acrylic acid and chloroform solutions. PTFE was also used for tubing exposed to these chemicals at inlet and exit points.

Both the 25 μm and 10 μm gauge stainless steel mesh, used in microcapsule filtration, were obtained from TWP Inc, USA. In-place filtering of microcapsules reduces the need for transfer of the solution from the reaction vessel, thus allowing the whole manufacturing process to be contained *in situ*. The overall yield of microcapsules is improved as less material is lost in process steps. In addition, tighter control over the

size of microcapsules produced can be obtained by changing the mesh sizes used for filtering operations. Stainless steel mesh has advantages over similar filtration methods as it is reusable, corrosion resistant, has a uniform pore size and is easy to handle.

On removing the centrifugation washing step from the original method, the ethanol concentration needed to be raised within the reactor during washing. A dialysis step was implemented to gently add ethanol solution while maintaining the volume in the reactor at a constant level. A simple model was developed to determine the ethanol concentration over time based on the following diagram (Figure 3-5). It has been assumed the tank is well mixed and maintains a constant volume due to matched inlet and outlet flows.

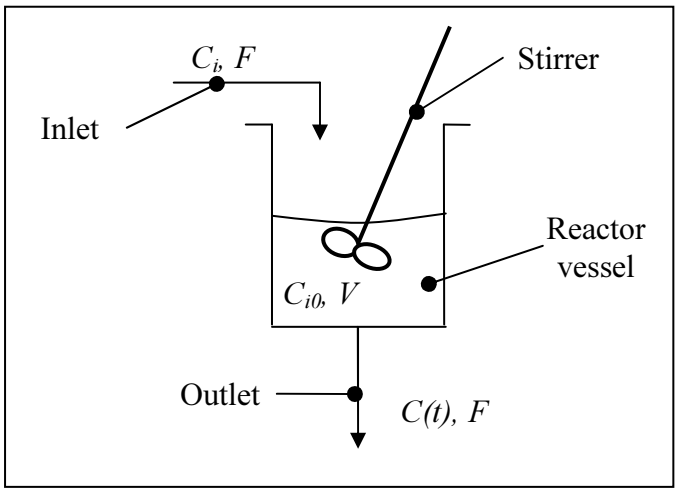

Figure 3-5: Schematic of reactor use to model ethanol concentration during the solvent exchange dialysis step

C_i is the concentration of the inlet (% v/v), C_{i0} the initial ethanol concentration in the reactor (% v/v), $C(t)$ the ethanol concentration of the outlet (% v/v) over time designated t (s), F the flowrate into the reactor (L s^{-1}) and V the volume of liquid in the reactor (L). A mass balance around the reactor leads to Equation 3-2.

$$C(t) = \frac{FC_i t + VC_{io}}{V + Ft} \qquad \textbf{(3-2)}$$

Assuming a fixed flowrate of 0.001 L s^{-1} and a reactor liquid volume maintained at 1 L the idealised concentration over time within the reactor can be plotted. Based on this

model, a 2 L ethanol solution with a concentration of 30 % (v/v) raises the reactor outlet concentration to 20 % (v/v) over the course of the washing procedure. The ethanol concentration over time can be represented graphically as plotted in Figure 3-6.

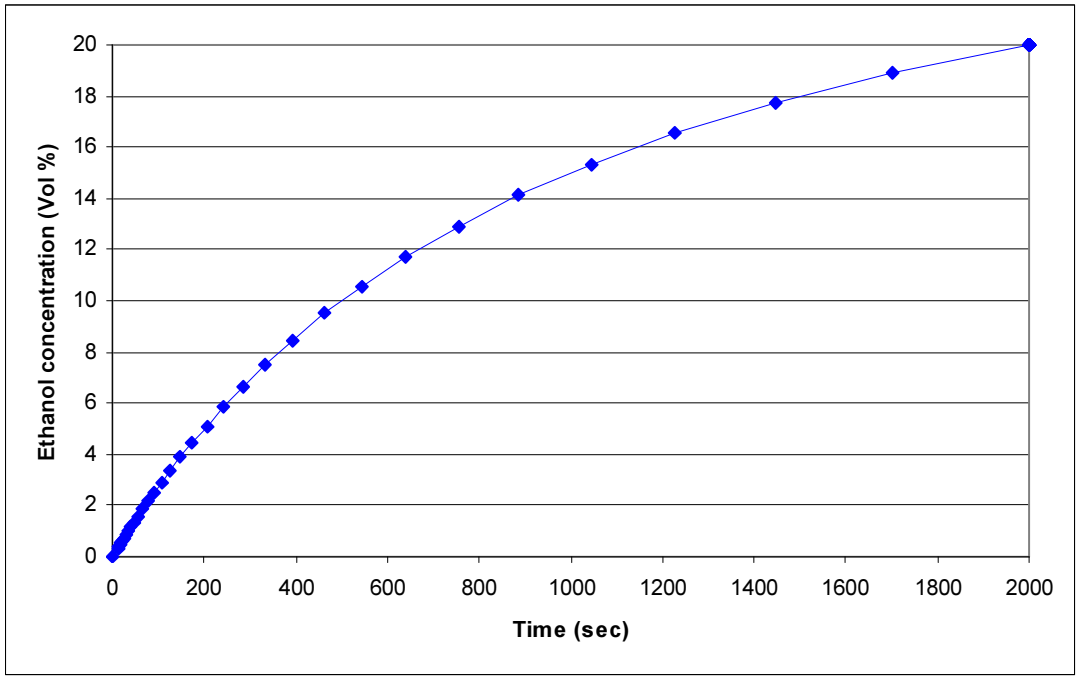

Figure 3-6: Ethanol concentration over time during washing of microcapsules in polymerisation reactor

This model does not account for ethanol diffusional resistance into the microcapsules, reactor liquid level fluctuations or the volume occupied by the polyamide polymer, which were all rejected.

3.5. Quartz tube bank reactor

A larger-scale reactor was designed for UV grafting in an attempt to mimic the flow characteristics of a Taylor – Couette reactor described by Forney & Pierson (2004). Direct implementation of a Taylor – Couette system for UV grafting in this project was considered less feasible. Additional rotor turning equipment would be required as well as expensive, large diameter quartz glass cylinders to allow for the transmission of UV light at 254 nm. Similar flow characteristics could be achieved by coupling a plug flow reactor to the existing CSTR emulsification reactor. A disadvantage to this approach is

the use of mechanical agitation in the CSTR, rather than gentle fluidisation for mixing as suggested by Lee *et al.* (2003). Agitation in the tank by impellor during grafting has the potential to damage microcapsules and increase instances of contact, promoting agglomeration as PAA chains crosslink. However, as the reaction needs to be under an inert atmosphere, nitrogen or helium gas would be required as a fluidising agent. This would significantly increase the cost of production, detrimental to scale-up.

To ensure uniform grafting, a plug flow profile was targeted along with a reduction in the hold-up volume. This allowed more concentrated microcapsule slurries to be grafted, effectively minimising the amount of acrylic acid required. This is desirable as acrylic acid is costly as well as being a potential environmental pollutant. A summary of the final design is presented in Figure 3-7. The assembly was housed in an enclosed box to prevent emission of UV-C radiation to the surroundings. Detailed drawings including dimensions can be found in Appendix A.4.

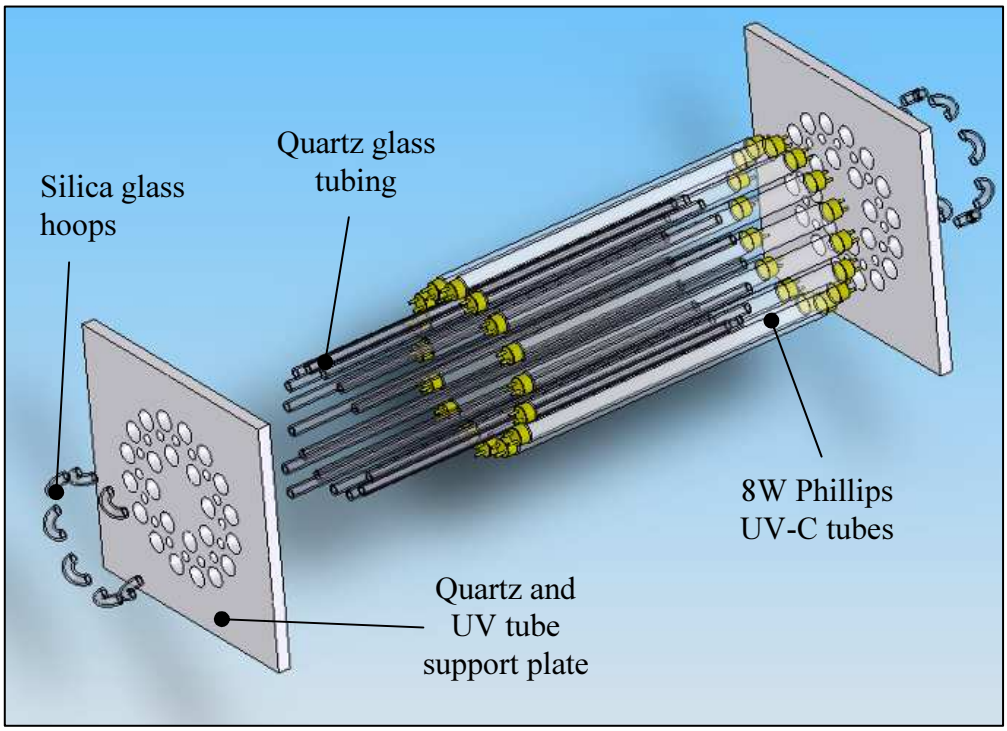

Figure 3-7: Quartz tube bank UV grafting reactor; 16 quartz tubes with a 5 mm ID, 300 mm in length set at a pitch circle diameter (PCD) of 97mm, 16 Phillips TUV 8 W tubes set at a PCD of 120 mm

Quartz glass tubes were required for UV transmittance at 254 nm and obtained from Technical Glass Products Inc, USA. Silica glass hoops were formed to join each straight

quartz tube. Two layers of heat shrink tubing were used to seal each of these joints; an internal Teflon heat shrink layer to provide chemical resistance, covered by a polyolefin protective layer. The modified design had significant advantages over the bench scale trial reactor as the microcapsules were sealed in a closed system during irradiation, reducing oxidation of free radical groups. A more uniform UV exposure could also be achieved due to an improved mixing regime.

A key design parameter in the construction of an UV grafting reactor is the radiation intensity received by each tube. A simple model was developed to allow for sizing of the reactor based on the relative pitch circle diameters of the quartz and UV tubes. To determine the intensity of radiation received by a quartz tube, the distance to the UV tube providing the irradiation must be calculated. With reference to Figure 3-8, the distance from the centre of a UV tube to the centre of a quartz tube can be calculated using Equation 3-3.

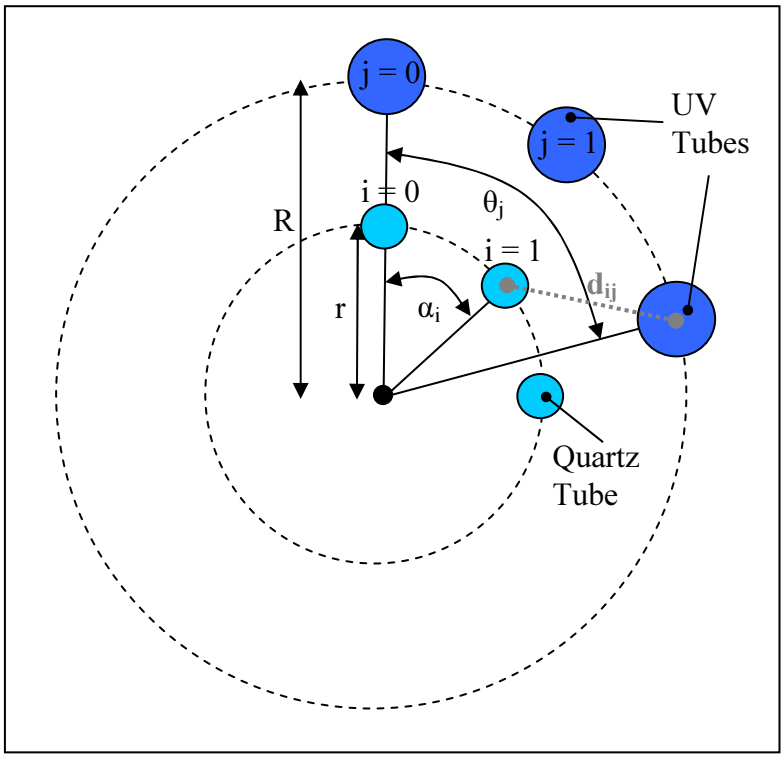

Figure 3-8: Schematic of layout of tubes for calculation of UV intensity at the centre of quartz tubes in UV grafting reactor

$$d_{ij} = \sqrt{\left(2r\sin\frac{\omega_{ij}}{2}\right)^2 + (R-r)^2 - 4r(R-r)\left(\sin\frac{\omega_{ij}}{2}\right)\cos\left(\frac{\pi+\omega_{ij}}{2}\right)} \qquad \textbf{(3-3)}$$

R represents the radius at which the UV tubes lie from the centre of the grafting reactor (mm), r the radius at which the quartz tubes lie from the centre of the grafting reactor, α_i the angle between quartz tube 0 and quartz tube i (rads), θ_j the angle between quartz tube 0 and UV tube j (rads), and d_{ij} the distance between quartz tube i and UV tube j. The angle ω (rads) is an absolute value and defined as follows, based on angles taken from Figure 3-8 above (Equation 3-4).

$$\omega_{ij} = \left|\theta_j - \alpha_i\right| \qquad \textbf{(3-4)}$$

However, it should be noted that not every UV tube irradiates every quartz tube due to interference from adjacent quartz tubes. When the reactor tubes are loaded with microcapsule solution, negligible levels of UV light will be transmitted. The limits of the angle θ_j can be specified by determining the angle required to cause tube interference. This is based Figure 3-9 under the assumption that each bank of tubes is equally spaced around the centre of the reactor and radiation travels from centre to centre between tubes (Equation 3-5). A complete derivation of this equation can be found in Appendix A.2.

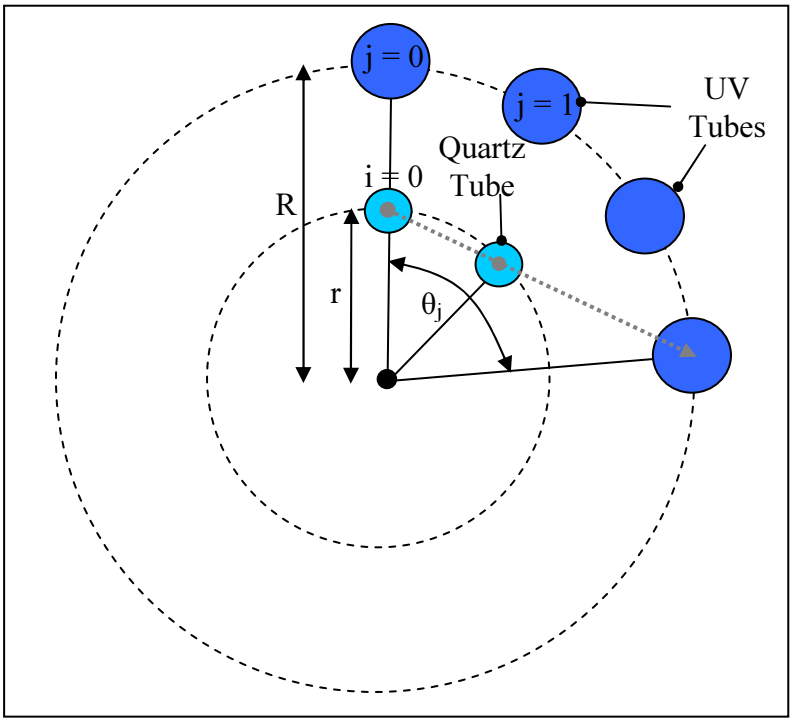

Figure 3-9: Schematic of tube layout for calculation of limits of angle ω due to quartz tube interference

$$\omega_{ij} < \left| \frac{\alpha_i}{2} + \cos^{-1}\left(\frac{r \cos \frac{\alpha_i}{2}}{R} \right) \right| \quad and \quad \omega_{ij} > 2\pi - \left(\left| \frac{\alpha_i}{2} + \cos^{-1}\left(\frac{r \cos \frac{\alpha_i}{2}}{R} \right) \right| \right) \qquad \textbf{(3-5)}$$

Many of the UV tubes on the opposite side of the pitch circle diameter (PCD) will still contribute to the light intensity received by a quartz tube, but their contribution is significantly smaller and has been ignored in this model to reduce complexity.

Once the distance (d_{ij}) has been calculated between each quartz tube (i) and each UV tube (j), for allowable angles of ω, the approximate intensity, denoted I_i (mW cm^{-2}), at the centre of each quartz tube can be calculated by Equation 3-6.

$$I_i = \sum_j \frac{\varepsilon}{4\pi {d_{ij}}^2 + 2\pi L d_{ij}} \qquad \textbf{(3-6)}$$

This model does not take into account reflection from quartz tube surfaces, the decrease in lamp output over its lifespan or the contribution from opposite UV tubes. It is intended as a sizing guide only. A spreadsheet was compiled using the above equations to determine the influence of various tube arrangements. A copy has been included in Appendix B.1. The final tube arrangement using 16 UV-C tubes delivers a calculated intensity of 19 mW cm^{-2} to each quartz tube. This pattern has the quartz tubes on a PCD of 97 mm and the UV tubes on a 120 mm PCD. A benefit of this arrangement is a uniform UV irradiation for each quartz tube due to the symmetry of the quartz and UV tube patterning.

3.5.1. Reactor flow characterisation

Flow characteristics within a reactor can be found by residence time distribution studies using a simple tracer test, injecting a pulse of known concentration and measuring the outlet concentration over time (Levenspiel, 1999). Tracer tests were performed on the grafting reactor to determine the flow characteristics. The flow type and the deviation from ideal flow give an estimate as to the amount of mixing occurring during

irradiation, as well as the residence time within the system. Both these factors contribute to an even distribution of surface free radical sites during grafting.

Tracer tests were conducted using a concentrated methylene blue solution. The system was maintained at constant head by using a vacuum line to remove liquid exceeding a total system volume of 500 ml. Prior to injection of the methylene blue dye, the system was purged of air with distilled water and a pump setting of 600 using a Cole Palmer 100/1 drive coupled to a Teflon diaphragm head. The pump was stopped for the introduction of 800 μL of tracer delivered using a glass syringe. Once the pump was started, samples were taken every 5 pulses up to 30 pulses, whereupon every pulse was collected thereafter until 80 pulses had been completed. Absorbance was taken at 664 nm in a spectrophotometer using disposable plastic curvettes.

The reactor volume was determined by loading the quartz tubing with distilled water before connection of a compressed air line to gently push the water into a measuring cylinder. This was weighed to determine the mass of water contained in the system. The volumetric-flowrate was determined similarly with a timed mass of water collected from the exit of the quartz tubes. Finally, the period of the pulses was calculated by timing 20 pulses of distilled water exiting the reactor. All measurements were performed in triplicate to ensure accuracy.

A dispersion model was fitted to the tracer response data, characterised by the dimensionless group D/uL. This is also known as the vessel dispersion number, where D is the dispersion coefficient ($m^2\ s^{-1}$), u the fluid velocity ($m\ s^{-1}$) and L the path length. Large values of D/uL represent significant deviation from plug flow whereas small values indicate little spreading hence good plug flow (Levenspiel, 1999). For instance, a value of D/uL less than 0.01 represents near ideal plug flow and was the target for design of the reactor system.

The average residence time of the tracer $\bar{t}_i$, was calculated using Equation 3-7 (Levenspiel, 1999), where the subscript i denotes each successive data point collected. The variable t represents time (s), C the concentration of the outlet ($kg\ m^3$) and Δt_i the

time interval (s) between concentration measurements. Equations 3-7 to 3-14 are from (Levenspiel, 1999).

$$\bar{t}_i = \frac{\Sigma t_i C_i \Delta t_i}{\Sigma C_i \Delta t_i} \qquad \textbf{(3-7)}$$

The variance of the outlet curve, σ^2, was found using Equation 3-8. This is a measure of the spread of the tracer as it progresses through the vessel.

$$\sigma^2 = \frac{\Sigma t_i^{\,2} C_i \Delta t_i}{\Sigma C_i \Delta t_i} - \bar{t}_i^{\,2} \qquad \textbf{(3-8)}$$

The input was considered to be a sharp spike, with a variance of zero, allowing the vessel dispersion number to be calculated using Equation 3-9.

$$\frac{\sigma^2}{\bar{t}_i^{\,2}} = 2\left(\frac{D}{uL}\right) \qquad \textbf{(3-9)}$$

A second model, using tanks in series, provided a useful guide as to the approximate number of ideal continuously stirred tank reactors (CSTRs) mimicked by the system. This was found from Equation 3-10, where N represents the number of idealised CSTRs.

$$N = \frac{\bar{t}_i^{\,2}}{\sigma^2} \qquad \textbf{(3-10)}$$

A secondary approach was taken to further confirm the flow profile in the reactor. The method of least squares was used to fit axial dispersion model equations to the experimental data. For small deviation from plug flow, characterised by a vessel dispersion number less than 0.01, the axial dispersion model was applied (Equation 3-11).

$$E_\theta = \frac{1}{\sqrt{4\pi(D/uL)}} \exp\left[-\frac{(1-\theta)^2}{4(D/uL)} \right] \qquad \textbf{(3-11)}$$

The dimensionless variable θ represents a normalised time value as described in Equation 3-12.

$$\theta = \frac{t}{\bar{t}_i} \qquad \textbf{(3-12)}$$

If the flow deviates from plug flow by a large extent, defined as a dispersion number in excess of 0.01, a modified family of equations as described below can be used to find the E curve (Equation 3-13).

$$E_\theta = \frac{1}{\sqrt{4\pi(D/uL)}} \exp\left[-\frac{(1-\theta)^2}{4\theta(D/uL)} \right] \qquad \textbf{(3-13)}$$

Experimental data was directly compared to this curve when the time values were normalised as above and the E_θ curve calculated from tracer outlet concentrations using Equation 3-14, where V is the reactor volume (m^3) and M the mass of tracer injected (kg).

$$E_\theta = \frac{V}{M} C_i \qquad \textbf{(3-14)}$$

The results from tracer tests conducted on the external loop grafting reactor are presented in section 5.6.

Chapter 4 Experimental materials and methodology

This chapter focuses on the equipment and methods used in the production, grafting and characterisation of PAA bonded microcapsules. Most emphasis was placed on development of an UV method of grafting and characterisation of the resulting grafted capsules. Figure 4-1 shows the order of experimental work performed.

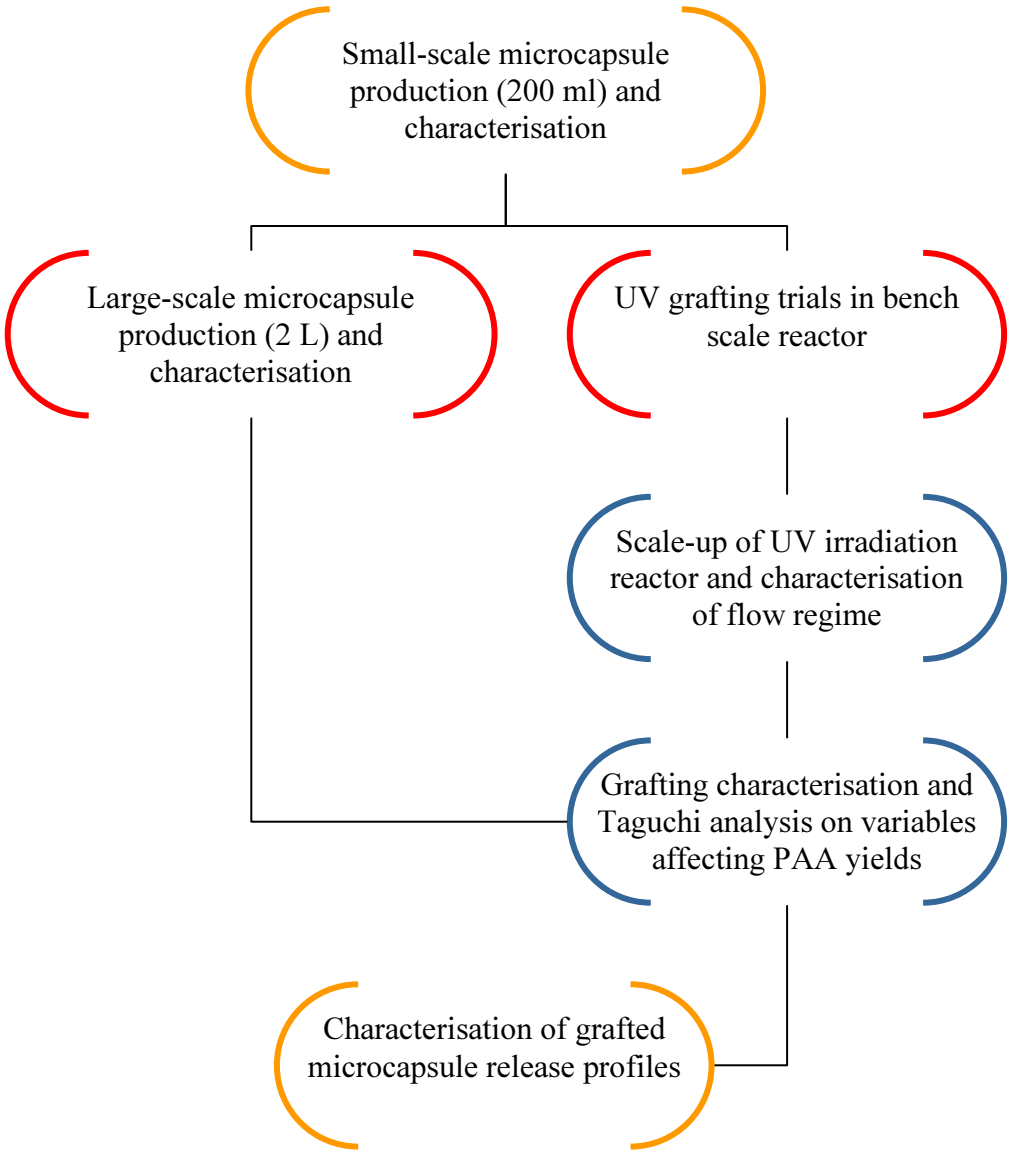

Figure 4-1: Organisation of experimental procedure in scaled production of PAA grafted polyamide microcapsules

Experiments were primarily undertaken in the Special Purposes Laboratories, Department of Chemical and Process Engineering, at the University of Canterbury. A small amount of work on microcapsule production, prior to scale-up, was performed in the Materials Engineering Laboratory at the University of Waikato. The aim of the experimental work was to produce a sufficiently large quantity of microcapsules for release profile testing. A higher rate of release was expected at pH 3 than pH 7 due to pore constriction caused by swelling of PAA grafted functional gates at pH 7.

4.1. Materials and equipment

Details of reagents used during experiments, including purities and suppliers, are located in Table 4-1.

Table 4-1: List of chemicals used for experiments including purities and suppliers

Chemical	Abbreviation	Purity	Supplier
6 – carboxytetramethylrhodamine	TAMRA	N/S	Molecular probes, USA
Acrylic acid	AAc	99 %	Sigma-Aldrich, USA
Alpha-lactalbumin	α-lac	> 85 %	Sigma-Aldrich, USA
Ammonia	NH_3	33 %	BDH Lab supplies, England
Ammonium chloride	NH_4Cl	99.5 %	BDH Lab supplies, England
Blue dextran 2000	-	N/S	Amersham Biosciences, Sweden
Chloroform	-	99 %	BDH Lab supplies, England
Citric acid	-	99.5 %	May and Baker Ltd, England
Cyclohexane	-	99.5 %	BDH Lab supplies, England
Cytochrome C		95 %	Sigma-Aldrich, USA
Dichloromethane	DCM	> 99 %	Merck and Co, Inc, Germany

Table 4-1. (continued)

Diethyl ether	DEE	99 %	Ajax Finechem Ltd, New Zealand
Diethylene triamine		99 %	Sigma-Aldrich, USA
Dimethyl formaldehyde	DMF	99.8 %	Sigma-Aldrich, USA
Di-sodium phosphate	-	99 %	BDH Lab supplies, England
Ethanol	EtOH	96 %	Anchor, New Zealand
Ethylene diamine	-	99 %	Sigma-Aldrich, USA
Fluorescein	-	N/S	Chemistry Department, University of Canterbury
Hydrochloric acid	HCl	37 %	Merck and Co, Inc, Germany
Methylene blue	-	N/S	BDH Lab supplies, England
Mono-sodium phosphate	-	> 99 %	BDH Lab supplies, England
N – hydroxysuccinimide	NHS	>97 %	Fluka, Germany
N, N′ - dicyclohexylcarbodiimide	DCC	99 %	Fluka, Germany
Nitrogen gas	OFN	Zero grade	BOC gases, New Zealand
p – toluene sulfonyl chloride	TsCl	> 98 %	Sigma-Aldrich, USA
Phosphate buffered saline	PBS	N/S	Sigma-Aldrich, USA
Polyethylene glycol 5000 monomethyl ether	mPEG 5000	N/S	Fluka, Germany
Sodium carbonate	Na_2CO_3	99.5 %	Pronalys, New Zealand
Sodium chloride	NaCl	99.9 %	BDH Lab supplies, England
Sodium dodecyl sulfate	SDS	N/S	Ajax Finechem Ltd, New Zealand
Sodium hydroxide	NaOH	> 98 %	Fluka, Germany
Sodium sulfate	Na_2SO_4	N/S	N/S
Terephthaloyl dichloride	TDC	98 %	Merck and Co, Inc, Germany
Triethylamine	TEA	99 %	Sigma-Aldrich, USA
Tri-sodium citrate	-	99 %	Ajax Finechem Ltd, New Zealand

In addition, a range of specialised equipment was required for scale-up and characterisation of grafted microcapsules. Details of the equipment used, with reference to the section of work undertaken, are briefly explained below. Figure 4-2 shows the layout of the experimental apparatus used for 2 L scale microcapsule production.

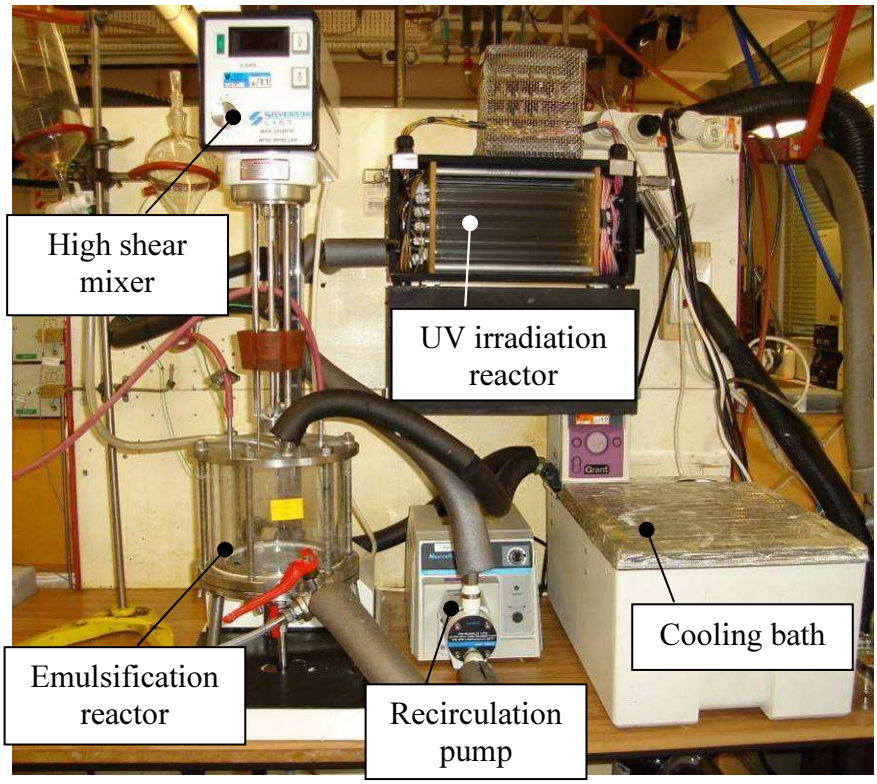

Figure 4-2: Equipment layout for production and PAA grafting of 2 L microcapsule batches

Unless otherwise specified, all emulsification and mixing steps in microcapsule production were performed using a Silverson L4RT Laboratory mixer (Advanced Packaging Systems Ltd, New Zealand). For emulsification steps a high shear emulsification head was used with a medium perforated emulsion screen. Temperature control of the emulsification reactor was achieved using a Grant Instruments water bath (Biolab Ltd, New Zealand) coupled with a FTS systems LC – 80 liquid cooler unit (SP Industries Inc., USA). Sonication for preparation of the emulsion organic phase involved the use of a 250HT Soniclean ultrasonic bath (Alphatech Systems Ltd, New Zealand). A Heraeus 3 L centrifuge (Kendo Laboratory Products, Germany) facilitated separation of microcapsules on the 200 ml scale during washing steps. Deionised water used throughout the experiments for equipment rinsing and microcapsule washing was produced in a Millipore Elix S system (Biolab Ltd, New Zealand). This water had an ohmic resistance exceeding 15 MΩ. Images of the microcapsules were captured by

camera using an Olympus BX60F-3 light microscope (Olympus Corporation, Japan) coupled with an Ikegami CCD camera (Ikegami Tsushinki Co., Ltd, Japan). Freeze-drying of microcapsules for SEM viewing required the use of a Labanco Freezone 2.5 freeze drier (Total Lab Systems Ltd, New Zealand). Dry microcapsule characterisation was performed using a Jeol JSM-7000F SEM (JEOL Ltd, Japan). In addition, a Saturn Digisize S200 laser particle size analyser was used to detect the size distribution of a wet slurry of microcapsules (Micromeritics Instrument Corp., USA)

Circulation through the UV irradiation reactor was achieved by use of a Cole Palmer Masterflex control drive coupled to a Teflon diaphragm pump head (Biolab Ltd, New Zealand). Phillips T-UV 8 W tubes (Lamp Specialists South Island Ltd, New Zealand) were used to supply light at 254 nm for grafting. A Shimadzu FTIR-8201PC (Shimadzu Corp., Japan) was used to obtain infrared spectral data of grafted and ungrafted microcapsule samples following irradiation.

During release profile tests, measurements of pH were recorded by a Eutech Instruments 510 pH meter (Biolab Ltd, New Zealand) and measurements of conductivity using a Mettler-Toledo MC126 meter (Global Science & Technology Ltd, New Zealand) while housed in a temperature controlled Ratek Orbital mixer platform (Biolab Ltd, New Zealand). The absorbance of resulting samples was measured, using quartz curvettes at 280 nm and plastic curvettes at 664 nm, with an Amersham Biosciences Ultrospec 2100 Pro spectrophotometer (Amersham Biosciences, Sweden). In conjunction, microcapsule release characterisation was undertaken on a Lecia LAS AF TCS SP5 confocal microscope (Lecia Microsystems, Germany) in the School of Biological Sciences at the University of Canterbury. Finally, an XK 5 / 5 column (Amersham Biosciences, Sweden) was packed with grafted microcapsules allowing pulse response characteristics to be determined when attached to an AKTA 10 chromatography unit (Amersham Biosciences, Sweden).

4.2. Small scale microcapsule production and characterisation

Microcapsules were first prepared on a 200 ml scale according to the method proposed by Chu (2004) and revised by Lin (2006), as detailed in section 4.2.1. During scale-up the average emulsion droplet size was kept constant using the method presented in section 4.2.2. This was to ensure the total surface area for the polymerisation reaction was kept proportional to the scale factor of the process, thus maintaining a constant membrane thickness during scale-up.

4.2.1. 200 ml batch scale microcapsule production

To confirm the validity of previous methods published on microcapsule production and gain familiarity with the process steps required, small scale synthesis of capsules was carried out initially (Lin *et al.*, 2006).

1. 0.9 g of TDC granules were milled to a fine powder and added to 7.5 ml chloroform combined with 2.5 ml cyclohexane before ultrasonic exposure for 30 minutes. The mixture was left stirring overnight at room temperature. Stock TDC was stored with a desiccant to prevent degradation by atmospheric water.
2. A 160 ml surfactant solution of 1 % (w/v) sodium dodecyl sulfate (SDS) was prepared and added to a 250 ml beaker.
3. The saturated TDC solution was centrifuged at 2500 rpm for 8 minutes to remove undissolved solid. The resulting clear solution was added to the SDS surfactant.
4. The mixture was cooled to 10 ^{o}C and emulsified using the standard mixing head with medium emulsion screen at 800 rpm for 10 minutes.
5. Following emulsification, 10 ml ethylene diamine, 5ml diethylene triamine and 20 ml 1.18 mol L^{-1} sodium carbonate were added to the beaker. Mixing was continued at a reduced speed of 200 rpm for a further 60 minutes.
6. The microcapsules produced in step 5 were centrifuged at 800 rpm for 8 minutes and the supernatant was decanted. This washing procedure was repeated twice

with 30 % (v/v) 4 ^{o}C ethanol and three times using 4 ^{o}C distilled water to remove residual solvent.

7. Microcapsules were freeze-dried for storage.

4.2.2. Emulsion dispersion testing

The influence of impeller speed on the emulsion droplet size was tested for both 2 L and 200 ml batch production. The method for emulsion droplet sizing on the 2 L scale was as follows:

1. 10 g milled TDC powder was added to 100 ml 3 : 1 chloroform / cyclohexane mixture and sonicated for 1 hour.
2. 1.6 L SDS 1 % (w/v) was cooled to 10 ^{o}C in a jacketed reactor while stirring with the high shear emulsification set to 110 mm below the liquid surface.
3. The organic phase solution was centrifuged twice at 2000 rpm for 10 minutes before addition to the jacketed reactor. The mixture was emulsified at 800, 1000 or 1200 rpm for 30 minutes.
4. Microcapsule samples were taken from equal depth and images of the dispersion captured at 10 x optical zoom.
5. These images were enlarged consistently and 200 horizontal droplet diameters were recorded in a defined area as shown in Figure 4-3.

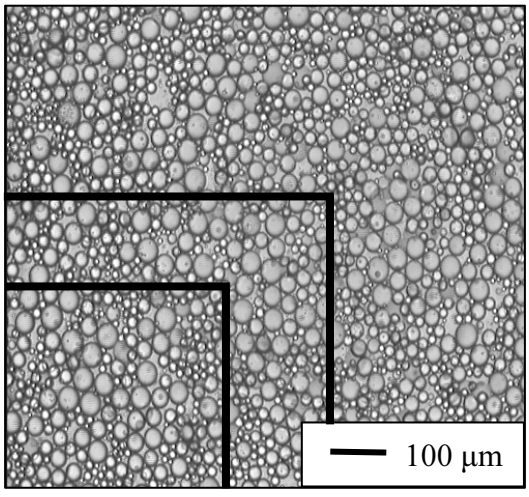

Figure 4-3: Emulsion droplet sizing area for particle size distribution analysis of optical micrographs

The diameter distribution was converted to a volume frequency distribution (Vf_i) using Equation 4-1.

$$Vf_i = \frac{D_i^{\,3} n_i}{\sum_{i=j}^{i=1} D_i^{\,3} n_i} \times 100 \qquad \textbf{(4-1)}$$

Subscripts *i* and *j* denote the number of droplet size intervals and the total number of size intervals respectively. D_i is the average diameter for interval *i* and n_i the number of droplet diameters falling within that interval. The emulsion sizing method was repeated at the 200 ml production scale using lesser quantities of reaction reagents

4.3. UV grafting trials in bench scale reactor

To initially test the method for UV grafting of acrylic acid to polyamide, a polymer film was prepared for irradiation in the apparatus shown in Figure 3-2. Section 4.3.1 details the casting method for production of this film. The UV irradiative method for grafting PAA to this film is given in section 4.3.2, followed by grafting of PAA to microcapsules, produced on the 200 ml, scale in section 4.3.3.

4.3.1. Polyamide film preparation and casting

Polyamide resin beads were mixed with ethanol in a 10 % (w/v) solution over a 60 °C heater pad for 2 hours. Once a viscous solution had formed, the liquid was cast on a glass plate using a 5 μm casting block. The film was submerged in water and allowed to solidify for an hour. After drying overnight at room temperature, the film was refrigerated.

4.3.2. UV irradiative grafting of PAA to polyamide film

The UV irradiative bench reactor, as detailed in Figure 3-2, was used to expose the surface of polyamide films and microcapsules to UV-C radiation of wavelength 254 nm. The intensity of the light was set at 1 mW m^{-2} by maintaining a distance of 68 mm from the tube to the base of the glass sample dishes. Polyamide film swatches 20 mm x 20 mm were added to 10 % (w/v) acrylic acid 6 mm below the liquid surface. The system was purged with nitrogen gas for 10 minutes, prior to irradiation, to remove oxygen gas from the chamber. After UV exposure for one hour, samples were thoroughly washed in deionised water, to remove excess monomer, and then refrigerated.

4.3.3. UV irradiative grafting of PAA to 200 ml scale polyamide microcapsules

The bench scale UV irradiative reactor was used to graft PAA to samples of microcapsules prepared by the method detailed in section 4.2.1. Glass sample dishes were prepared containing 6 mm of 10 % (w/v) acrylic acid and 5 ml of microcapsule slurry. These samples were treated with one hour of UV radiation under an inert atmosphere of nitrogen gas. Following irradiation, samples were washed three times with deionised water using a membrane filter apparatus. A back titration method, detailed in section 4.5.1, was used to quantify the number of carboxyl groups present.

4.4. Large-scale microcapsule production and characterisation

The finalised methodology for production of microcapsules on a 2 L scale is presented in section 4.4.1. However, unwanted agglomeration of microcapsules caused significant difficulties during the development of this method. Agglomeration was observed in two key production steps; the addition of the amine reactants to the organic emulsion and the addition of ethanol solution during the dialysis of microcapsules following the polymerisation step. A Taguchi analysis was performed on variables influencing the

stability of the suspension during the dialysis step with ethanol solution (section 4.4.2). Second, the effect of the volume of sodium carbonate added to the emulsion during the reaction was determined (Section 4.4.3). Third, the causes of agglomeration due to the speed of addition of the amine solution to the emulsion were studied (section 4.4.3). Finally, the conclusions drawn from these experiments provided the basis for a final set of experiments testing the influence of TDC monomer concentration on microcapsule dispersion according to the procedure provided in section 4.4.3.

4.4.1. Scaled polyamide microcapsule production

The method for microcapsule production prescribed in section 4.2.1 was scaled by a factor of ten. The scaled method below was finalised following experiments on the causes of microcapsule agglomeration, details of which are included in subsequent sections.

1. 4 g milled TDC powder was added to 100 ml 3 : 1 chloroform / cyclohexane mixture before sonication for 1 hour.
2. 1.6 L SDS 1 % (w/v) was cooled to 10 ^{o}C in a jacketed reactor while stirring with the high shear emulsification head set to 110 mm below the liquid surface.
3. The organic phase solution was centrifuged twice at 2000 rpm for 10 minutes before addition to the jacketed reactor.
4. The mixture was emulsified at 10 ^{o}C using the standard mixing head with the medium emulsion screen at 800 rpm for 20 minutes.
5. A pitched six-bladed impeller was introduced and 200 ml of 1.18 mol L^{-1} Na_2CO_3 gradually added to the emulsion while stirring at 100 rpm.
6. 40 ml ethylene diamine, previously mixed with 20 ml diethylene triamine, was added dropwise via a dropping funnel. Stirring was continued at a speed of 100 rpm for a further 60 minutes.
7. The reactor was drained and a 10 μm stainless steel mesh filter added, along with stainless steel baffles. Mixing was continued at 100 rpm and the microcapsules dialysed with 2 L of 30 % (v/v) ethanol and 8 L of deionised water. Dialysis was begun at a constant flow rate of 30 ml min^{-1} with a volume

of 1 L maintained in the reactor. The flowrate was increased over the course of the dialysis as particulate matter was removed.

8. The microcapsule slurry was drained, collected as a filter cake and stored in a suspension of deionised water.

The yield of dry microcapsules was determined by measurement of the total dry solids in a slurry of known mass (m_{slurry}). In triplicate, 5 ml samples were removed from the final suspension and added to 10 ml beakers of known weight (m_{bi}). The loaded beakers were subsequently weighed (m_{bl}), before introduction to a temperature controlled oven maintained at 103 ^{o}C. Samples were weighed again the next day (m_{bf}) and the total dry capsule yield determined by Equation 4-2.

$$m_{dry\,capsules} = \frac{\left(m_{bf} - m_{bi}\right)}{\left(m_{bl} - m_{bi}\right)} m_{slurry} \qquad \textbf{(4-2)}$$

4.4.2. Taguchi analysis on causes of agglomeration

A Taguchi analysis was undertaken to provide an estimate of individual percentage contributions of variables believed to cause microcapsule agglomeration during scale-up. A summary of the levels of each variable tested is reported in Table 4-2.

Table 4-2: Variables tested in prevention of microcapsule agglomeration

Variable	Level 1	Level 2
Ethanol concentration % (v/v)	30	45
Washing temperature (^{o}C)	4	25
SDS concentration % (w/v)	0	1
Tween 80 concentration % (w/v)	0	0.5
Speed of addition of solution	Fast	Slow
Solution degassed	Yes	No

A L_8 matrix array with six two level factors and a single interaction was used to plan a series of experiments, detailed in Table 4-3 (Roy, 1990). The interaction was designed

to determine the effect temperature had on the influence of ethanol concentration in relation to the dispersion of the microcapsules.

Table 4-3: L_8 Taguchi array for investigation into causes of microcapsule agglomeration

	Ethanol Conc.	Temp	Interaction	SDS Conc.	Tween 80 Conc.	Addition speed	Degassing
	% (v/v)	(^{o}C)		% (w/v)	% (w/v)		
A	30	4	-	0	0	Fast	Yes
B	30	4	-	1	0.5	Slow	No
C	30	25	-	0	0	Slow	No
D	30	25	-	1	0.5	Fast	Yes
E	45	4	-	0	0.5	Fast	No
F	45	4	-	1	0	Slow	Yes
G	45	25	-	0	0.5	Slow	Yes
H	45	25	-	1	0	Fast	No

A 2 L batch of microcapsules was produced with a TDC concentration of 0.5 mol L^{-1} following steps 1 – 6 of the method detailed in section 4.4.1. Slurries, 5 ml in volume were removed by pipette and mixed with 10 ml of solutions of each of the eight combinations of variables provided by the Taguchi array (Table 4-3). An optical microscope was used to view microcapsule samples at 10 x zoom. A rating out of ten was assigned to each experiment based on the approximate fraction of dispersed microcapsules.

4.4.3. Emulsion stability during production steps

A 2 L emulsion was prepared by steps 1 – 4 of the method described in section 4.4.1. Slurries of 5 ml volume were removed and mixed with volumes of Na_2CO_3 equivalent to 100, 150, 200, 250 and 300 ml aliquots in 2 L scale production. Optical micrographs were taken at 10 x zoom to observe the dispersion of the microcapsules. The speed of addition of the amine solution was varied using the same emulsion once the optimal volume of Na_2CO_3 had been established. Two methods of delivery were tested; swift pouring from a measuring cylinder and dropwise addition by dropping funnel. In each

case the microcapsules were viewed under an optical microscope to determine if agglomeration occurred.

The final set of emulsion stability testing experiments involved a reduction in the molar concentration of TDC. The amine volume delivered was reduced proportionally to ensure a constant ratio between the monomer reactants was maintained. TDC concentrations of 0.5, 0.25, 0.2 and 0.1 mol L^{-1} were used to produce microcapsules by the method described in section 4.4.1. Microcapsules were characterised using an optical microscope at 10 x zoom.

4.5. Taguchi analysis on variables affecting PAA grafting yields

A second Taguchi method was used for the design of an experiment to investigate the relative influence of each variable on the grafting yield. Quantisation of the graft yields was achieved by a back titration method, presented in section 4.5.1. A L_9 Taguchi array was selected to allow for four variables, each with three levels, to be tested as described in Table 4-4.

Table 4-4: Variables tested for influence on grafting yield of acrylic acid to microcapsule surfaces

Variable	Level 1	Level 2	Level 3
Graft temperature (^oC)	30	40	50
Monomer concentration (% w/w)	10	20	30
UV graft time (hours)	0.5	1	1.5
Post irradiation reaction time (hours)	1	2	3

The L_9 array provided a guide for 9 experiments which reduced the otherwise impractical number of experiments required to test each combination of variables (Table 4-5).

Table 4-5: L_9 Taguchi array for investigation into variables influencing acrylic acid graft yield

	Graft Temperature	Monomer Concentration	UV graft time	Post irradiation reaction time
	(^oC)	(% w/w)	(hours)	(hours)
Exp 1	30	10	0.5	1
Exp 2	30	20	1	2
Exp 3	30	30	1.5	3
Exp 4	40	10	1	3
Exp 5	40	20	1.5	1
Exp 6	40	30	0.5	2
Exp 7	50	10	1.5	2
Exp 8	50	20	0.5	3
Exp 9	50	30	1	1

The general experimental procedure used for the grafting trials was as follows:

1. 500 g of ungrafted microcapsule slurry from a 5 L stock solution was deaerated for 10 minutes with N_2 gas.
2. The quartz glass irradiative reactor tubes were purged with demineralised water and dried with N_2 gas to remove traces of oxygen.
3. The microcapsule slurry was added to the emulsification reactor and circulated through the external irradiative grafting reactor until the solution reached the desired graft temperature. The mixture was stirred at 100 rpm with a circulation pump speed setting of 600. A positive pressure of N_2 was maintained to prevent oxygen contamination.
4. The AAm was precisely weighed and sparged with N_2 gas for 10 minutes to remove oxygen. The deaerated AAm was placed in a 500 ml dropping funnel, under an N_2 atmosphere, and raised to the graft temperature in a temperature-controlled cabinet.
5. The UV tubes were activated when the slurry reached the specified graft temperature. During UV exposure the system was maintained at ± 1 °C.
6. The UV tubes were turned off after the irradiation period had passed and circulation through the irradiative reactor was continued. AAm was added under

positive N_2 pressure and the temperature maintained at ± 1 °C for the specified post irradiation period.

7. Once the post irradiation reaction time had been observed 1 L of deionised water was added to the emulsification reactor and the microcapsules were drained from the system. The 10 μm filter mesh was inserted and the microcapsules were washed with 9 L of deionised water delivered in 1 L volumes.
8. The slurry was removed as a moist filter cake and stored in deionised water at 4 ^{o}C.

4.5.1. Back titration of carboxylic groups

Characterisation of microcapsule grafting was performed primarily through back titration to quantify the number of carboxyl groups present. A secondary confirmation was achieved through FT/IR analysis of freeze-dried capsules. The back titration method, adapted from work by Lin *et al.* (2006), is presented below:

1. 5 ml grafted slurry samples (V_{slurry}) were taken in triplicate from the bulk grafted slurry of known weight (m_{slurry}, g) and neutralised with 5 ml of 0.05 mol L^{-1} NaOH solution overnight.
2. A second set of 5 ml control samples were removed and filtered separately through a sintered glass funnel. Each sample was washed with three 5 ml volumes of deionised water then transferred to a conical flask. These controls were then neutralised with 5 ml 0.05 mol L^{-1} NaOH solutions overnight.
3. The following day, unfiltered samples from step 1 were removed and passed through the sintered glass funnel. These samples were washed with three 5 ml volumes of deionised water and transferred to a clean conical flask.
4. All samples were back titrated against 0.025 mol L^{-1} HCl (C_{HCl}) using phenolphthalein as an indicator. Hydrochloric acid volumes were recorded for neutralisation of the controls ($V_{HCl\ control}$, ml) and samples ($V_{HCl\ sample}$, ml).

The graft yield (Y) was subsequently calculated by Equation 4-3, where ρ_{slurry} is the slurry density (g ml^{-1})

$$Y = \frac{m_{slurry} C_{HCl} \left(V_{HCL\ control} - V_{HCL\ sample} \right)}{\rho_{slurry} V_{slurry} m_{dry\ capsules}} \qquad \textbf{(4-3)}$$

4.6. Characterisation of grafted microcapsule release profiles

Release profiles were required to determine the effect of surface grafting on the diffusion characteristics of microcapsule membranes and whether higher grafting yields were more advantageous than lesser levels of grafting. Three independent approaches were taken to testing the release profiles; bulk release of a slurry in a beaker (section 4.6.1), fluorescent recovery after photo bleaching (FRAP) as viewed by confocal microscopy (section 4.6.2) and compound retention in a packed chromatography column (section 4.6.3).

4.6.1. Bench scale tests

Microcapsules were loaded with a variety of compounds including cytochrome C (Lin *et al.*, 2006), alpha lactalbumin, methylene blue, sodium chloride (Chu *et al.*, 2004) and methylene blue conjugated dextran. The generalised release procedure was as follows for all compounds, excluding sodium chloride:

1. Approximately 30 mg of trial 'drug' was added to a 30 ml microcapsule slurry.
2. The pH was adjusted to 3 with a known volume of 2 mol L^{-1} HCl acid solution and left to equilibrate overnight.
3. The following day, the pH was adjusted to 7 using 2 mol L^{-1} NaOH and left to equilibrate for 30 minutes.
4. The resulting slurry was filtered and washed quickly with three 20 ml volumes of pH 7 phosphate buffer before re-suspension in 30 ml pH 7 buffer.
5. 1.5 ml samples were removed every 5 minutes for 30 minutes. A syringe was used with a 1.2 μm in-line filter to separate microcapsules from the free solution. Absorbance readings were taken at 280 nm in quartz glass curvettes.
6. After 30 minutes the pH was lowered to 3 using a known volume of 2 mol L^{-1} HCl.

7. Sampling was continued every 5 minutes for another 30 minutes.

A variation on the above release test was used for detecting sodium chloride release from ungrafted microcapsule samples. The method, based on that of Chu *et al.* (2004), had the advantage that no sampling was required as salt concentration was detected using a conductivity probe. The basic procedure is illustrated below:

1. A 10 ml slurry of ungrafted microcapsules of known weight was added to a 80 ml beaker.
2. Approximately 585 mg of NaCl was added to the suspension.
3. A rubber bung was used to seal the beaker and the contents were left to equilibrate overnight.
4. A known weight of deionised water was swiftly introduced to the beaker and conductivity measurements recorded every minute for 10 minutes then every 5 minutes thereafter.

4.6.2. Confocal microscopy

Confocal microscopy was used to test diffusion rates into individual microcapsules. The first aim using this equipment was to demonstrate dye diffusion into an ungrafted sample. 10 μL of fluorescein at a concentration of 0.01 mg ml^{-1} was mixed with a 10 μL sample of ungrafted microcapsules. Fluorescence from 500 – 550 nm was observed using excitation with a 488 nm laser running at 3 % power. Fluorescent recovery was then recorded after briefly photobleaching a target microcapsule with 100 % laser intensity.

The second aim was to explore differences in diffusion rates for grafted microcapsules. Due to the pH sensitivity of fluorescein at pH 3, where all fluorescence is lost, this marker was unsuitable for comparison of release rates from grafted microcapsules at pH 3 and 7. Instead, a PEG conjugated rhodamine dye was used, similar to a peptide conjugated rhodamine synthesised in work by Brunner *et al.* (1998). This fluorophore has a lower pH sensitivity to acidic pH than fluorescein. Production of PEG rhodamine dye required two synthesis steps; the production of methylether PEG amine and the

coupling of this PEG derivative to 6 – carboxytetramethylrhodamine (TAMRA) fluorescent dye.

The PEG amine was produced from a monomethylether PEG 5000 (mPEG) base using a Tosylated mPEG intermediate. The method for production of the Tosyl group on the mPEG chain was adapted from work by Nho (2004). Conversion of the Tosyl functional group to an amine terminus was based on a method outlined by Harris & Kozlowski (1997). Table 4-6 outlines the ratios and amounts of reactants used in production of this intermediate.

Table 4-6: Detail of reactants and ratios required for Tosylation of mPEG 5000

Reagent	Molecular weight (g mol^{-1})	Mass (g)	Moles	Molar ratio
mPEG	5000	10	0.002	1
TEA	101.19	1.53	0.015	7.5
TsCl	190.65	1.73	0.009	4.5

1. The mPEG 5000 was added to a 200 ml round bottomed flask (RBF) followed by the TEA and 20 ml anhydrous DCM.
2. Separately, the Tosyl chloride was dissolved in 10 ml DCM and added dropwise to the RBF.
3. The mixture was stirred at 40 °C for 6 hours.
4. The solution was cooled to room temperature and 25 ml DCM was added preceding 50 ml of saturated NaCl solution. This mixture was stirred vigorously for 10 minutes then filtered through cotton wool into a dropping funnel.
5. The lower organic phase was separated and 25 ml DCM added to aqueous phase
6. Extraction steps 4 – 5 were repeated twice more until no emulsion was observed during separation in the dropping funnel.
7. The organic phase was filtered through anhydrous sodium sulfate and concentrated under vacuum.
8. The resulting dry crude product was dissolved in 10 ml DCM then charged with 100 ml diethyl ether to precipitate the PEG product.
9. This solution was stirred for 30 minutes and then filtered to remove the precipitate. The crystallisation, in step 8, was repeated a second time.

10. The final product was dried under vacuum overnight.

The Tosyl mPEG was then converted to an amine mPEG by the following method:

1. The dry Tosyl mPEG was dissolved in 78 ml deionised water and adjusted to pH 12 with 1 mol L^{-1} NaOH solution.
2. The pH was maintained at 12 for 1 hour with periodic addition of 0.1 mol L^{-1} NaOH as required.
3. This solution was added to 17 g NH_4Cl dissolved in 170 ml ammonia and stirred at room temperature for 48 hours.
4. A vacuum was used to concentrate the reaction solution to a third of the original volume.
5. The mPEG was extracted into 50 ml of DCM and passed through cotton wool into a dropping funnel.
6. The aqueous phase was separated from the organic phase and extracted into DCM twice more following the procedure in step 5.
7. The organic solution was filtered through sodium sulfate and concentrated under vacuum.
8. The dry crude product was dissolved in 10 ml DCM then charged with 100 ml diethyl ether to precipitate the PEG product.
9. This solution was stirred for 30 minutes and then filtered to remove the precipitate. The crystallisation, in step 8, was repeated a second time.
10. The final product was dried under vacuum overnight.

Coupling of the mPEG amine to TAMRA dye was the final step in production of the PEGylated rhodamine fluorophore. The TAMRA dye was first activated with an N – hydroxysuccinimide (NHS) ester to facilitate the coupling. Table 4-7 provides the ratios and amounts of reactants involved in this final synthesis procedure.

Table 4-7: Reactants used for coupling of TAMRA dye to amine mPEG 5000

Reagent	Molecular weight ($g\ mol^{-1}$)	Mass (mg)	Moles ($x\ 10^{-5}$)	Molar ratio
TAMRA	430.45	5	1.16	1
NHS	115.9	1.48	1.278	1.1
DCC	206.33	2.876	1.394	1.2
mPEG-NH_2 (57% purity)	5015	102.2	1.16	1

1. Combined TAMRA and NHS were dissolved in 1 ml DMF and cooled to 0 °C.
2. The DCC was dissolved separately in 0.5 ml DMF and subsequently added dropwise to the chilled reaction mixture.
3. The solution was agitated at room temperature for 8 hours before the addition of the PEG amine.
4. The reaction was left overnight and the solution was concentrated under vacuum the next day.

Nuclear magnetic resonance (NMR) was used to confirm the presence of the conjugated dye. Following confirmation of a successful dye coupling, fluorescence recovery after photobleaching (FRAP) was used to observe differences in diffusion rates into grafted microcapsules.

1. 800 µL microcapsule slurries from Taguchi experiment 9 (Table 4-5) were mixed with 200 µL of 0.086 g ml^{-1} PEGylated rhodamine dye and incubated overnight at room temperature.
2. 800 µL volumes of buffer at pH 3 or 7 were added and the samples allowed to equilibrate for 12 hours.
3. The samples were centrifuged at 500 rpm and 800 µL of supernatant removed. The microcapsules were resuspended by gentle agitation.
4. 10 µL of slurry was introduced to a glass slide and viewed with 561 nm laser light at 5 % intensity with a Leica confocal microscope. Fluorescence was collected from 570 – 650 nm.
5. The laser light was increased briefly to an intensity of 100 % centred on a microcapsule to induce photobleaching.

6. Fluorescent recovery in the capsules was recorded over a 20 minute period after the laser intensity was returned to 5 %.

4.6.3. Packed column pulse testing

A 5 ml XK column was packed with grafted microcapsule slurry produced in experiment 9 of the Taguchi grafting analysis (Table 4-5). Packing was performed using pH 7 phosphate buffer, at a flowrate of 0.5 ml min^{-1}, connected to an AKTA explorer chromatography unit. A common testing procedure was used to observe the refractive index outlet response to a pulse input of mPEG 5000 in both citric acid (pH 3) and phosphate buffer (pH 7).

1. The column was equilibrated for 3 column volumes (CV) with buffer at a flowrate of 0.2 ml min^{-1}.
2. A 2 ml pulse of 10 mg ml^{-1} mPEG 5000 was injected at the same flowrate.
3. Following this, 3 CV of buffer were used to elute the PEG solution while recording refractive index response at the outlet.

Chapter 5 Results

This chapter details the results obtained from experiments using methodology established in Chapter 4. Where applicable, error estimates have been included to give an indication of the precision of the results. The results are presented in the order given by Figure 4-1, beginning with the small-scale production of microcapsules in section 5.1 and working towards the characterisation of scaled method microcapsule release profiles in sections 5.8, 5.9 and 5.10.

5.1. 200 ml batch scale microcapsule characterisation

Microcapsules were successfully produced on a 200 ml scale with an average dry weight yield of 200 – 250 mg. It was noted that some agglomeration occurred during microcapsule washing following centrifuge separation. Figure 5-1 shows typical microcapsules produced on the 200 ml scale. Some non-spherical microcapsules were observed as well as polymer debris from broken or partially formed spheres.

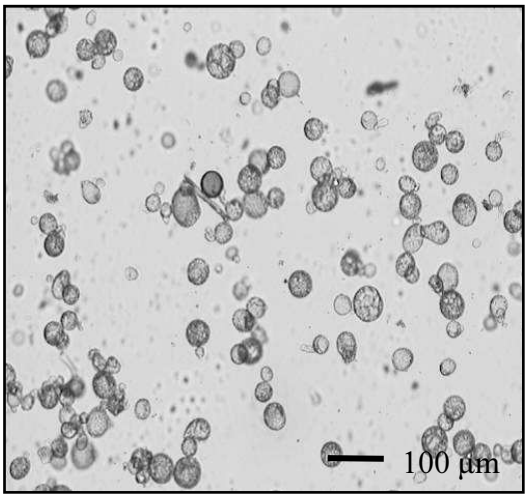

Figure 5-1: Optical micrograph of microcapsules produced on the 200 ml batch scale

The method was scaled to produce 2 L sized batches following successful production of microcapsules on this scale.

5.2. Emulsion dispersion testing

The average particle diameter was calculated at regular intervals over a 30 minute period for 2 L emulsions created with rotor speeds of 1200, 1000 and 800 rpm (Figure 5-2). These average droplet sizes were compared to those of the original 200 ml method to enable selection of an equivalent emulsification regime.

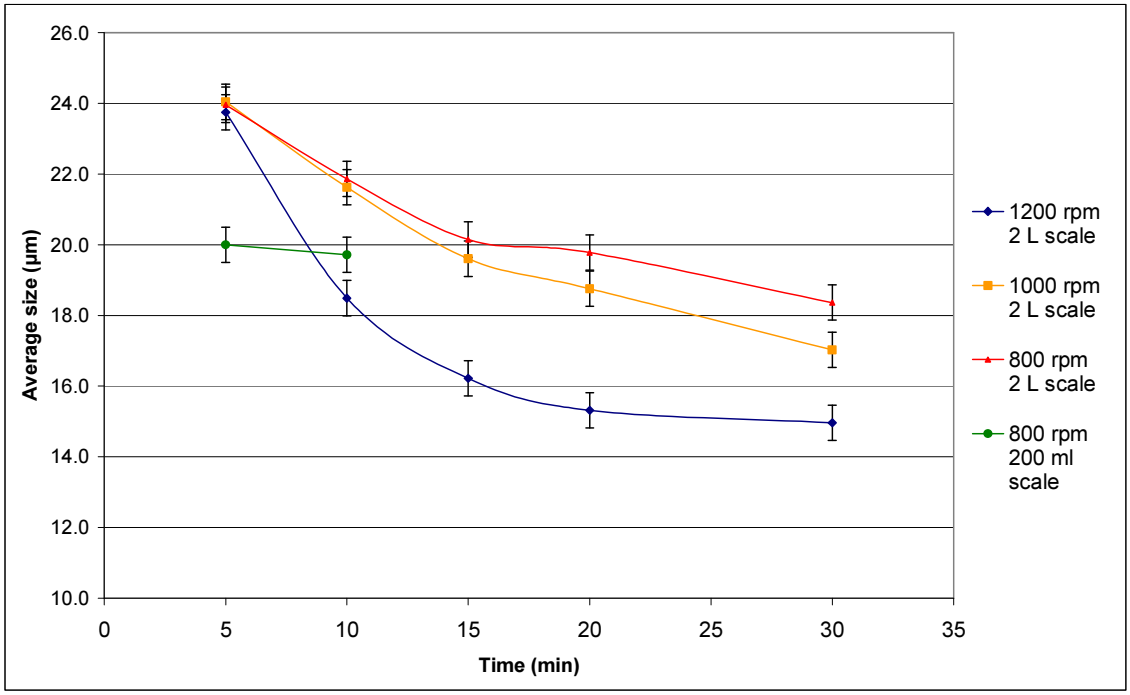

Figure 5-2: Average emulsion droplet size over time during microcapsule production

In addition, a size distribution analysis was performed on the emulsion data at each rotor speed, to give an estimate of dispersion (Figures 5-3, 5-4 and 5-5). Droplets were grouped into 5 µm intervals and plotted against volume frequency percent, calculated by Equation 4-1. Each sample for droplet sizing was removed from the centre of the reactor at equal depth and was assumed to be representative of the total volume.

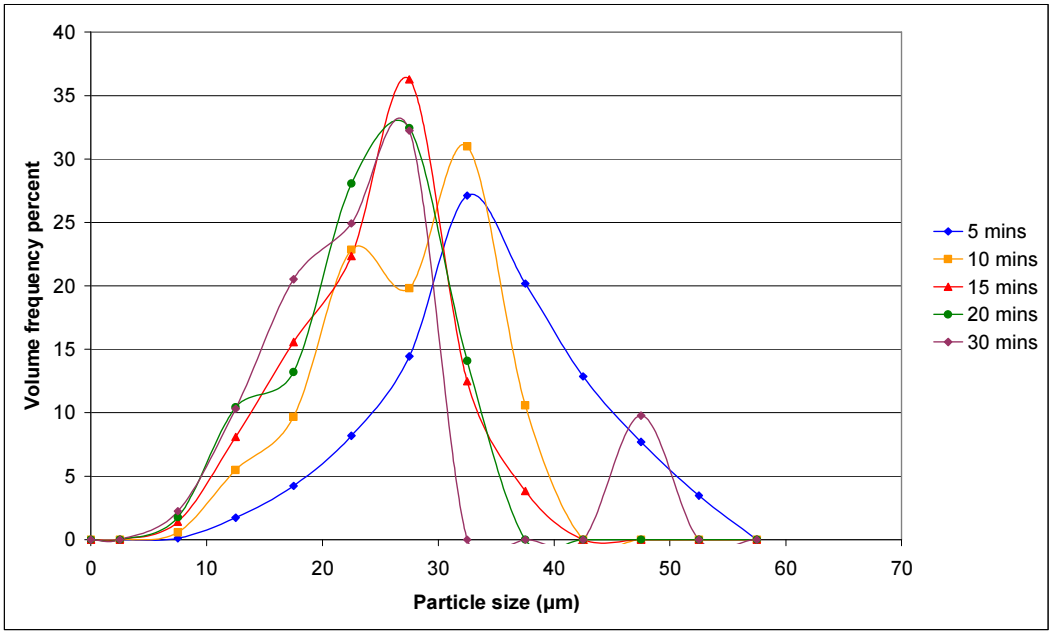

Figure 5-3: Droplet size distribution of emulsion over time when emulsified at 1200 rpm

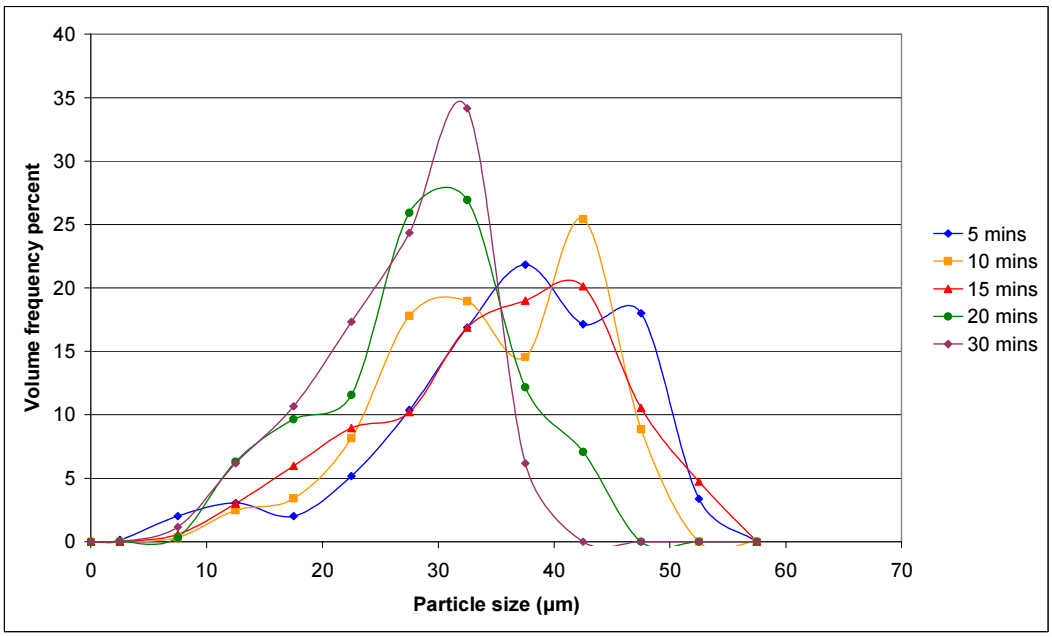

Figure 5-4: Droplet size distribution of emulsion over time when emulsified at 1000 rpm

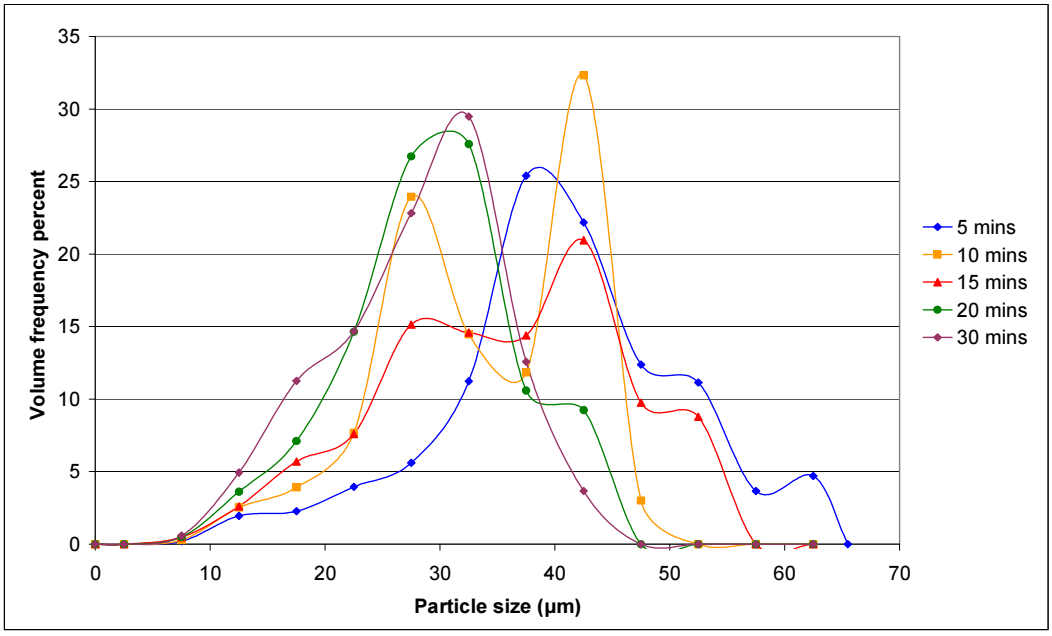

Figure 5-5: Droplet size distribution of emulsion over time when emulsified at 800 rpm

An increased emulsion monodispersivity was observed as agitation time increased. This is shown by a decrease in the standard deviation of the droplet diameter data (Figure 5-6). The lowest standard deviation values were observed for the highest rotor speed of 1200 rpm.

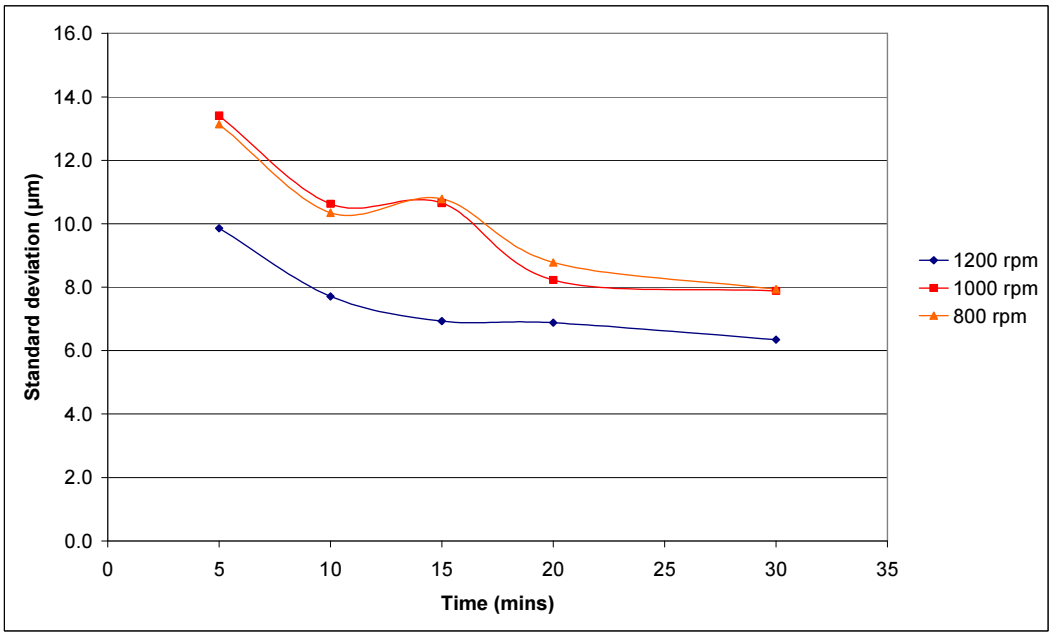

Figure 5-6: Standard deviation of emulsion droplet populations over time, for varied impeller speeds

5.3. UV grafting results from bench scale reactor

Initial UV grafting trials, using polyamide films irradiated in the bench top reactor (Figure 3-2), yielded a positive graft of $3.2 \times 10^{-3} \pm 2.6 \times 10^{-3}$ mmol cm^{-2} equivalent to 230 ± 190 μg cm^{-2}. This range was determined through averaging results from a triplicate repeat.

In addition, a microcapsule sample was irradiated in the bench scale reactor according to the method described in section 4.3.3. Back titration analysis showed a graft yield of 0.561 ± 0.460 mmol g^{-1}, averaged from a triplicate repeat.

5.4. Agglomeration prevention experiments

Characterisation of the degree of agglomeration was performed on a visual basis using a light microscope at 10 x optical zoom. The sample micrographs presented in Figure 5-7 show the differences between agglomerated and dispersed microcapsules produced by the 2 L batch method.

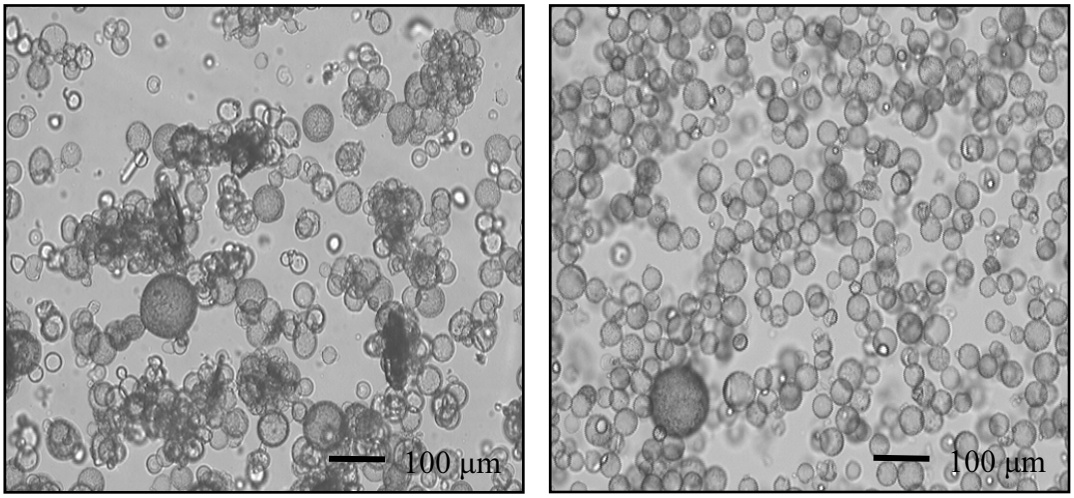

Figure 5-7: Agglomerated (left image) and dispersed (right image) microcapsules

A Taguchi experimental design method was applied to determine likely causes of unwanted microcapsule agglomeration (Section 4.4.2). Table 5-1 below provides a

summary of the results from the experiments prescribed by the L_8 Taguchi array (Table 4-3).

Table 5-1: Summary of results from Taguchi microcapsule agglomeration investigation during ethanol washing

	Dispersed fraction of capsules	
	Repeat 1	Repeat 2
Experiment A	9.5	9
Experiment B	2	4
Experiment C	9	9
Experiment D	7	7
Experiment E	1	1
Experiment F	1	3
Experiment G	5	5
Experiment H	2	2

The statistical analysis of variance (ANOVA) performed on the data is summarised below (Table 5-2) and shown in full in Appendix B.2. Each variable has a calculated percentage contribution to the cause of agglomeration. Variables 'pooled' were deemed to be insignificant at 95 % confidence limits and were grouped with the percentage contribution of the error term. ANOVA testing of two or more levels of each variable allows for projection of probable conditions for optimum performance.

Table 5-2: Contributions of each variable to instances of microcapsule agglomeration during ethanol washing

Variable	Contributing variable	Percentage contribution (%)	Optimum performance
Ethanol concentration (Vol %)	45	53.2	Low EtOH Concentration
Washing temperature (^{o}C)	25	9.3	High Temp
Ethanol concentration / temperature interaction		-	
SDS concentration % (w/v)	1	16.6	Low/No SDS
Tween 80 concentration % (w/v)	0.5	6.0	Low/No Tween
Speed of addition of solution		-	
Solution degassed	No degassing	10.6	Degas solution
Error		4.3	

Most significant was the ethanol washing concentration (45 % v/v) which contributed 53.2 % to instances of agglomeration. This provided a basis for experiments in which the ethanol washing concentration was further lowered. However, agglomeration was still observed when demineralised water was solely used during washing. Addition of sodium carbonate solution to the slurry, prior to washing, was found to delay the onset of agglomeration. Na_2CO_3 acts as a buffer for the microcapsule polymerisation, neutralising HCl derived from the condensation reaction. These observations led to subsequent experiments investigating the influence of Na_2CO_3 concentration on microcapsule formation.

Figure 5-8 below shows the effect of sodium carbonate buffer volume on the stability of microcapsules during polymerisation. Significant agglomeration was observed in samples B, C and E. By comparison, sample D and sample F were relatively free of agglomeration. Of note are the larger microcapsules seen in both of these images, none of which were present in the original emulsion (A). Image F, although dispersed, did not produce microcapsules as the emulsion remained unreacted.

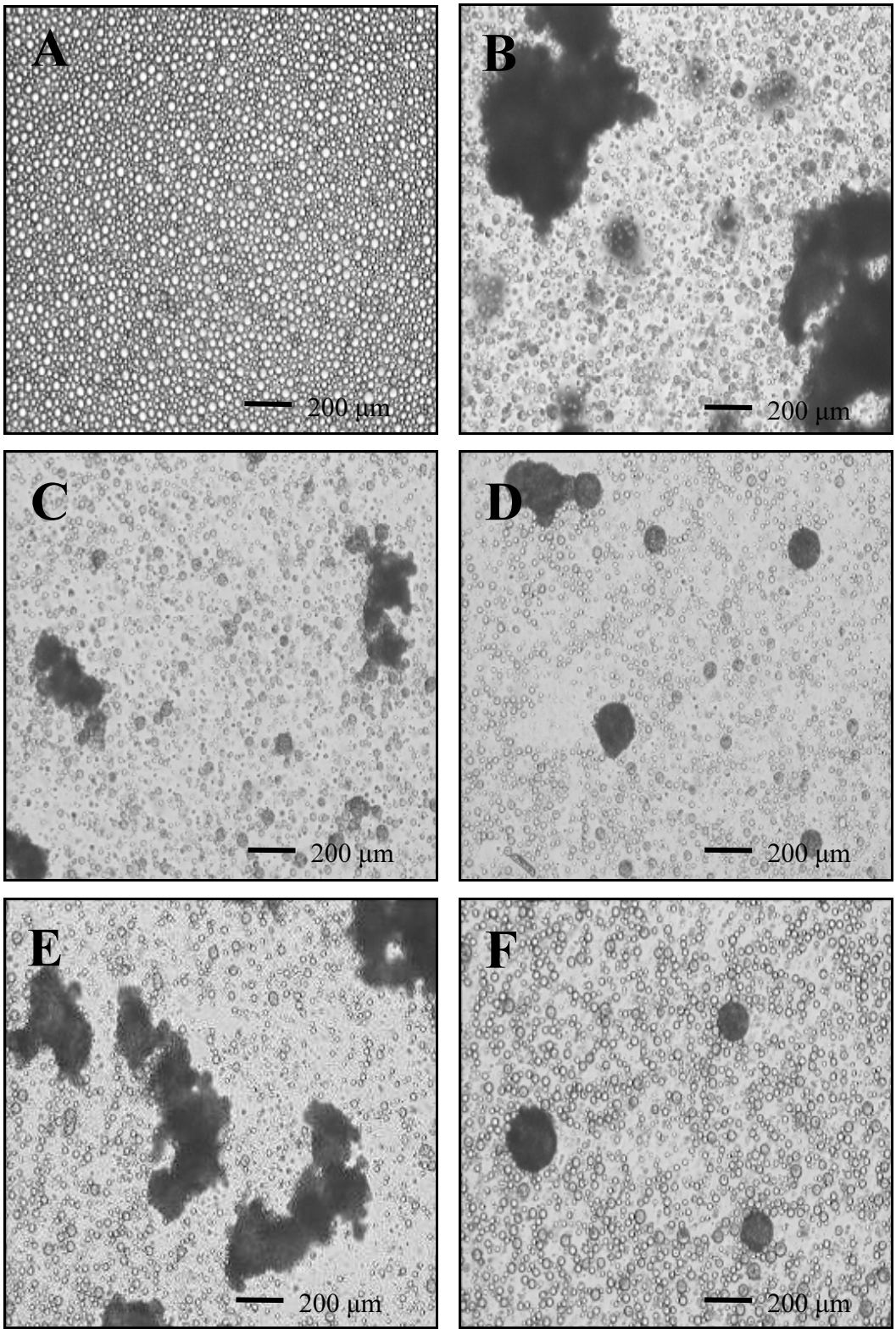

Figure 5-8: Optical micrographs of microcapsule formation after addition of varied volumes of 1.18 molL^{-1} Na_2CO_3 buffer; (A) initial emulsion, (B) 100 ml Na_2CO_3 equivalent, (B) 150 ml Na_2CO_3 equivalent (B) 200 ml Na_2CO_3 equivalent (B) 250 ml Na_2CO_3 equivalent (B) 300 ml Na_2CO_3 equivalent

Next, an investigation was undertaken to determine how microcapsule agglomeration was influenced by the speed at which the amine mixture was added to the reaction vessel. A sharp temperature spike was observed during fast amine addition and the microcapsules produced tended to be non-spherical in shape. Dropwise addition of amines from a dropping funnel yielded more spherical microcapsules (Figure 5-9).

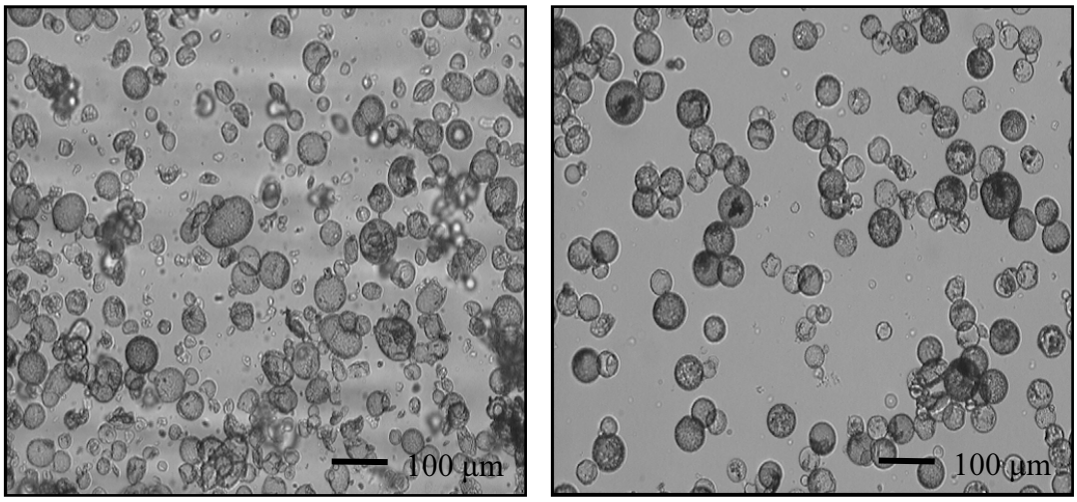

Figure 5-9: Microcapsules produced through swift addition of amine (left image) and microcapsules produced by dropwise amine delivery (right image)

A final set of experiments were undertaken to determine if the excess TDC monomer in the organic phase was reacting with the residual amines in free solution or the microcapsule exteriors during solvent exchange in the washing steps. Systematic lowering of the TDC concentration in the organic chloroform / cyclohexane phase yielded the observations summarised in Table 5-3.

Table 5-3: Observations during investigation into TDC monomer influence on microcapsule formation

Monomer concentration	Observations
0.5 mol L^{-1}	Complete agglomeration noted after 1 L of 30 % (v/v) ethanol solution delivered.
0.25 mol L^{-1}	Slight agglomeration noted after washing with 2 L 30 % (v/v) ethanol and 6 L deionised water.
0.2 mol L^{-1}	Good dispersion of microcapsules observed after washing with 2 L 30 % (v/v) ethanol and 6 L deionised water.
0.1 mol L^{-1}	No agglomeration detected after washing with 2 L 30 % (v/v) ethanol and 6 L deionised water, but microcapsules appeared unstable. Signs of membrane collapse and coalescence of unreacted organic emulsion droplets detected.

The most desirable slurry characteristics were achieved using a TDC monomer concentration of 0.2 mol L^{-1} in the organic phase. This concentration was selected for preparation of a bulk slurry for AAm UV grafting experiments.

5.5. Characterisation of scaled production microcapsules

Microcapsule dry mass yields in the range 1.01 – 1.20 g were calculated by total dry solid analysis of 2 L production batches (Equation 4-2). Samples from randomly selected scaled microcapsule batches were characterised by both SEM microscopy and laser particle size analysis. An average microcapsule diameter of 53.5 μm was calculated from batch data detailed in Table 5-4.

Table 5-4: Particle size distribution data taken from three batches produced on the 2L scale

	Batch A	Batch B	Batch C	Average
Mean (μm)	56.0	59.2	45.5	53.5
Mode (μm)	47.5	51.1	45.0	47.9

The size distribution is characterised by multi-modal peaks as seen in Figure 5-10. The same method was used in the preparation of all batches. They were prepared on different days as required and refrigerated prior to particle size analysis.

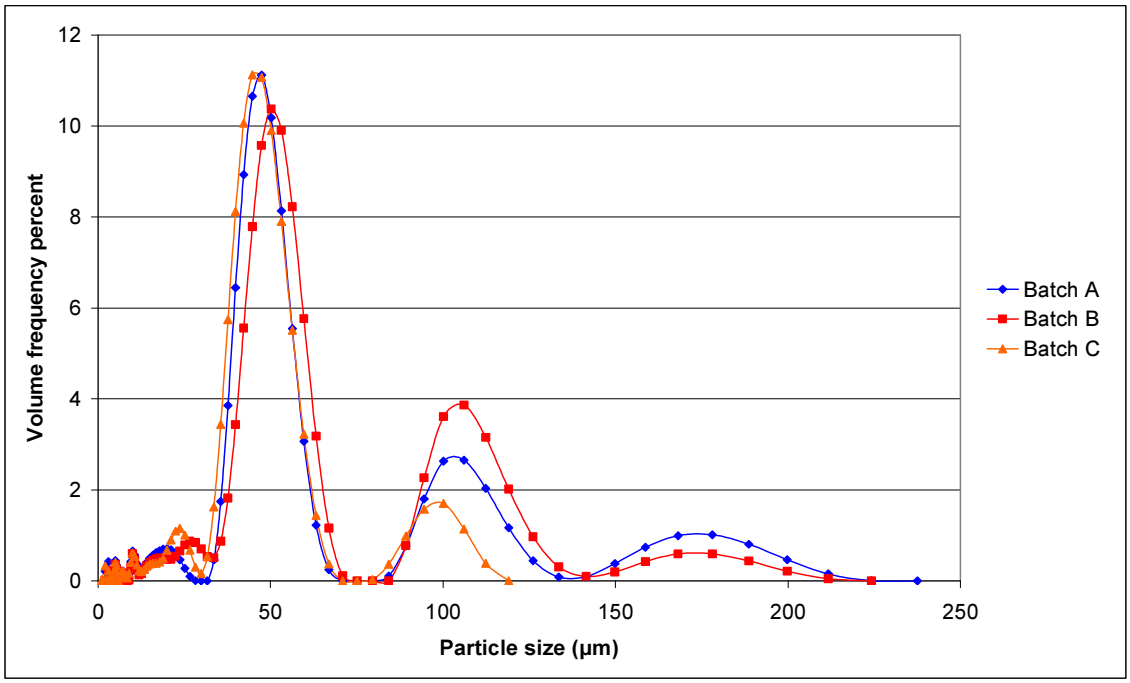

Figure 5-10: Particle size analysis averaged from triplicate results for three batches of scaled production

The particle size analysis revealed three distinct particle populations at 50, 110 and 175 µm. Batch C had a smaller average diameter than batches A and B and was distinguished by the absence of a particle population at 175 µm.

Scanning electron micrographs were taken of microcapsules produced in batch A. Samples were first prepared by freeze-drying, followed by sputtering of a gold layer. Initially, observations were made of the external surface of a representative microcapsule within the sample population (Figure 5-11). Microcapsules were determined to be spherical in nature with smooth external surfaces, periodically permeated by pores.

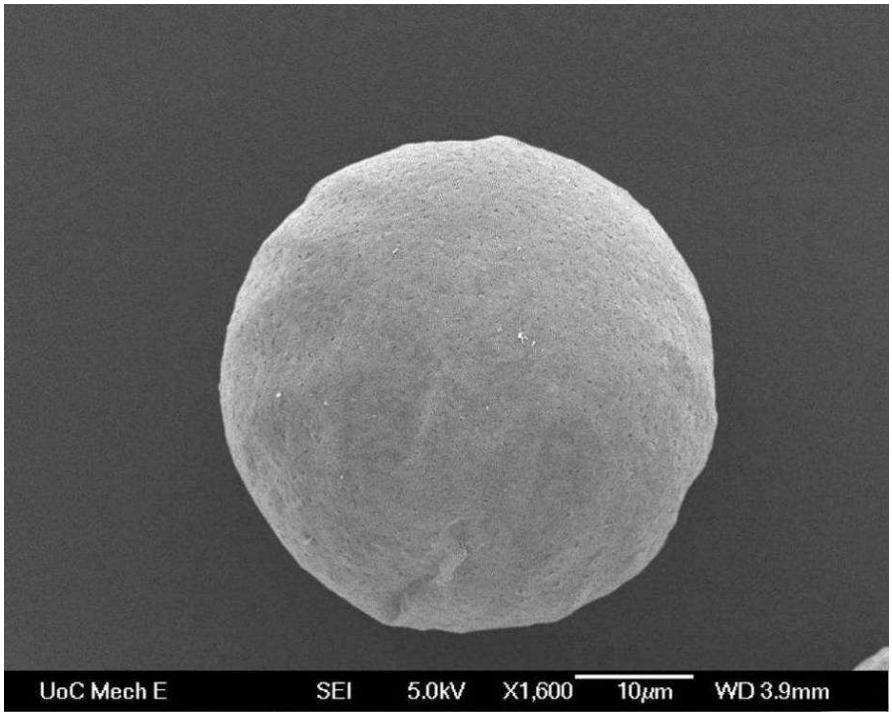

Figure 5-11: Porous polyamide microcapsule from Batch A viewed at 1600 x zoom

A SEM was captured of the microcapsule population to determine the proportion of broken microcapsules after the freeze-drying operation (Figure 5-12). The majority of microcapsules were observed to have withstood freeze-drying.

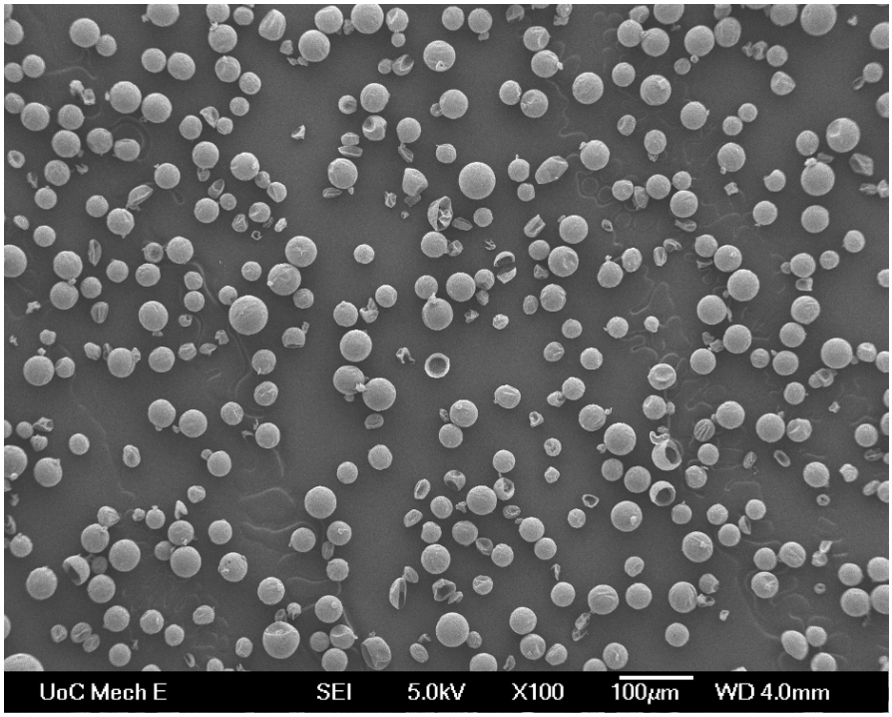

Figure 5-12: Sample population of microcapsules viewed under low magnification

A hollow microcapsule structure was confirmed by location of a split capsule (Figure 5-13). The internal void showed no evidence of internal partitioning. Lighter areas on the micrograph were due to the effects of charging, caused by uneven distribution of the gold coating on the microcapsule membrane.

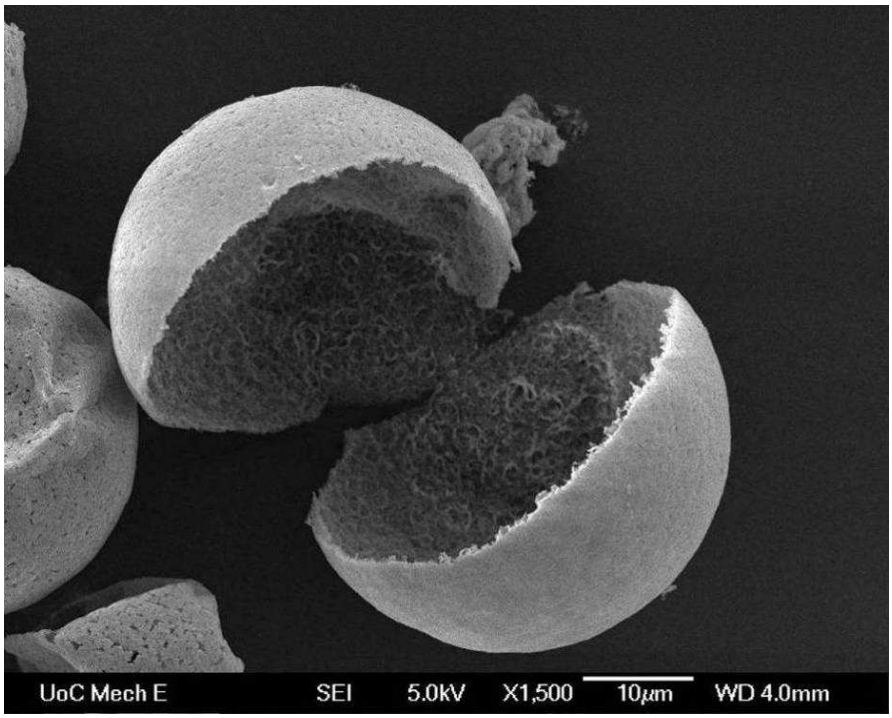

Figure 5-13: Split microcapsule showing internal void and thin shell membrane viewed at 1500 x zoom

A comparison was made between the structure of the external and internal microcapsule membrane surfaces (Figures 5-14; 5-15). The outer shell of the microcapsule was smooth and sporadically permeated by irregular shaped pores. Little polymer debris was observed on the outer surfaces, indicating no significant agglomeration during the washing step.

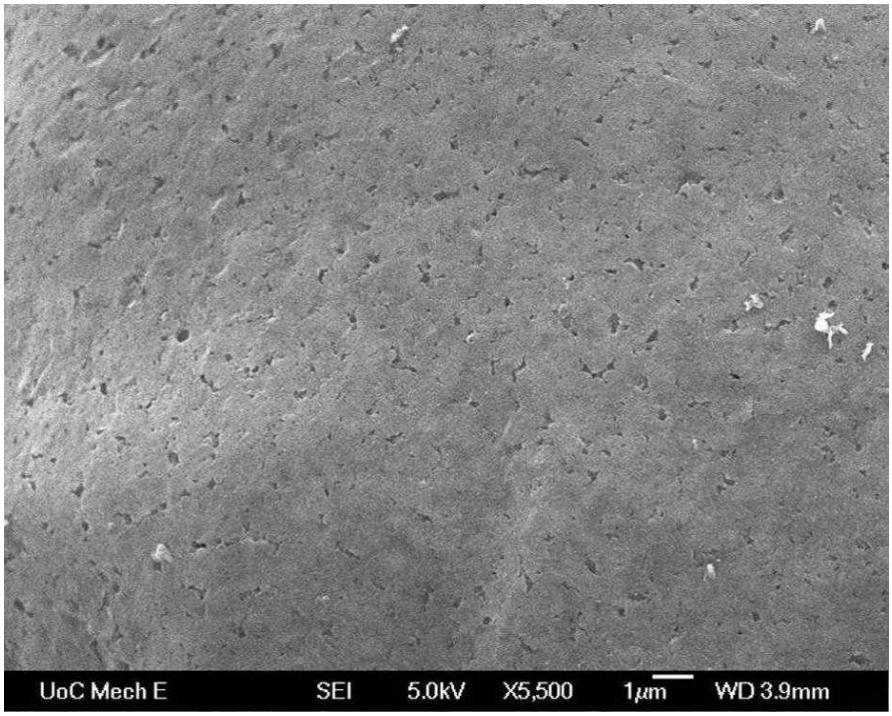

Figure 5-14: External membrane surface showing porous nature at 5500 x zoom

In contrast, the internal membrane surface was observed as a rough structure. This prevented the detection of any pores that might have permeated the membrane (Figure 5-15).

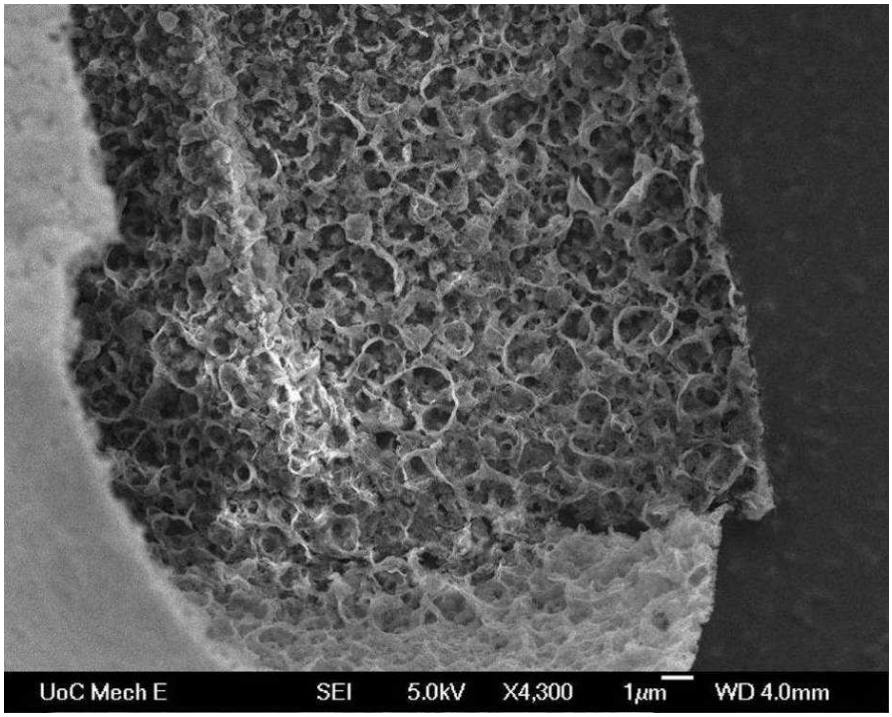

Figure 5-15: Internal membrane surface of split microcapsule viewed at 4300 x zoom

Finally, a cross-section of the membrane was viewed at a higher resolution. An even membrane shell thickness of approximately 0.5 μm was observed with a highly porous structure (Figure 5-16).

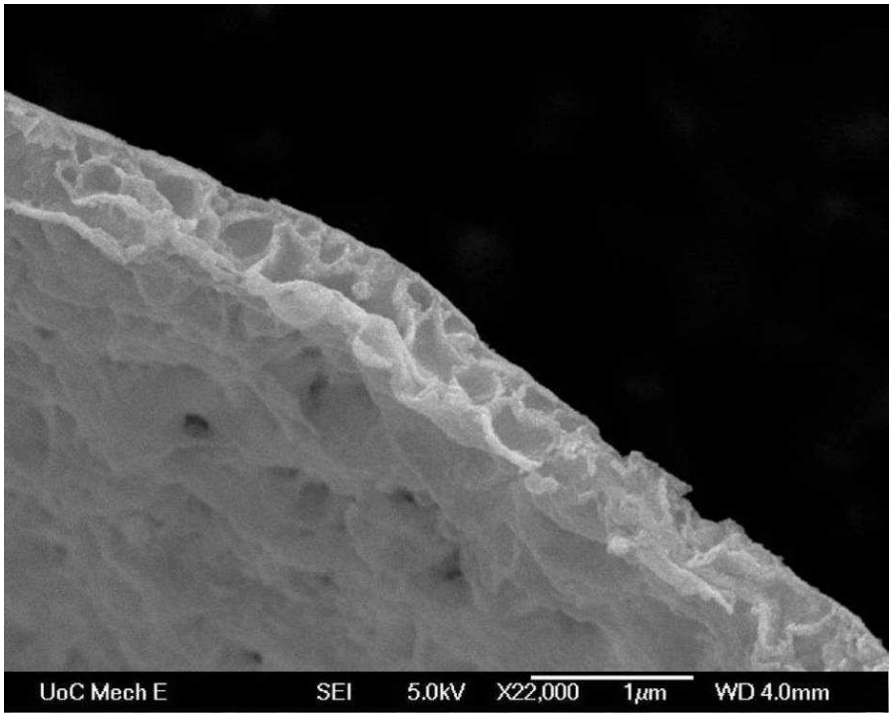

Figure 5-16: Cross-sectional view of a typical microcapsule membrane at 22000 x resolution

Visualisation of the membrane microcapsule structure confirmed the suitability of the scaled production method for further experimentation in grafting trials.

5.6. Grafting reactor flow characterisation

The external loop UV grafting reactor, depicted in Figure 3-7, was characterised to determine the flow regime and key flow variables. The reactor was found to have a holdup volume of 114 ml within the quartz glass tubes. An average liquid residence time of 44 seconds was calculated for a pump drive setting of 600. This pump setting produced a pulse frequency of 0.987 s^{-1}, corresponding to a UV irradiation time of 11.3 minutes per hour of circulation. From the data gathered, a Reynolds number of 1310 was determined for the maximum fluid velocity, assumed to be twice that of the average fluid velocity in the quartz tubes of 0.131 m s^{-1}.

Injection of methylene blue tracer dye showed a consistent outlet response curve (Figure 5-17). The tracer test was performed in triplicate to ensure accuracy of the method. Two independent methods were used to validate the results; a mass balance on the methylene blue dye and a calculation of the residence time of the dye. An average of 80.6 % of the injected mass of methylene blue was recovered in the reactor exit stream. The average calculated residence time from the tracer tests was 43.6 seconds.

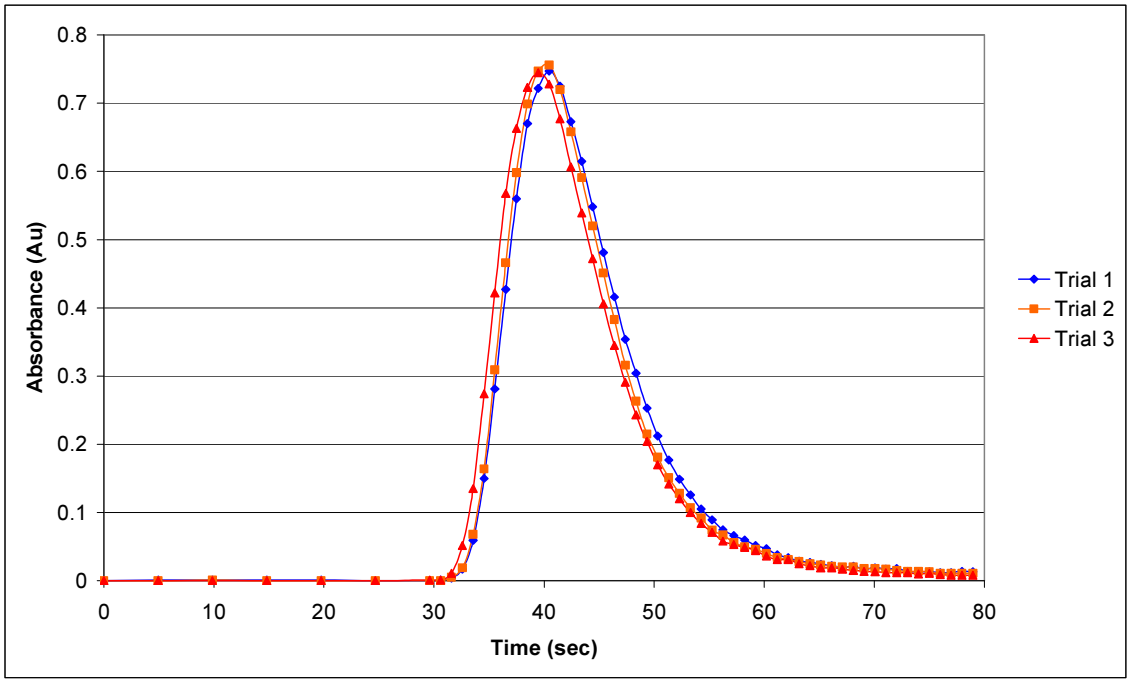

Figure 5-17: Tracer absorbance curves for spike injection of methylene blue dye

Calculation of the vessel dispersion number by Equation 3-9, gave an average value of 0.014, indicating only mild deviation from ideal plug flow. The axial dispersion model (Equation 3-13) for dispersion numbers in excess of 0.01 was fitted to tracer runs using the non-linear regression method of least squares (Figure 5-18). An average vessel dispersion number of 0.01 was determined by this method.

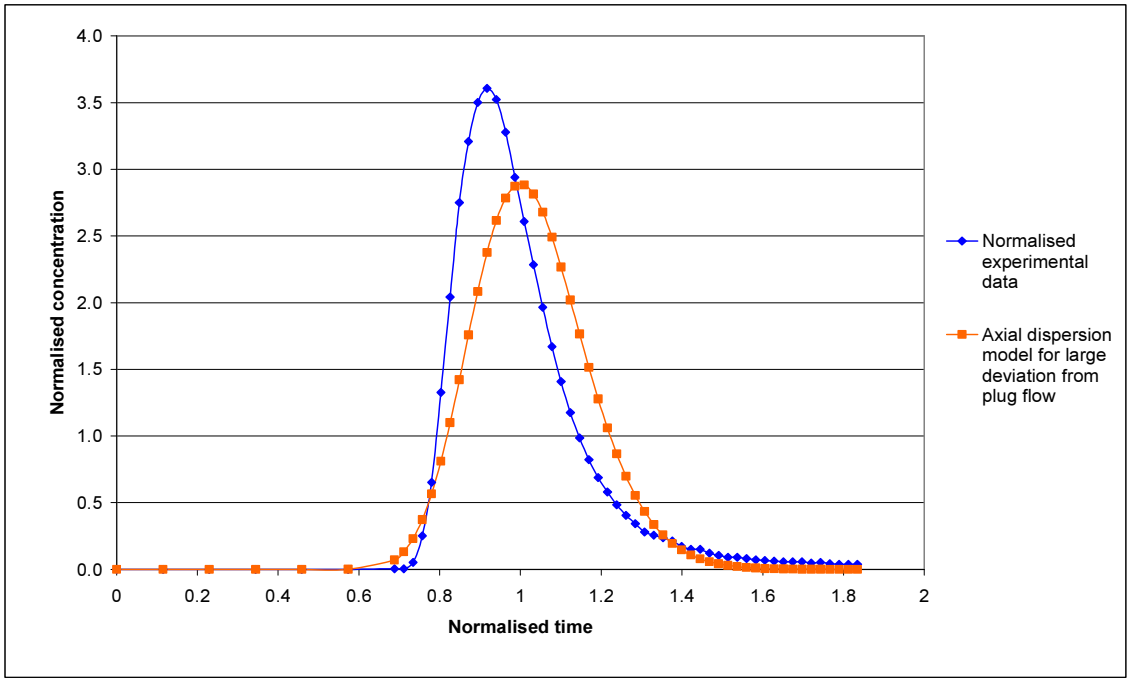

Figure 5-18: Axial dispersion model for large deviation from plug flow as fitted to normalised Trial 1 data

However, significant tailing on the response curve from a tracer input, accompanied by an earlier than expected response curve, was indicative of stagnant regions within the reactor (Levenspiel, 1999). A compartment model was used to account for this deviation by separating the reactor volume into two compartments; V_d was the volume of the reactor occupied by stagnant regions (m^3) and V_p the plug flow volume (m^3). This is schematically represented in Figure 5-19.

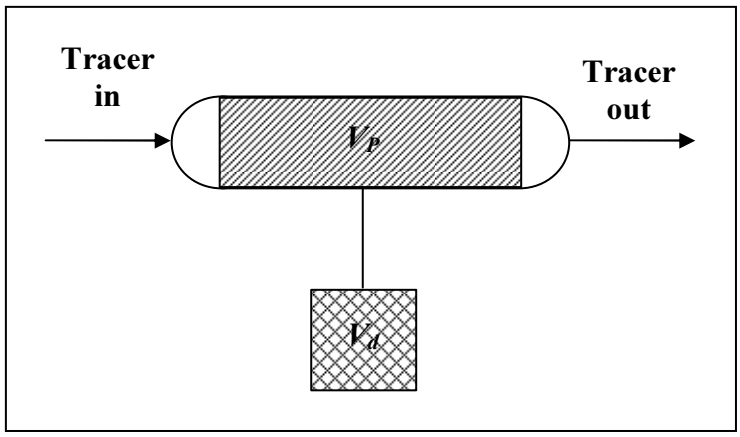

Figure 5-19: Diagrammatic representation of compartment model accounting for non ideal plug flow

New dimensionless normalised time values (θ_p) based on the adjusted volume V_p were calculated to reduce the effect of the tracer tailing.

$$\theta_p = \frac{t\nu}{V_p} \qquad \textbf{(5-1)} \qquad \textbf{(Levenspiel, 1999)}$$

A stagnant volume of 6.8 ml was calculated, accounting for 6 % of the total volume, by subtracting the theoretical reactor volume from the volume determined by experiment. Axial dispersion models for small and large deviation from plug flow were fitted, by linear regression, to the normalised experimental data modified by Equation 5-1 (Figure 5-20).

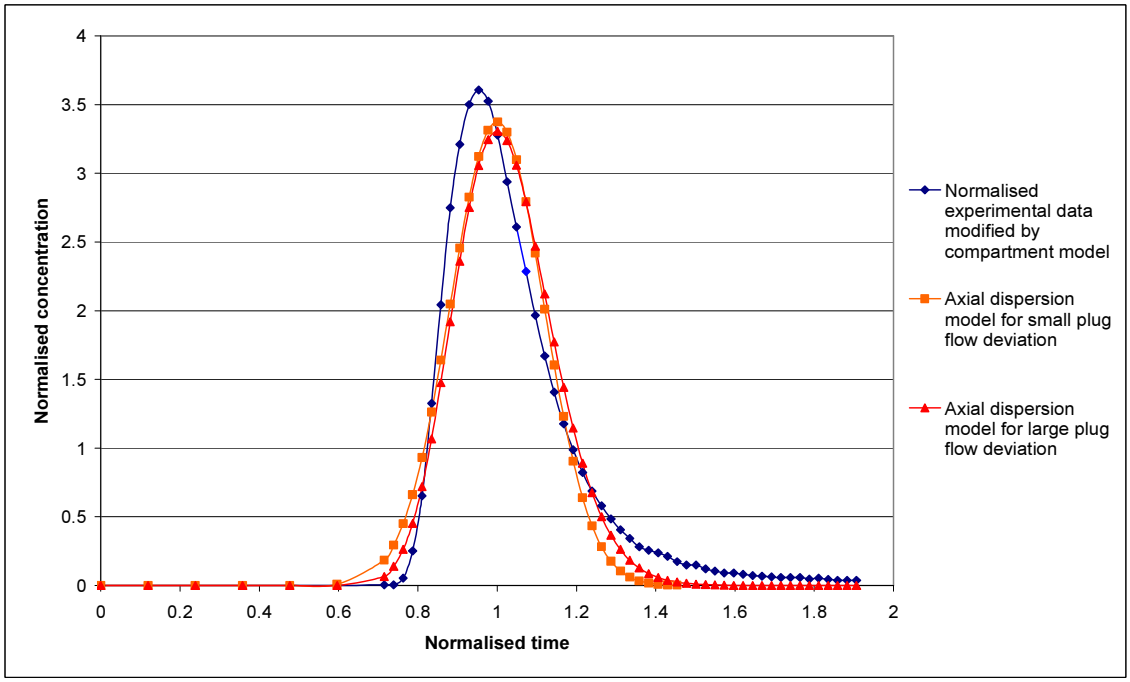

Figure 5-20: Axial dispersion models as fitted to normalised Trial 1 data modified by the compartment model

The dispersion model for small deviation from plug flow provided the best fit and gave an average vessel dispersion number of 0.008 across the three trial runs. This indicated that the flow profile was predominantly ideal plug flow when stagnant regions were accounted for.

The number of tanks in series approximating the system was calculated using Equation 3-10. An average total of 35.8 CSTRs in series were required to achieve the same flow characteristics as observed in the tracer tests.

5.7. Taguchi analysis on variables affecting PAA grafting

Both FT/IR and the back titration method described in section 4.5.1 were used to characterise acrylic acid polymerisation by UV in large scale batches. Using potassium bromide pellet FT/IR spectroscopy, an elevated peak was observed at 1720 cm^{-1} when ungrafted microcapsules were compared to grafted counterparts from the same bulk slurry.

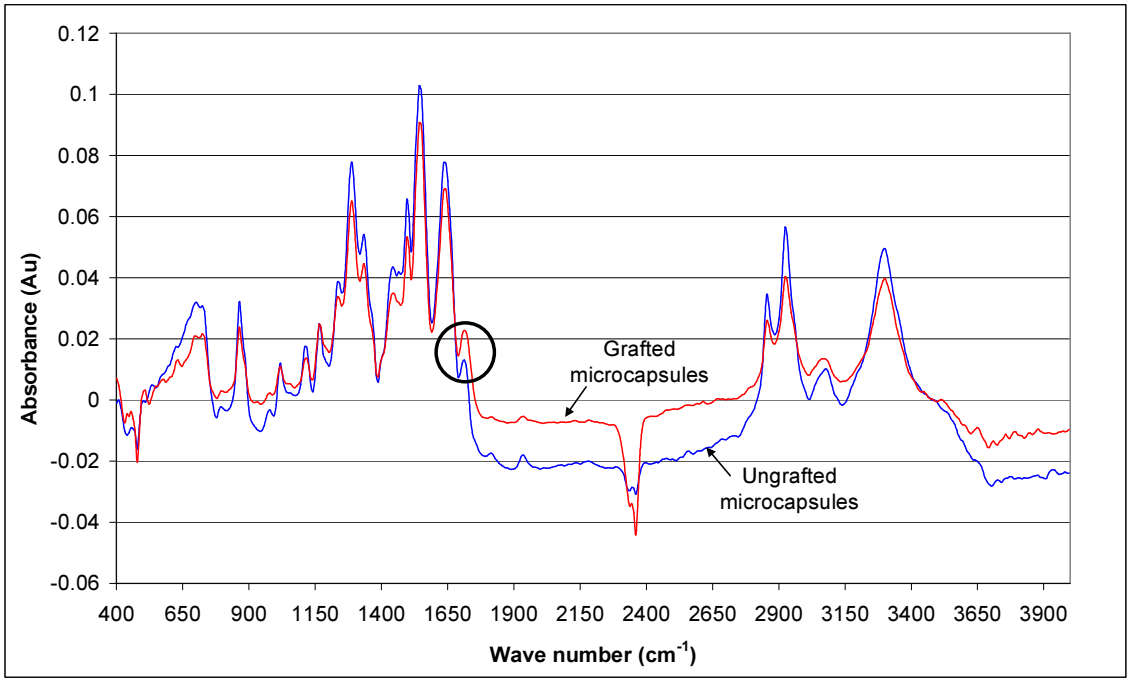

Figure 5-21: FT/IR spectrum for grafted microcapsules compared to ungrafted microcapsules

The grafted microcapsule spectrum exhibited a shift in the region of 1700 – 2900 cm^{-1}. However, the peak at 1720 cm^{-1} was greater in magnitude relative to surrounding peaks than in the ungrafted sample. This confirmed the presence of the carboxyl bond found in PAA.

Back titration of microcapsules produced in each of the Taguchi grafting experiments yielded the following results in Table 5-5:

Table 5-5: Polyacrylic acid graft yields for Taguchi experiments on variables affecting UV grafting

Experiment number	Grafting yield (mmol g^{-1})
1	0.55
2	0.80
3	0.39
4	0.77
5	0.52
6	0.54
7	1.00
8	1.05
9	1.13

An ANOVA test on the grafting yields was performed under the assumption that microcapsules with higher levels of grafting are more responsive to pH and therefore more desirable. As detailed in Table 5-6, an elevated temperature had the largest positive influence on the grafting yield, followed by a longer irradiation time. The percentage contributions from variables termed 'pooled' were merged with the error contribution term at a 95 % confidence limit.

Table 5-6: Contributions of process variables to grafting yields of PAA on microcapsules

Variable	Contributing variable	Percentage contribution (%)	Optimal performance
Temperature (^{o}C)	50	77.6	High Temperature
Acrylic acid concentration (% w/w)	-	Pooled	-
UV irradiation time (hours)	3	16.6	Longer irradiation
Post irradiation reaction time (hours)	-	Pooled	-
Error		5.8	

5.8. Batch microcapsule release characteristics

The first bench scale release tests were performed using cytochrome C as a model protein. A sharp change in the concentration of cytochrome C in free solution was observed when the pH of the surroundings was lowered from 7 to 3 (Figure 5-22). The rate of release suggested diffusion was not the controlling parameter. Alternative reasons to explain this behaviour have been proposed in section 6.9 of the discussion.

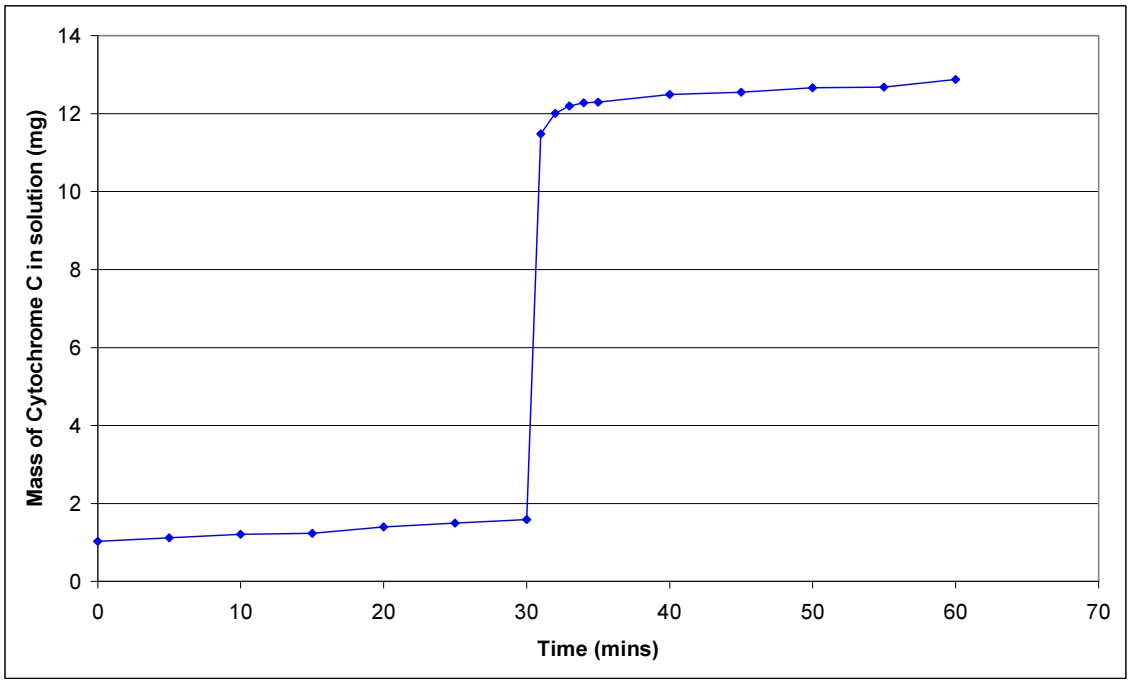

Figure 5-22: Release profile for cytochrome C from grafted microcapsule slurry during pH step change

Other test compounds were less successful; methylene blue and methylene blue conjugated dextran both showed an affinity for microcapsule membranes, while α-Lac aggregated at low pH, causing a reduction in the detected concentration. The NaCl test procedure showed no increase in conductivity over a 30 minute time span. These findings led to the use of a packed column for bulk microcapsule pH tests.

5.9. Confocal microscope release profiles

Ungrafted microcapsules were first tested to establish the permeability of the pores in the external membrane (Figure 5-14). The FRAP method from section 4.6.2 showed fluorescein diffusion into an individual microcapsule (Figure 5-23).

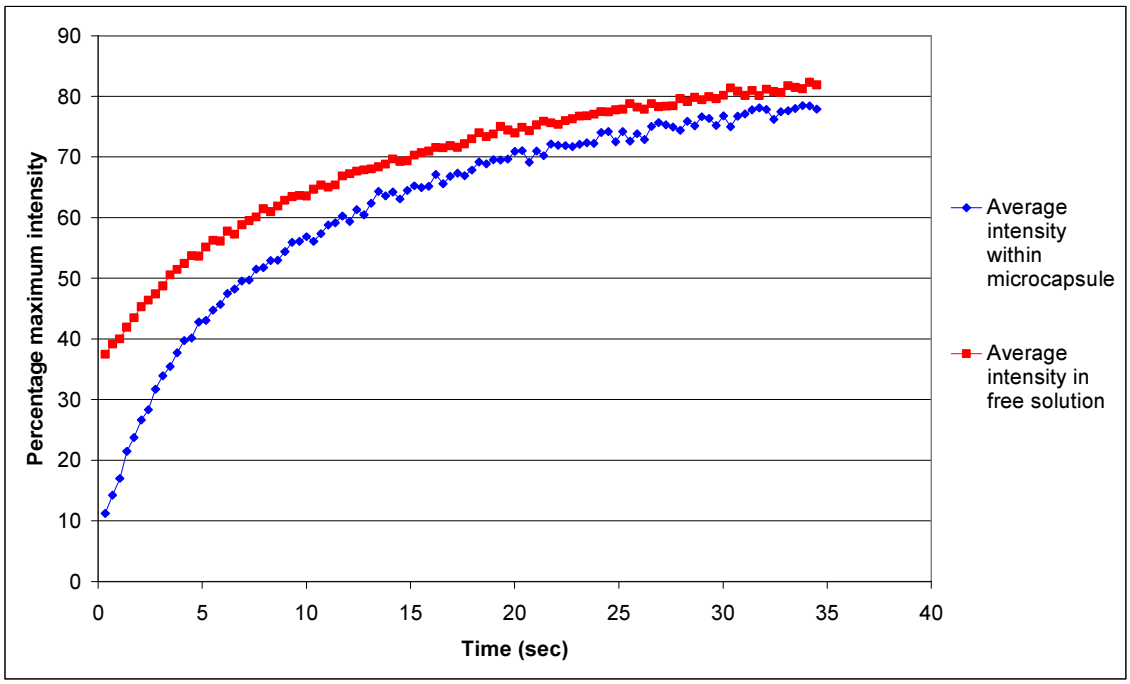

Figure 5-23: Fluorescence recovery of fluorescein in an ungrafted microcapsule following photobleaching

FRAP analysis at varied pH was performed on grafted microcapsules using TAMRA mPEG 5000 fluorescent dye. Confirmation of the synthesised dye structure was obtained by NMR (Figure 5-24).

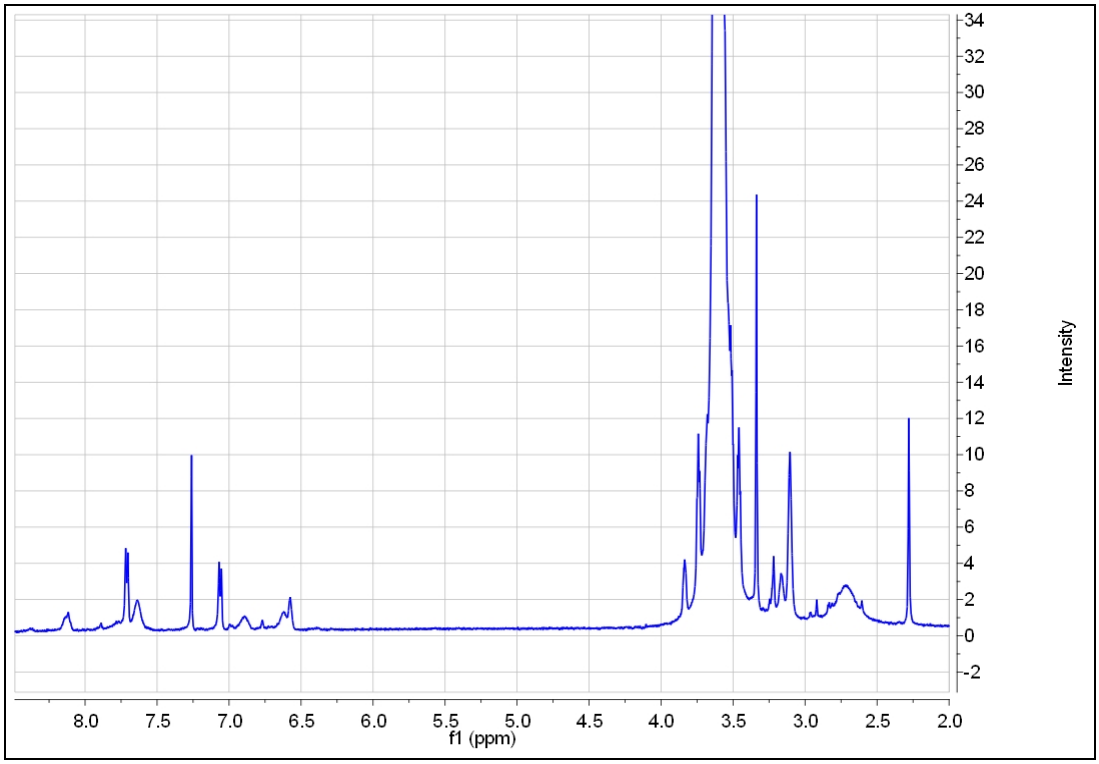

Figure 5-24: NMR spectrum for PEGylated rhodamine dye

Peaks in the range of 6.5 to 8.5 ppm confirmed the presence of aromatic rings associated with TAMRA dye and unreacted Tosyl groups. The characteristic peak at 2.28 ppm was indicative of a positively charged amine derivative in the dye structure. The high intensity peak at 3.6 ppm was due to coupled and uncoupled mPEG 5000 in the sample. Fluorescent recovery of TAMRA mPEG 5000 was observed in internal microcapsule voids at both pH 3 and 7 (Figure 5-25). The bright colour of the microcapsules indicated a strong affinity of the dye for the polyamine membranes.

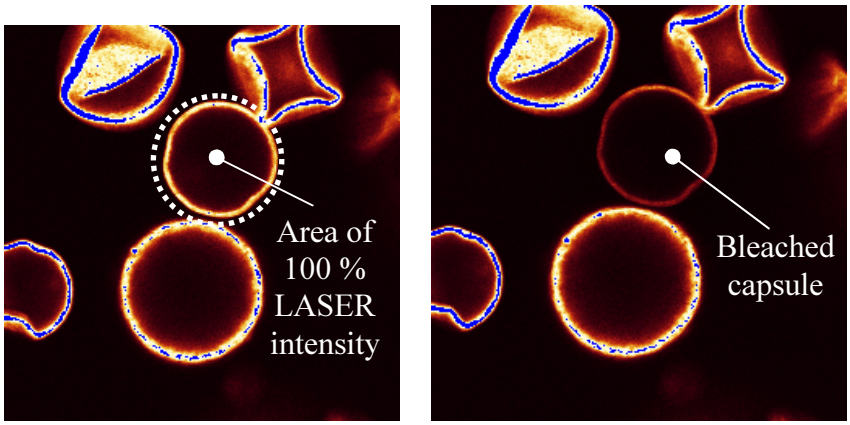

Figure 5-25: Microcapsule fluorescence preceding (left) and following (right) photobleaching with a laser intensity of 100 %. In this image, blue labelling indicates image saturation

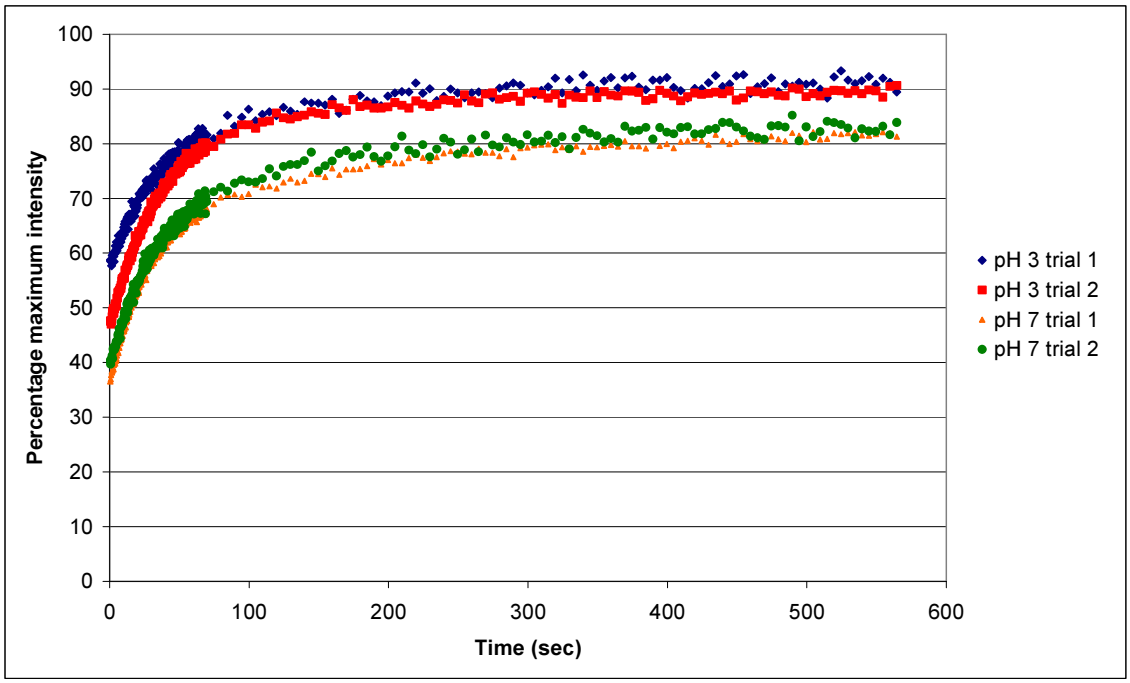

Figure 5-26: Fluorescence recovery of PEG 5000 rhodamine dye within microcapsule internal voids at pH 3 and 7 following photobleaching

The PEGylated rhodamine dye exhibited sensitivity to pH; lower emissions were observed at pH 3 than at pH 7. The fluorescence profiles were scaled accordingly, as a percentage of the original maximum intensity prior to photobleaching, allowing for comparison shown in Figure 5-26.

5.10. Packed column release tests

Refractive index measurements of a pulse of mPEG 5000 at the outlet of a packed column of microcapsules provided highly repeatable response curves (Figure 5-27). The response at pH 3 had a 2.9 % greater spread than the response at pH 7. Peak integration revealed the area of the curves to be within 0.5 mV ml of each other.

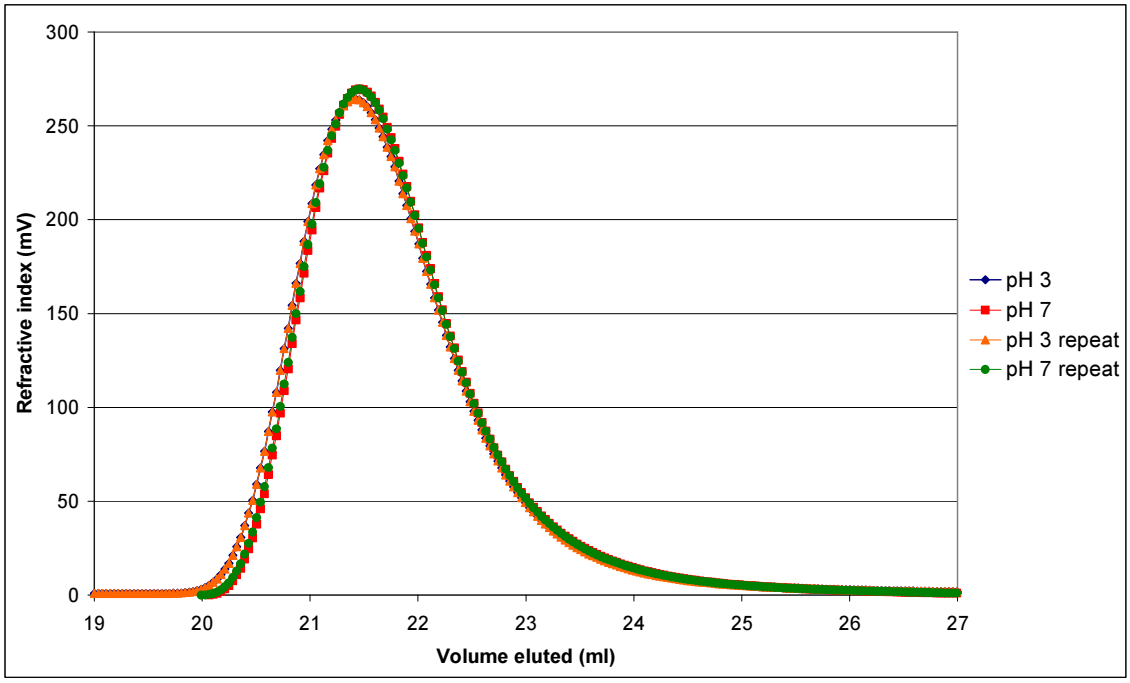

Figure 5-27: Pulse response of 5 ml column packed with microcapsules to a 2 ml solution of 10 mg ml^{-1} mPEG 5000 solution

Chapter 6 Discussion

Chapter 6 explores some of the main ideas drawn from the results section and compares these to published literature. Within this section, the methodology and experimental techniques are critically examined. Finally, the outcomes of the research are presented with reference to the project objectives; in particular the implications of the findings with respect to scale-up of the process.

6.1. 200 ml scale microcapsule production and characterisation

A high proportion of microcapsules produced on the 200 ml batch scale were non-spherical in shape (Figure 5-1). Distortion of the microcapsule shape may lead to non-uniform grafting on membrane surfaces. An irregular PAA attachment is likely to introduce error when the graft yield is correlated to the microcapsule release rate. Experiments on the rate of amine addition to the emulsion, described in section 5.4, showed similar microcapsule deformation during rapid addition of the amine monomers (Figure 5-9). Improvement in microcapsule shape was observed when a slower amine addition rate was set. The cause of deformation during the rapid addition of the amine monomers may be linked to the associated temperature rise observed. A higher temperature reduces the surface tension of the surfactant, which reduces the stability of the emulsion (Chatzi *et al.*, 1991b). In conjunction, a higher temperature promotes a faster polymerisation reaction by increasing the diffusion rate of monomer across the droplet interface. Shear forces induced by the impeller in the reaction vessel may cause droplet oscillation, which can lead to the production of misshapen microcapsules when coupled with a faster rate of reaction.

A high reaction rate may have a secondary influence on the microcapsule membrane shape. A fast reaction rate is likely to produce a less structured porous membrane. Microcapsules produced in this manner would have non-uniform membrane cross

sections, leading to a crumpled or irregular appearance when viewed under the microscope (Figure 5-1).

Figure 5-1 shows significant microcapsule debris in free solution. Particulate matter will reduce the mesh filtering efficiency, requiring more frequent cleaning operations. A likely cause of this microcapsule breakdown is the use of the high shear impeller during microcapsule polymerisation. Despite a reduced speed, shear forces between the emulsion screen and the impeller head probably continue to cause breakage when the forming membrane shells are still thin. This finding led to the use of a pitched six-bladed angled impeller for mixing during the polymerisation step.

Lin *et al.* (2006) reported yields of 100 – 140 mg of dry microcapsules per 200 ml batch. The higher reported microcapsule yields in this project can be explained by a higher TDC monomer concentration in the organic solvent, resulting from differences in preparation methods. A longer sonication period and a lengthened mixing period are likely to have increased the concentration of TDC in solution. Observed agglomeration, stemming from excess TDC monomer reacting during the solvent exchange washing steps, will contribute to a higher observed mass yield. Direct measurement of the TDC concentration in solution would be useful for future production, to ensure repeatability of the method.

6.2. Emulsion dispersion testing

To ensure a comparable microcapsule product following scale-up, the average emulsion droplet size at the 2 L scale was matched to the 200 ml scale. Matching of the emulsion droplet size to that of the original method is essential to maintain a constant total surface area for polymerisation. This is required to ensure a consistent microcapsule shell thickness, consumption rate of TDC monomer and consumption rate of amine monomers. The simplest variable to change during production was the impeller speed, which influenced the amount of shear force exerted upon the organic phase droplets at the blade tips.

Emulsion droplet dispersion tests on the 2 L scale showed that droplet size decreases over time with continuous mixing. This observation is congruent with those reported by Chatzi *et al.* (1991) and Koishi *et al.* (1969). A plateau effect was noted at an impeller speed of 1200 rpm, as the average droplet size tended towards a minimum of 15 μm (Figure 5-2). This was not as pronounced with slower mixing speeds, indicating more time may have been required for the rate of coalescence to match the rate of droplet formation. Once again, this explanation is supported by observations published by Chatzi *et al.* (1991b). As expected, an increase in mixing time improved the monodispersity of the emulsion. This was best indicated by a decrease in standard deviation of the raw data as time progressed (Figure 5-6). Contrary to expectation, exceptions to this trend were noted at stirring speeds of 800 and 1000 rpm, following 15 minutes of mixing. This is most likely due to experimental variation introduced by a limited sample population of 200 diameters. A larger sample size would reduce some of this variance, allowing for a more accurate droplet size distribution analysis. The most monodisperse emulsion was attained at the highest mixing speed of 1200 rpm. This agrees with measurements made by Yan *et al.* (1992), who found a narrower droplet dispersion at high rpm than at low rpm.

Figures 5-3, 5-4 and 5-5 show a progressive reduction in the number of large diameter microcapsules over time. Similarly, a narrowing of the droplet size distribution may be seen in these figures. Interestingly, particles less than 5 μm in size were not observed in any of the emulsions studied. This seems to suggest a lower limit of stability exists. More stabilising agent, a lower temperature or a higher mixing speed is likely to be required to further reduce the droplet size.

The results from the emulsion dispersion testing indicated a mixing speed of 800 rpm, for 20 minutes, should be selected for 2 L scale production. The average droplet diameter at this setting most closely correlated to that of the 200 ml scale production method. The calculated average droplet size for 1000 rpm mixing over 15 minutes was also found to be similar to that of the 200 ml production method. However, comparison of this droplet size distribution curve (Figure 5-4) with the 800 rpm curve after 20 minutes, in Figure 5-5, showed the emulsion produced at the lower speed had a larger proportion of particles in the 25 – 30 μm range. This was more favourable for two reasons; first, microcapsule diameters were reported in this size range by Lin *et al.*

(2006) and second, if a 25 μm filter mesh was to be used for filtration, a greater proportion of microcapsules could be recovered than from filtration of the 1000 rpm production method. Agglomeration testing on the microcapsules revealed more influential factors controlling the microcapsule size distribution during the polymerisation reaction. These factors will be discussed in greater depth in section 6.4.

Inaccuracy in the emulsion droplet sizing method was primarily introduced by the limited resolution of the camera used to collect the optical micrographs. An error of 0.5 μm was attributed to each of the diameter measurements. Unfortunately, use of a laser diffraction particle size analyser was impractical for emulsion sizing. The stability of the emulsion would have been affected by dilution of the SDS surfactant in the sample chamber, causing coalescence of droplets. In future, a software package could be used to analyse emulsion micrographs, allowing for automatic determination of droplet boundaries and calculation of droplet diameters.

6.3. Bench scale UV grafting

Successful grafting of PAA to polyamide films was achieved using UV irradiation. This result strongly suggested UV assisted attachment of PAA to polyamides was a viable technique for use in scale-up of the microcapsule grafting process. Initial use of a polymer film enabled the simple removal of both unreacted and homopolymerised monomer by thorough washing with deionised water. These factors had the potential to contribute to an inflated graft yield.

Only a tentative comparison can be made with the values from literature due to a large calculated experimental uncertainty. The calculated graft yield of 230 ± 190 μg cm^{-2} lies within the range achieved by Lei & Liao (2001) using a corona discharge method. A similar graft range was published by Choi *et al.* (2004). The high experimental uncertainty stemmed from the back titration assay of carboxyl groups. Volumetric errors were compounded during the calculation using Equation 4-3. A potentiometric titration method would help to reduce these errors, as would preparation of the stock reagents on a mass basis.

A polyamide microcapsule graft yield of $3.2 \times 10^{-3} \pm 2.6 \times 10^{-3}$ mmol cm^{-2} is within the range reported by Lin *et al.* (2006). Again, this figure has a high associated experimental error due to the same limitations in the back titration as detailed above. In addition, homopolymerised PAA could not be separated from the final microcapsule slurry, the effect of which is an inflated graft yield. Despite these limitations, an advantage of the back titration method is the establishment of a background acidity level. Subsequent subtraction of this value from the sample measurement allows for graft yield comparison between batches by negating the effect of differences in washing procedures. However, a reduction in the background level of AAm by thorough washing is essential to ensure a minimal experimental error.

It was thought that scale-up of the UV grafting process to a circulation system would require significantly higher irradiation intensities to achieve similar grafting yields to the bench scale reactor. The reason being that a high intensity would be needed to achieve a greater slurry penetration depth and shorten the exposure time required to ensure an even grafting of each microcapsule.

6.4. Microcapsule agglomeration testing

Agglomeration was first observed during the microcapsule washing steps, most notably after the addition of ethanol to the slurry. Instances of agglomeration were also observed on addition of the amine phase to the emulsion. Agglomeration was unwanted as the drug release characteristics are likely to be affected by an uneven distribution of the pH responsive PAA functional gates. As seen in Figure 5-7, the agglomeration appears to be caused by a gel matrix binding the capsules together. This matrix formation was uncontrolled, so microcapsule diffusion rates were likely to be inconsistent and drug delivery unpredictable. Furthermore, agglomerated microcapsules often presented poor structural characteristics, frequently appearing collapsed or broken.

Results provided by the Taguchi analysis on the microcapsule washing step were key in determining the cause of the agglomeration (Table 5-1). A high ethanol concentration was determined to be the most influential contributor to the cause of agglomeration. To a lesser extent, a high washing temperature was determined to cause more frequent

agglomeration than a low wash solution temperature and it was clear supplementary washing solution additives, such as SDS, were not required. In addition, a degassed ethanol washing solution tended to cause less agglomeration of microcapsules. Ethanol concentration was thought to affect the reaction mixture by altering the solubility of the organic phase in the aqueous phase. Work published by Lynn *et al.* (2001) indicates solvent exchange of chloroform at sub-ambient temperature will occur at a faster rate than at room temperature. The detrimental effect of this characteristic is the removal of excess TDC monomer into free solution, allowing for subsequent reaction with aqueous amine monomers or the external surfaces of the microcapsules. Excess TDC reactant will be present if the microcapsule membrane impedes the diffusion rate sufficiently during emulsion polymerisation, resulting in a TDC conversion of less than 100 %. A lower ethanol concentration should result in less TDC monomer transfer to free solution. Correspondingly, a less severe agglomeration was observed at ethanol concentrations below 30 % (v/v). An improvement in microcapsule dispersion was observed with washing solutions at room temperature. Chloroform exhibits a lower solubility in aqueous solution at room temperature and as a result less reactant is transferred to free solution for agglomeration reactions to occur.

Degassed washing solutions have a reduced dissolved gas content. Evolution and attachment of gaseous bubbles to microcapsules in untreated washing solutions effectively lowered the density of the bulk slurry. This density change caused microcapsule flotation and made the slurry more difficult to suspend. As a result, microcapsules appeared less dispersed, promoting instances of contact and increasing the chance of agglomeration. Addition of SDS to the washing mixture was detrimental to the stability of the microcapsule slurry. The binding of SDS at the water / monomer interface, as suggested by Chatzi *et al.* (1991b), was prevented by the polymer membrane and did not aid in inter-capsule repulsion. Potentially, excess SDS in free solution could cause the microcapsules to congregate by a hydrophobic mechanism, promoting the chance of agglomeration by close proximity during washing.

To investigate agglomeration caused by amine addition, the effect of sodium carbonate volume on the emulsion stability during the reaction was examined (Figure 5-8). The experiment showed a lack of system buffering caused agglomeration, while too much buffer retarded the reaction and prevented the formation of stable microcapsules. This

suggested the optimal concentration of sodium carbonate slows the reaction sufficiently, to allow ordered membrane formation, while not completely preventing the polymerisation. An optimal volume of 200 ml of 1.18 mol L^{-1} Na_2CO_3 should be added to the emulsion before the addition of amine monomer, to ensure dispersed microcapsule formation. This volume fits with the reported equivalent volumes delivered in small scale production methods (Lin *et al.*, 2006; Chu *et al.*, 2004).

A reduction in the amount of observed agglomeration was observed as the TDC monomer concentration was lowered. This reduction was likely due to near complete consumption of the TDC by excess amine monomer in the aqueous solution during membrane polymerisation. Little agglomeration was noted during the subsequent washing steps. The concentration of the TDC in the chloroform phase during solvent exchange was assumed to be too dilute to initiate a reaction with the residual amines. However, a limit to the reduction of the TDC concentration was discovered. Microcapsules produced with a TDC concentration of 0.1 mol L^{-1} were fragile and prone to collapse during washing operations. In future, SEM images could be used to correlate the thickness of the microcapsule membranes with varied TDC monomer concentrations and polymerisation times. Control over the membrane thickness may provide a method to control diffusion based release rates, allowing particular thicknesses to be selected for individual applications.

Rapid addition of the mixed amine monomers to the emulsion was observed to produce misshapen microcapsules. Similar mechanisms to those described for misshapen 200 ml scale microcapsules production are believed to cause this deformation (Section 6.1). The primary variable influencing deformation is thought to be the emulsion temperature, raised by exothermic polymerisation reactions. Dropwise addition of the amine monomer was most successful in reducing the rate of temperature increase. However, dropwise addition is impractical on scales larger than 2 L production. A spray operation, to mist the amine into the vessel, may be a viable alternative. Introduction of the amines to the reactor by airbrush was successfully tested on the 2 L scale, resulting in uniform, spherical microcapsules. Further scale-up of the manufacture method will require careful design of the cooling jacket to provide an adequate heat transfer rate to dissipate the exothermic release from the polymerisation reactions. The surface area-to-volume ratio of a vessel diminishes with an increasing diameter. Cooling coils inside

the reactor may help improve this ratio by providing a larger surface area for heat transfer. However, consistent flow dynamics between scales should be maintained to ensure emulsion stability and adequate mixing.

6.5. 2 L scale microcapsule production and characterisation

The performance of the scaled method may be evaluated by monitoring a few key indicators; process time, cost and product quality. During scale-up, significant savings were made in process time and energy cost. Replacement of the energy intensive freeze-drying step from small-scale production (Table 6-1) with a dialysis washing step (Table 6-2), was the primary improvement made to the 2 L scale manufacture method. The selection of an aqueous phase UV irradiation method allowed the dialysis substitution to be made, reducing the total process time from over 24 hours to 6.3 hours.

Table 6-1: Timeline of production for microcapsules produced on the 200 ml scale

Task name	Duration	Timeline																								
	hrs	1	2	3	4	5	6	7	8	9	10	11	12	13	14	15	16	17	18	19	20	21	22	23	24	25
Reactant preparation	2																									
Emulsification time	0.17																									
Reaction time	1																									
Centrifuge washing	1																									
Freeze drying	20																									

Table 6-2: Timeline for microcapsules produced on the 2 L batch scale

Task name	Duration	Timeline						
	hrs	1	2	3	4	5	6	7
Reactant preparation	2							
Emulsification time	0.33							
Reaction time	1							
Dialysis washing	3							

Evaluation of the quality of microcapsules produced on the 2 L was achieved by comparison with results from the literature, as discussed in the following paragraphs.

The scaled batch mass yield of 1.0 – 1.2 g dry microcapsules is proportional to the lower end of the mass yield range reported by Lin *et al.* (2006) on the 200 ml scale. However, particle size analysis of microcapsules produced on the 2 L scale unexpectedly revealed a multi-modal distribution with several distinctive peaks. A multi-modal distribution suggested the influence of mechanical shear forces in the

microcapsule formation (Chatzi *et al.*, 1991b), yet comparison of the microcapsule size distribution to that of the pre-reaction emulsion revealed a much higher mean microcapsule diameter. The mesh filtering operation accounts for some of this difference in the mean microcapsule size, as significant proportions of microcapsules less than 10 μm were removed during dialysis. More unexpected was an observed shift in the modal diameter. A proposed explanation of this shift is coalescence caused by addition of sodium carbonate buffer to the reaction mixture, prior to the mixed amine monomers. The concentration of SDS in the solution is reduced by the Na_2CO_3 volume, effectively lowering the stabilising effect of the surfactant. This will lead to droplet coalescence at the new conditions until a stable drop size is reached. As suggested in section 6.1, the problem will be compounded following the addition of the amine monomer and the associated temperature rise of the reactants. Further reduction of the solution viscosity will increase the rate of coalescence, raising the modal diameter. These findings suggest cooling loads need to be carefully monitored to ensure reactants can be added in reasonable time, while maintaining a stable temperature in the vessel.

The 2 L batch microcapsules produced in this project were significantly larger in diameter than those produced by both Lin *et al.* (2006) and Chu *et al.* (2001). These reported methods used centrifugation as a separation technique during washing. The filtering operation used in this work is likely to have expanded the size distribution range of the slurry, by removing a large proportion of microcapsules under 10 μm. An average microcapsule diameter of 53.5 μm is advantageous in large scale processing. Filter steps will have a low filtercake pressure drop and dialysis of the slurry can be achieved under the influence of gravity alone, without the need for vacuum pressure on the outlet. Microcapsules are less likely to be damaged or crushed by this gentle method of separation. Despite these advantages, microcapsules produced with larger diameters have limitations; the overall mechanical strength of the microcapsule may be decreased. Also, the surface-to-volume ratio is lower and may not produce as sharp a release profile as smaller diameter capsules. Both of these factors are influenced by the microcapsule shell thickness which may be adjusted, by altering the TDC monomer concentration or polymerisation time, to find an optimum between mechanical strength and the desired rate of diffusion.

Coalescence of emulsion droplets on addition of the amine reactants, as described above, provides a possible explanation for the reduction in agglomeration seen when the organic phase TDC monomer concentration is reduced. Chu *et al.* (2001) indicated the interfacial polymerisation reaction proceeds by the diffusion of amine reactants across the membrane. Presumably this diffusion rate is limited by an increasing membrane thickness. It follows that the total droplet surface area will determine the final TDC monomer concentration inside the microcapsules. Amine reactants in free solution should always be present in excess following polymerisation. The average microcapsule diameter is inversely proportional to the average microcapsule surface area. Hence, doubling the diameter of the microcapsules from the original method will halve the total surface area for reaction. A direct result of this diameter increase will be the presence of twice as much reactant inside the microcapsules as required, increasing the likelihood of an agglomeration reaction during the washing procedure. This finding has significant implications for scale-up of the method. Cost savings could potentially be made in production, as larger diameter microcapsules will require less monomer reactants than smaller diameter microcapsules for the same internal void capacity. Cost minimisation will be essential to increase the chances of commercialisation of the product. Based on these findings, a thorough study into microcapsule membrane thickness verses monomer concentration should be undertaken to better quantify this relationship.

Scaled microcapsules, viewed using scanning electron microscopy, were particularly promising. Microcapsules appeared spherical in shape with smooth external surfaces (Figure 5-11). A SEM image of a sample microcapsule population confirmed the microcapsules were predominantly unbroken after freeze-drying (Figure 5-12). It appeared microcapsule membranes produced by the scaled method were robust and able to withstand some processing operations. This observation validated the use of the pitched six-bladed impeller at 100 rpm during polymerisation. Comparison of Figure 5-11 with the SEM image captured by Lin *et al.* (2006) in Figure 2-3, revealed a less aggregated microcapsule population. This dispersion should allow for a uniform graft distribution on microcapsule surfaces during UV irradiation, important for consistent release characteristics.

The large internal microcapsule void fraction indicated a substantial volume for drug retention (Figure 5-13). This void did not appear to contain internal partitions. This

observation suggested a uniform rate of diffusion into and out of the microcapsules could be expected, limited primarily by the effective membrane pore size.

Micrographs of the external microcapsule surface revealed a sporadic distribution of unsymmetrical pores permeating the surface (Figure 5-14). However, these pores did not appear to completely transect the membrane. The microcapsule surface was otherwise smooth and consistently formed. When the internal membrane surface was viewed, a rough uneven structure was observed (Figure 5-15). Pore openings could not be detected on this internal surface. These observations agree with those made by Chu *et al.* (2001). A similar membrane structure was observed when a comparison of a scaled microcapsule cross section (Figure 5-16) was made with Figure 2-1 (Chu *et al.*, 2001). However, the microcapsules produced in this project were noted to have a thinner membrane. This is possibly due to the reduced TDC monomer concentration used in the organic phase to eliminate agglomeration during washing.

Finally, the introduction of the dialysis washing step produced an unexpected lowering in the bulk microcapsule slurry density. Chloroform solvent has a specific gravity (SG) of 1.49 and cyclohexane has a SG of 0.779 (Green *et al.*, 1998). When combined in a 3 : 1 ratio the organic phase has an average SG of 1.31, more dense than that of the aqueous solution with a SG of approximately 1. As a result, microcapsules will have a higher density than the surrounding solution immediately following production. The relative solubility of each of the solvents in the aqueous washing solution is best assessed by comparison of polarity indices for each of the components. Chloroform has a polarity index value of 4.1, closer to an aqueous phase polarity of 7.86 (30 % v/v ethanol) than to cyclohexane with a polarity index of 0.2 (Byers, 2003). Thus, chloroform will be extracted into the washing solution preferentially over cyclohexane and replaced by aqueous solution. Removal of sufficient chloroform from the organic phase will lower the average SG below that of the surrounding aqueous solution. This density change is believed to cause flotation of the microcapsules. The low density microcapsule slurry was observed to have a greater flux rate during the filtration operation, presumably through reduction of capsule contact with the mesh. In future, this phenomenon may be a useful indicator for determining adequate solvent removal from the microcapsules.

6.6. Grafting reactor flow characterisation

Reactor flow characterisation showed laminar flow within the quartz tubes with only a mild deviation from ideal plug flow. Due to the pulsatile nature of the diaphragm pump flow, the Reynolds number calculation was made using the maximum liquid velocity. This velocity was assumed to be twice that of the average calculated velocity in the quartz tubes. The Reynolds number of less than 2000 suggests a laminar flow profile. However, several other factors are believed to induce turbulence in the reactor. The diaphragm pump operation introduces a momentary flow reversal after each stroke. This reversal was not taken into account in the Reynolds number calculation and was found to cause some mixing of the slurry within the glass tubes. In addition, inertial mixing effects were experienced as a result of fluid pockets travelling in tight circular paths around the glass hoops connecting each of the quartz glass lengths. Finally, mismatched joins at the glass hoop / quartz tubing junctions introduced turbulent mixing and regions of stagnation. It is these stagnant regions that are believed to cause the mild deviation from plug flow, as indicated by a calculated vessel dispersion number of 0.014. This theory was verified by compartment modelling of the reactor. A closer fit of the axial dispersion model was achieved for the compartment modified experimental data than for unmodified experimental data (Figure 5-18). As expected, a lower dispersion number was calculated following compartment model modification of the experimental data. The vessel dispersion number of 0.08 indicates only slight deviation from ideal plug flow regime, when stagnant regions are accounted for.

6.7. Production and characterisation of UV grafted microcapsules

As expected, grafting on the 2 L scale required an UV intensity increase of 18 mW cm^{-2} to achieve detectable grafting levels. The UV grafting process was evaluated using the same performance indicators as applied to the evaluation of the microcapsule production method developed in this work. Removal of a second freeze-drying step following the grafting procedure was the primary cost saving action. Process timelines

were not readily compared, as the UV grafting method requires further optimisation to achieve a functional graft yield. This is discussed further in subsequent paragraphs.

FT/IR spectroscopy provided, in addition to the back titration method, confirmation of carboxyl groups in the grafted microcapsule slurry (Figure 5-21). A peak wave number of 1720 cm^{-1} lies within the range identified by Timus *et al.* (2000). The presence of PAA most probably accounts for the increase in peak height at this wave number for grafted samples. Interference of atmospheric water, due to the hygroscopic nature of potassium bromide, is likely to have caused an elevated response in the range below 1000 cm^{-1}.

Future scale-up of microcapsule production will require more detailed experimental data on PAA graft kinetics and variables affecting graft yield on microcapsule surfaces. By estimating the influence of each variable upon the final grafting yield, probable optimal grafting conditions can be established. This provides definitive starting settings for more quantitative experiments. The Taguchi analysis concluded that elevated temperatures contributed most significantly to a high graft yield (77.6 %). A more minor contribution of 16.6 % was calculated for longer irradiation times at 95 % confidence limits. Despite the determination of probable optimal conditions it is not certain whether an increased grafting yield is actually responsible for a more controlled drug release action as discussed further below.

The maximum calculated graft yield of 1.13 mmol g^{-1} was much higher than the yields reported by Lin *et al.* (2006) using a plasma discharge method. Homopolymersation of the AAm is a potential cause of this difference. Both the back titration and FT/IR characterisation methods provide no distinction between AAm grafted onto polyamide surfaces and homopolymerised monomer. This limitation reduces the level of certainty in the recorded graft yields. Separation of homopolymer, prior to the carboxyl group assay, would be ideal but proved challenging to implement. PAA acid homopolymer is more stable than its AAm precursor, proving insoluble in a wide range of solvents and difficult to separate on size. A potential option is to separate grafted microcapsules from homopolymer based on SG differences. In conjunction, a different method for determination of carboxyl group concentration should be explored with lower

uncertainty than the back titration method. The Cu^{2+} - EDTA complex assay developed by Timus *et al.* (2000) is a possible avenue of investigation.

Despite the uncertainty associated with the back titration method, the Taguchi analysis clearly indicated a higher temperature induces more polymerisation of AAm. Likewise, a longer irradiation period contributed positively to the observed graft yield. However, few conclusions can be drawn as to the optimum graft conditions for PAA attachment to microcapsule surfaces. A better understanding of the kinetics of the reactions, described in Equations 2-1 to 2-7, is required to determine the influence of the competing homopolymerisation reaction on the graft yield. AAm is reported to have an increased risk of homopolymerisation at temperatures exceeding 60 °C (2007, "Summary MSDS for ACRYLIC ACID"). The same source highlighted safety concerns using acrylic acid at elevated temperatures due to a flash point of 50 °C. A brief literature search revealed 4-methoxyphenol is a strong inhibitor of the AAm chain polymerisation reaction (Liu *et al.*, 2006). In addition, dissolved oxygen in the solution strengthens the 4-methoxyphenol inhibition action by inducing the formation of peroxide groups which prevent further chain propagation (Li & Schork, 2006). These polymerisation termination mechanisms may be useful for a robust kinetic study of PAA grafting to microcapsules by UV irradiation.

Interestingly, microcapsules following grafting were denser than the aqueous phase. There are two possible explanations for this observed increase in microcapsule SG; the removal of residual cyclohexane from inside the microcapsules during the graft operation and the attachment of grafted PAA chains. Despite the bulk density increase, microcapsules continued to filter at a high flux rate allowing for rapid washing.

6.8. Equipment design evaluation

Both the jacketed emulsification reactor and UV grafting reactor proved to be adequately functional and robust during all experiments. However, several aspects of both designs were identified for further improvement in functionality.

The jacket surrounding the emulsification reactor was effective for maintaining a 2 L volume of liquid at low temperature, until the addition of the amine reactants, when internal heat generated by the resulting polymerisation reaction sharply raised the liquid temperature. To maintain the polymerisation reaction at lower than ambient temperatures a larger surface area is required to facilitate a greater rate of heat dissipation to the cooling jacket. A second limitation in the jacket design was the heat loss from stainless steel flanges and fittings which prevented the reactor liquid temperature exceeding 60 ^{o}C during grafting operations. This could be improved through better insulation of the stainless steel reactor or by placing the entire system in a temperature controlled environment. Both of these improvements would reduce the effect of ambient temperature fluctuations.

The emulsification reactor proved challenging to seal from atmospheric contamination and so required a positive pressure of N_2 to prevent oxygen introduction during UV grafting. In future designs, a sealed impeller gland would allow for a reduction in the nitrogen flowrate to the reactor. A facility for the addition of chemicals under an inert atmosphere, such as a manifold system, would further reduce the chance of oxygen contamination. A direct result of this improvement would be an increased graft yield.

The stainless steel mesh filter operation saved time and was more practical to implement than centrifugation, especially as microcapsule density changes were observed during washing. Mesh fouling was occasionally encountered during washing if the initial flowrate exceeded 30 ml min^{-1}. The introduction of reactor baffles reduced this problem by increasing the turbulence intensity at the mesh surface. Sonication of the mesh immediately following filtration was found to reduce build up of dry polymer in the pores. To increase mesh life, impeller contact should be avoided during mixing.

Improvements to the jacketed reactor which could be made for future scale-up include;

- A Teflon coated hollow core silicon O ring for sealing the filter flanges rather than the current Teflon gasket tape, which requires periodic replacement.
- A thermocouple pocket for temperature measurement below the liquid surface.
- A sealed impeller gland.
- A manifold system for introduction of reagents under an inert atmosphere.

- A gate valve instead of the current ball valve to provide tighter control on the outlet flow.

The external loop grafting reactor proved to be as robust as the jacketed vessel. Teflon heat shrink tube was used to join the glass hoops to the quartz tubing. It was found an additional layer of polyolefin heat shrink tubing was required to provide an adequate seal. This sealing method was tested up to a maximum flowrate of 1000 ml min^{-1}. If scaled further, a reactor consisting of continuous quartz tubing or flanges to seal quartz glass tubes should be investigated. A flange-based design may be the most practical to implement as it would permit an easier cleaning operation and damaged tube replacement procedure.

The plug flow characteristics exhibited by the reactor, when coupled to a CSTR, combined to produce highly favourable conditions for uniform grafting. In future reactor designs, elimination of the void spaces created during connection of the glass tubing to the reactor would provide a lower vessel dispersion number. This would result in a flow regime more closely resembling ideal plug flow.

An increase in temperature of the microcapsule slurry was observed during the irradiative grafting. This was caused by radiative heat transfer from the operating UV tubes. A cooling fan was unable to provide sufficient convective cooling and compressed air was used to supplement the air flow. Ambient temperature fluctuations were noted to have a significant effect on the required cooling load in the reactor. This variation could be negated if the system was housed in a temperature-controlled environment.

Improvements to the irradiative reactor design for future scale-up include;

- Use of a flange-based system for sealing straight lengths of quartz glass tubing to improve reactor robustness and ease of cleaning.
- Temperature control in the irradiative graft reactor housing to maintain isothermal conditions during grafting, without the need for manual adjustment of the airflow.

- A viewing port for observation of the quartz tubes to ensure no air bubbles are contaminating the graft slurry during irradiation.

6.9. Microcapsule release profiles

Release profile testing was performed to determine the effectiveness of the grafted microcapsule PAA functional gates in retaining compounds at pH 7, prior to release at pH 3. A slow rate of diffusion is required at pH 7 to retain drugs or formulations for the 24-hour particle residence period in the rumen. The release at pH 3 should be comparatively swift to ensure delivery of the contents before the microcapsules are passed from the digestive tract.

6.9.1. Batch scale release profile testing

Initial release profiles, using cytochrome C as a model protein, were distinguished by a sharp solution concentration increase as the pH was lowered from 7 to 3 (Figure 5-22). cytochrome C was recommended for use as a model compound in the literature (Lin *et al.*, 2006). The rate at which the mass of protein in free solution increased, suggested the release mechanism was not solely due to diffusion across the microcapsule membrane. Cytochrome C protein has an isoelectric point (pI) in the range of 10 – 10.5 (Van Gelder & Slater, 1962). This indicates cytochrome C carries a net positive charge in the pH range used for microcapsule release testing. PAA chains on microcapsules loaded at pH 3 have a neutral charge and so little interaction with the positively charged cytochrome C was observed at these conditions. However, isolation of the microcapsule contents by pH adjustment to 7 caused the PAA chains to gain strong negative charges. At these altered conditions, an electrostatic interaction is likely between the negatively charged PAA chains and the positively charged cytochrome C. A reversal in this affinity was subsequently seen when the pH was returned to 3 to enable release of the microcapsule contents. This ion exchange type interaction explains the sharp change in cytochrome C concentration detected in the slurry solution. Future protein selection is critical to preventing ion exchange interaction, invalidating diffusion-based microcapsule release profile results. Ideally, a protein pI of 7 or less is required to

prevent binding to the PAA functional gates. Alternatively, a neutral molecule such as mPEG 5000 may be selected for release profile testing.

Experiments using methylene blue, alpha lactalbumin and methylene blue labelled dextran model compounds did not provide detectable release profiles. Alpha lactalbumin was selected as a model protein due to an isoelectric point in the range 4.2 – 4.5 (Jeng *et al.*, 1997). Methylene blue and dextran derivatives were selected due to low biotoxicity and ranged molecular weights. However, it was found that microcapsule samples taken for solution absorbance measurement had poor repeatability. Microcapsule separation by the in-line filter method introduced variability to the results, possibly as a result of crushed microcapsules releasing prematurely their contents. Other complications arose during testing, including; a strong microcapsule membrane affinity for both dextran coupled as well as native methylene blue dye and an observed aggregation of α-lactalbumin at pH 3, thereby lowering the detected concentration in solution over time.

Testing of NaCl release by conductivity measurement did not yield a detectable release. It was noted that small temperature changes and solution evaporation influenced the conductivity readings, despite being sealed while housed in a temperature-controlled environment. The small molecular size of NaCl may have led to a very rapid release through the microcapsule pores, before stable conductivity readings could be taken. Despite this, the lack of interference of this testing method is considered a significant advantage and the release profile of a higher molecular weight salt should be explored in future.

6.9.2. Diffusion experiments using confocal microscopy

Fluorescence recovery of fluorescein dye into ungrafted polyamide microcapsules was recorded to establish functionality of the membrane pores for drug diffusion. Figure 5-23 showed a rapid recovery of the fluorescence within the microcapsule, after photobleaching suggesting diffusion was not hindered significantly by the membrane. However, fluorescein dye was observed to have a strong affinity for the membrane surfaces.

As fluorescein is not fluorescent at pH 3, another dye was required for testing with fluorescence at both acidic and neutral pH. PEGylated rhodamine dye fit this criteria and was used for further studies investigating the effect of solution pH on FRAP (Figure 5-23). The presence of aromatic rings of TAMRA dye was confirmed by NMR spectroscopy after mPEG coupling (Figure 5-24). A calculation, based on the purity of amine modified mPEG and the assumption the coupling achieved 100 % conversion, determined a dye purity of 57 %. This calculation allowed for the matching of PEGylated and native dye concentrations to ensure a concentration independent dye diffusion rate.

High photostability of mPEG TAMRA dye led to the use of a longer bleach time to ensure a sufficient reduction in fluorescence within the loaded microcapsules. Greater photostability was observed during photobleaching of mPEG TAMRA than for the fluorescein fluorophore. Results were scaled to a percentage of the maximum observed intensity for direct comparison (Figure 5-26). The shape of the resulting recovery curves was very similar at pH 3 and 7. The timeframe of recovery indicates grafted microcapsules from Taguchi experiment 9 did not retain 5000 molecular weight contents for a sufficient length of time to allow for release at a later stage. Dye recovery was observed to a maximum of 90 % of the original intensity. The lower level of recovery suggests that dye binding to the membrane surfaces is influencing the observed fluorescence inside the microcapsules. Incubation of the dye with the microcapsules prior to confocal experiments allows a saturation of the binding sites on the membrane. Some of these bound dye molecules will be inactivated during photobleaching, yet they continue to occupy binding sites. It follows that not all of these sites will be available for binding of actively fluorescent molecules during the recovery phase and so a lower intensity will be observed. The difference in photostability of the dye at varied pH may account for the differences in maximum recovery at pH 3 and 7.

Experiments using confocal microscopy provided visual quantification of microcapsule diffusion characteristics. These experiments highlighted the importance of dye selection for release studies. Ideally, a dye should be selected that shows little affinity for microcapsule membranes, low pH sensitivity and medium photo-stability for simple photobleaching.

The findings from this study highlight interesting challenges for drug delivery using polyamide microcapsules as vectors. Membrane affinity interactions may reduce the range of compounds suitable for delivery, dependant on electrostatic charge, hydrophobicity and molecular weight. Further characterisation of the polyamide membrane is required to determine the likely relative influences of each of these physical properties on bulk release profiles.

6.9.3. Pulse response of a packed column

A packed column was used to determine bulk microcapsule drug retention characteristics. The use of a closed system avoided the influence of sample removal on the results. The microcapsules were expected to act in a similar manner to size exclusion media. Molecules, excluded from constricted microcapsule pores at pH 7, were expected to elute sooner than at a pH of 3, where diffusion into the pores would likely impede progress. However, comparison of the elution response to pulses of mPEG 5000 buffered at pH 3 and 7, showed similar outlet refractive index profiles. The response at pH 3 showed a 2.9 % broadening of the elution peak, possibly indicative of hindrance caused by an enlarged pore size.

Bed volume changes provide a second tentative explanation for the slight difference in release profiles at pH 3 and 7. Phosphate buffer was observed to have a higher conductivity than citric acid buffer at a 0.1 mol L^{-1} concentration. High salt concentrations are likely to cause shrinking of the microcapsules at pH 7. This may be offset to some degree by the swelling of the PAA chains. An overall reduction in the bed volume could account for the delayed response at pH 7.

The packed column elution response had an excellent repeatability at both pH 3 and 7, allowing for these tentative conclusions to be drawn from the data. The mPEG 5000 was an ideal choice of tracer being inert, stable across a pH range of 3 – 7, readily detected by RI and available in a variety of molecular weights. Despite the uncertainty concerning the pH responsive action of the particular sample tested, the packed column analysis method has merit for future study.

There was no decisive result that demonstrated a pH dependant release of model compounds from microcapsules grafted in batch 9 of the Taguchi analysis. There are several suggested reasons for this failure (Table 6-3). Release profile testing of each Taguchi experiment slurry would allow the 'more grafting is good' hypothesis to be evaluated.

Table 6-3: Suggested reasons for poor retention of trial compounds at pH 7 within grafted microcapsules from Taguchi experiment 9

Reasons for poor retention at pH 7	Recommended action
Homopolymer contamination inflating the graft yields at elevated graft temperatures	- Determine graft kinetics to evaluate ideal conditions for prevention of homopolymer formation - Develop a separation method for removal of homopolymer from grafted microcapsule slurries
Non-uniform grafting on microcapsule surfaces	- Increase turbulence intensity in quartz glass tubes by increasing the flowrate - Increase length of irradiation time
Pore size is too large to constrict effectively with PAA gates	- Lower the chloroform ratio in the organic solvent to reduce the membrane permeability
Insufficient graft density on microcapsule surfaces	- Increase length of irradiation time - Increase length of post irradiation polymerisation time

Chapter 7 Conclusions

Several key conclusions can be drawn from this study on both microcapsule production scale-up and the subsequent UV irradiative grafting method of PAA. In addition, an evaluation has been made of the success in meeting the central project objectives (Section 1.5).

Polyamide microcapsule production was successfully scaled from a 200 ml batch size to a 2 L batch size. In conjunction, the batch processing time was reduced from 24.2 to 6.3 hours by removal of the freeze-drying step present in the 200 ml production method. The increase of the average microcapsule diameter during scale-up appears to be caused by an insufficient cooling capacity of the emulsification reactor jacket. The resulting temperature increase reduced the surfactant viscosity during the exothermic membrane polymerisation reaction, increasing the rate of coalescence of the emulsion droplets. The subsequent reduction in total surface area available for polymerisation is believed to lead to residual TDC monomer within the organic emulsion phase. This excess monomer is likely to cause agglomeration by reacting with amine monomers in free solution during microcapsule washing by dialysis. It was found a reduction in the TDC organic phase concentration reduced instances of observed agglomeration, conducive to ensuring a consistent drug release profile. A dry basis mass yield of between 1.0 and 1.2 g per batch provided a sufficient quantity of microcapsules for scaled UV grafting trials.

The UV irradiative graft reactor revealed a flow regime with only mild deviation from ideal plug flow, characterised by a vessel dispersion number of 0.014. Compartment model modification of the experimental data showed the deviation from ideal plug flow was induced by stagnant regions in the reactor tubes. A positive PAA grafting yield was observed in microcapsule slurries irradiated with UV light at a calculated intensity of 19 mW cm^{-2}. Elevated temperature was found to be the most influential variable on the graft yield, followed by a longer irradiation period. However, the back titration and FT/IR characterisation methods failed to provide distinction between homopolymerised AAm and PAA attached to the microcapsule surfaces. Release profile characterisation

by batch release, confocal microscope FRAP and packed column retention did not detect any definitive action of the PAA functional gates between pH 3 and 7 for microcapsules produced in Taguchi experiment number nine. Sampling was found to influence the results of the batch release test. Dye selection for confocal microscope diffusion experiments proved critical. Both fluorescein and PEGylated TAMRA showed a strong affinity for microcapsule membranes. The packed column test method showed the most promising, repeatable results and should be considered for future release studies. The limitations discovered in microcapsule release profile testing highlighted possible implications for the delivery of bioactives. Affinity interactions between the PAA grafted chains or the microcapsule membranes and the bioactive compound may limit the efficiency of delivery based on charge, hydrophobicity or molecule size.

The primary project objective to develop a scaled method for production of PAA grafted microcapsules has been achieved in part. While a viable UV irradiation method for PAA polymerisation has been developed, a pH based release was unable to be determined at an observed graft yield of 1.13 mmol g^{-1}. The 2 L scale production method should enable rapid production of samples for *in-vivo* release testing once the PAA grafting mechanisms are better understood and have been optimised. A series of recommendations to aid in future development of the 2 L scale microcapsule production method are presented in Chapter 8.

Chapter 8 Recommendations

A number of recommendations for further study on the microcapsule production methods and equipment developed in this project have been identified:

- A study of PAA polymerisation reaction kinetics following UV irradiation of microcapsules, to determine favourable conditions for attachment of PAA chains to microcapsule surfaces.
- Development of an assay for the TDC monomer concentration in the organic solution.
- The use of cooling coils to increase the surface area for heat dissipation during emulsion polymerisation to prevent droplet coalescence.
- Exploration of a carboxyl group assay with a lower associated experimental error.
- Development of a method to separate homopolymerised monomer from the microcapsule slurry prior to carboxyl group concentration determination.
- A reduction in the irradiation reactor stagnant volume by elimination of irregular joins between the glass hoops and quartz glass tubes.
- The selection of a pH insensitive fluorescent dye, with little affinity for the microcapsule membrane, for use in confocal microscope FRAP diffusion studies.
- Individually test each grafted Taguchi experiment slurry, using the packed column method, to ascertain whether higher observed grafting provides desirable release characteristics than lower grafting levels.

The results obtained from experiments suggest some grafting has been achieved by UV irradiation. While this grafting was insufficient to provide the desired pH responsive release characteristics, the merits of using an aqueous irradiation approach have been clearly demonstrated. These results are encouraging for future development of UV grafting of PAA to polyamide microcapsules.

Chapter 9 References

Agustina, T. E., Ang, H. M., & Pareek, V. K. (2008). Treatment of winery wastewater using a photocatalytic/photolytic reactor. *Chemical Engineering Journal, 135*(1-2), 151-156.

Berkland, C., Kipper, M. J., Narasimhan, B., Kim, K., & Pack, D. W. (2004). Microsphere size, precipitation kinetics and drug distribution control drug release from biodegradable polyanhydride microspheres. *Journal of Controlled Release, 94*(1), 129-141.

Brunner, A., Minamitake, Y., & Göpferich, A. (1998). Labelling peptides with fluorescent probes for incorporation into degradable polymers. *European Journal of Pharmaceutics and Biopharmaceutics, 45*(3), 265-273.

Burrows, G. E. (1984). Methylene blue: effects and disposition in sheep. *Journal of Veterinary Pharmacology and Therapeutics, 7*(3), 225-231.

Byers, J. A. (2003). Solvent miscibility table. Retrieved 1/07/08, 2008, from http://www.chemical-ecology.net/java/solvents.htm

Cardinal, J. R. (1997). Intraruminal devices. *Advanced Drug Delivery Reviews, 28*(3), 303-322.

Chatzi, E. G., Boutris, C. J., & Kiparissides, C. (1991a). On-line monitoring of drop size distributions in agitated vessels. 1. Effects of temperature and impeller speed. *Ind. Eng. Chem. Res., 30*(3), 536-543.

Chatzi, E. G., Boutris, C. J., & Kiparissides, C. (1991b). On-line monitoring of drop size distributions in agitated vessels: 2. Effect of stabilizer concentration. *Ind. Eng. Chem. Res., 30*(6), 1307-1313.

Choi, H.-S., Kim, Y.-S., Zhang, Y., Tang, S., Myung, S.-W., & Shin, B.-C. (2004). Plasma-induced graft co-polymerization of acrylic acid onto the polyurethane surface. *Surface and Coatings Technology, 182*(1), 55-64.

Chu, L.-Y., Liang, Y.-J., Chen, W.-M., Ju, X.-J., & Wang, H.-D. (2004). Preparation of glucose-sensitive microcapsules with a porous membrane and functional gates. *Colloids and Surfaces B: Biointerfaces, 37*(1-2), 9-14.

Chu, L.-Y., Niitsuma, T., Yamaguchi, T., & Nakao, S.-i. (2003). Thermoresponsive transport through porous membranes with grafted PNIPAM gates. *AIChE Journal, 49*(4), 896-909.

Chu, L.-Y., Park, S.-H., Yamaguchi, T., & Nakao, S.-i. (2001). Preparation of thermo-responsive core-shell microcapsules with a porous membrane and poly(N-isopropylacrylamide) gates. *Journal of Membrane Science, 192*(1-2), 27-39.

Chu, L.-Y., Yamaguchi, T., & Nakao, S. (2002a). A Molecular-Recognition Microcapsule for Environmental Stimuli-Responsive Controlled Release. *Advanced Materials, 14*(5), 386-389.

Chu, L. Y., Park, S. H., Yamaguchi, T., & Nakao, S. i. (2002b). Preparation of Micron-Sized Monodispersed Thermoresponsive Core-Shell Microcapsules. *Langmuir, 18*(5), 1856-1864.

Clochard, M. C., *et al.* (2004). Tailoring bulk and surface grafting of poly(acrylic acid) in electron-irradiated PVDF. *Polymer, 45*(26), 8683-8694.

Cone, J. W., & van Gelder, A. H. (2006). Adaptation of the rumen microbial population to native potato starch degradation determined with the gas production technique and the nylon bag technique. *Journal of Animal Physiology & Animal Nutrition, 90*(11/12), p511-518.

Determan, A. S., Trewyn, B. G., Lin, V. S. Y., Nilsen-Hamilton, M., & Narasimhan, B. (2004). Encapsulation, stabilization, and release of BSA-FITC from polyanhydride microspheres. *Journal of Controlled Release, 100*(1), 97-109.

Dotson, N. A., Galvan, R., Laurence, R. L., & Tirrell, M. (1996). *Polymerization process modelling*: VCH Publishers Inc.

Fogler, H. S. (1999). *Elements of Chemical Reaction Engineering* (3rd ed.): Prentice Hall PTR.

Forney, L., & Pierson, J. (2004). Ultraviolet Disinfection: Academic Research Library database.

Forney, L. J., Goodridge, C. F., & Pierson, J. A. (2003). Ultraviolet Disinfection: Similitude in Taylor-Couette and Channel Flow. *Environmental Science and Technology, 37*(21), 5015-5020.

Forney, L. J., & Pierson, J. A. (2003). Photolytic reactors: Similitude in Taylor-Couette and channel flows. *AIChE Journal, 49*(5), 1285-1292.

Green, D. W., Perry, R. H., & Green, D. W. (1998). *Perry's Chemical Engineers' Handbook* (7th ed.): McGraw-Hill Professional Publishing.

Gupta, P., Vermani, K., & Garg, S. (2002). Hydrogels: from controlled release to pH-responsive drug delivery. *Drug Discovery Today, 7*(10), 569-579.

Harris, M. J., & Kozlowski, A. (1997). United States Patent No.

Hobson, P. N., & Stewart, C. S. (Eds.). (1997). *The rumen microbial system* (2nd ed.): Blackie Academic & Professional.

Hu, K., & Dickson, J. M. (2005). Development of pH-sensitive Pore-filled membranes for controlled release drug delivery: McMaster University.

Jabbari, E., & Nozari, S. (2000). Swelling behavior of acrylic acid hydrogels prepared by [gamma]-radiation crosslinking of polyacrylic acid in aqueous solution. *European Polymer Journal, 36*(12), 2685-2692.

Jeng, S.-Y., Bleck, G. T., Wheeler, M. B., & Jimenez-Flores, R. (1997). Characterization and Partial Purification of Bovine alpha-Lactalbumin and {beta}-Casein Produced in Milk of Transgenic Mice. *J. Dairy Sci., 80*(12), 3167-3175.

Jin, S., Liu, M., Zhang, F., Chen, S., & Niu, A. (2006). Synthesis and characterization of pH-sensitivity semi-IPN hydrogel based on hydrogen bond between poly(N-vinylpyrrolidone) and poly(acrylic acid). *Polymer, 47*(5), 1526-1532.

Koishi, M., Fukuhara, N., & Kondo, T. (1969). Studies on Microcapsules. II. Preparation of Polyphthalamide Microcapsules. *Chemical & pharmaceutical bulletin, 17*(4), 804-809.

Lacasse, F. X., Filion, M. C., Phillips, N. C., Escher, E., McMullen, J. N., & Hildgen, P. (1998). Influence of surface properties at biodegradable microsphere surfaces: Effects on plasma protein adsorption and phagocytosis. *Pharmaceutical Research, 15*(2), 312-317.

Lamprecht, A., Schäfer, U. F., & Lehr, C. M. (2000). Visualization and quantification of polymer distribution in microcapsules by confocal laser scanning microscopy (CLSM). *International Journal of Pharmaceutics, 196*(2), 223-226.

Lee, J. H.*, et al.* (2003). Design of two types of fluidized photo reactors and their photo-catalytic performances for degradation of methyl orange. *Applied Catalysis A: General, 244*(1), 49-57.

Lee, Y. M., Ihm, S. Y., Shim, J. K., Kim, J. H., Cho, C. S., & Sung, Y. K. (1995). Preparation of surface-modified stimuli-responsive polymeric membranes by plasma and ultraviolet grafting methods and their riboflavin permeation. *Polymer, 36*(1), 81-85.

Lee, Y. M., & Shim, J. K. (1997). Preparation of pH/temperature responsive polymer membrane by plasma polymerization and its riboflavin permeation. *Polymer, 38*(5), 1227-1232.
Lei, J., & Liao, X. (2001). Surface graft copolymerization of acrylic acid onto LDPE film through corona discharge. *European Polymer Journal, 37*(4), 771-779.
Levenspiel, O. (1999). *Chemical reaction engineering* (3rd ed.): John Wiley and Sons, Inc.
Li, R., & Schork, F. J. (2006). Modeling of the Inhibition Mechanism of Acrylic Acid Polymerization. *Ind. Eng. Chem. Res., 45*(9), 3001-3008.
Lin, Y., Fee, C. J., & Swan, J. E. (2006). Preparing Porous Polyamide Microcapsules with a pH-sensitive Chemical Valve.
Liu, T., DeSimone, J. M., & Roberts, G. W. (2006). Kinetics of the precipitation polymerization of acrylic acid in supercritical carbon dioxide: The locus of polymerization. *Chemical Engineering Science, 61*(10), 3129-3139.
Lynn, D. M., Amiji, M. M., & Langer, R. (2001). pH-Responsive Polymer Microspheres: Rapid Release of Encapsulated Material within the Range of Intracellular pH. *Angewandte Chemie International Edition, 40*(9), 1707-1710.
Manfred, K. (1959). Interfacial polycondensation. IV. Polyphthalamides. *Journal of Polymer Science, 40*(137), 337-342.
Massa, G., Mazzei, R., Garcia Bermudez, G., Filevich, A., & Smolko, E. (2005). Grafting of acrylic acid onto polypropylene films irradiated with argon ions. *Nuclear Instruments and Methods in Physics Research Section B: Beam Interactions with Materials and Atoms, 236*(1-4), 272-276.
Mathiowitz, E., & Cohen, M. D. (1989). Polyamide microcapsules for controlled release. I. Characterization of the membranes. *Journal of Membrane Science, 40*(1), 1-26.
Mazzei, R., Tadey, D., Smolko, E., & Rocco, C. (2003). Radiation grafting of different monomers onto PP foils irradiated with a 25 MeV proton beam. *Nuclear Instruments and Methods in Physics Research Section B: Beam Interactions with Materials and Atoms, 208*, 411-415.
McLellan, B. J. (2007). *Development of an Intraruminal Controlled-Release Device.* The University of Waikato, Hamilton.
Nho, K. O., KR), Hyun, Changmin (Seoul, KR), Lee, Junghun (Kyonggi-do, KR), Pak, Youngkyoung (Seoul, KR). (2004). United States Patent No.
O'Donnell, P. B., & McGinity, J. W. (1997). Preparation of microspheres by the solvent evaporation technique. *Advanced Drug Delivery Reviews, 28*(1), 25-42.
Pieracci, J., Crivello, J. V., & Belfort, G. (1999). Photochemical modification of 10 kDa polyethersulfone ultrafiltration membranes for reduction of biofouling. *Journal of Membrane Science, 156*(2), 223-240.
Pygall, S. R., Whetstone, J., Timmins, P., & Melia, C. D. (2007). Pharmaceutical applications of confocal laser scanning microscopy: The physical characterisation of pharmaceutical systems. *Advanced Drug Delivery Reviews, 59*(14), 1434-1452.
Ray, A. K., & Beenackers, A. A. C. M. (1998). Development of a new photocatalytic reactor for water purification. *Catalysis Today, 40*(1), 73-83.
Reeves, J. B., III, Blosser, T. H., Balde, A. T., Glenn, B. P., & Vandersall, J. (1991). Near Infrared Spectroscopic Analysis of Forage Samples Digested In Situ (Nylon Bag). *J. Dairy Sci., 74*(8), 2664-2673.

Richey, T., Iwata, H., Oowaki, H., Uchida, E., Matsuda, S., & Ikada, Y. (2000). Surface modification of polyethylene balloon catheters for local drug delivery. *Biomaterials, 21*(10), 1057-1065.

Rosa, G., Vahid, H.-A., & Hamid, M. (2004). Bioadhesion and biocompatibility evaluations of gelatin and polyacrylic acid as a crosslinked hydrogel in vitro. *Journal of Biomaterials Science, Polymer Edition, 15*, 1019-1031.

Rosiak, J. M., & Ulanski, P. (1999). Synthesis of hydrogels by irradiation of polymers in aqueous solution. *Radiation Physics and Chemistry, 55*(2), 139-151.

Roy, R. (1990). *A primer on the Taguchi method*: Van Nostrand Reinhold.

Schmaljohann, D. (2006). Thermo- and pH-responsive polymers in drug delivery. *Advanced Drug Delivery Reviews, 58*(15), 1655-1670.

Singer, V. L., & Johnson, I. D. (1997). *Fluorophore Characteristics: Making Intelligent Choices in Application-Specific Dye Selection.* Paper presented at the International Symposium on Human Identification

Summary MSDS for ACRYLIC ACID. (2007). *Chemwatch II Chemgold* Retrieved 1/07/08, from http://chemwatch.canterbury.ac.nz/

Taghizadeh, A., Danesh Mesgaran, M., Valizadeh, R., Shahroodi, F. E., & Stanford, K. (2005). Digestion of Feed Amino Acids in the Rumen and Intestine of Steers Measured Using a Mobile Nylon Bag Technique. *J. Dairy Sci., 88*(5), 1807-1814.

Timus, D. M., Cincu, C., Bradley, D. A., Craciun, G., & Mateescu, E. (2000). Modification of some properties of polyamide-6 by electron beam induced grafting. *Applied Radiation and Isotopes, 53*(4-5), 937-944.

Tokumura, M., Tawfeek Znad, H., & Kawase, Y. (2006). Modeling of an external light irradiation slurry photoreactor: UV light or sunlight-photoassisted Fenton discoloration of azo-dye Orange II with natural mineral tourmaline powder. *Chemical Engineering Science, 61*(19), 6361-6371.

Turmanova, S., Trifonov, A., Kalaijiev, O., & Kostov, G. (1997). Radiation grafting of acrylic acid onto polytetrafluoroethylene films for glucose oxidase immobilization and its application in membrane biosensor. *Journal of Membrane Science, 127*(1), 1-7.

Uchida, E., Uyama, Y., & Ikada, Y. (1990). A novel method for graft polymerization onto poly(ethylene terephthalate) film surface by UV irradiation without degassing. *Journal of Applied Polymer Science, 41*(3-4), 677-687.

Uchida, E., Uyama, Y., & Ikada, Y. (1993). Surface graft polymerization of ionic monomers onto poly(ethylene terephthalate) by UV-irradiation without degassing. *Journal of Applied Polymer Science, 47*(3), 417-424.

Van Gelder, B. F., & Slater, E. C. (1962). The extinction coefficient of cytochrome c. *Biochimica et Biophysica Acta, 58*(3), 593-595.

Vandamme, T. F., & Ellis, K. J. (2004). Issues and challenges in developing ruminal drug delivery systems. *Advanced Drug Delivery Reviews, 56*(10), 1415-1436.

Wei, X., Wang, R., Li, Z., & Fane, A. G. (2006). Development of a novel electrophoresis-UV grafting technique to modify PES UF membranes used for NOM removal. *Journal of Membrane Science, 273*(1-2), 47-57.

Wu, S. H. W., & Papas, A. (1997). Rumen-stable delivery systems. *Advanced Drug Delivery Reviews, 28*(3), 323-334.

Yan, N., Zhang, M., & Ni, P. (1992). Size distribution and zeta-potential of polyamide microcapsules. *Journal of Membrane Science, 72*(2), 163-169.

Yang, J.-M., & Yeh, M. J. H. T.-S. (1999). Preparation of poly(acrylic acid) modified polyurethane membrane for biomaterial by UV radiation without degassing. *Journal of Biomedical Materials Research, 45*(2), 133-139.
Yang, W. T., & Rånby, B. (1996). The role of far UV radiation in the photografting process. *Polymer Bulletin, 37*(1), 89-96.

Appendix A. Equipment design specifications

A.1 Derivation of Equation 3-3 for distance between UV tubes and quartz glass tubes

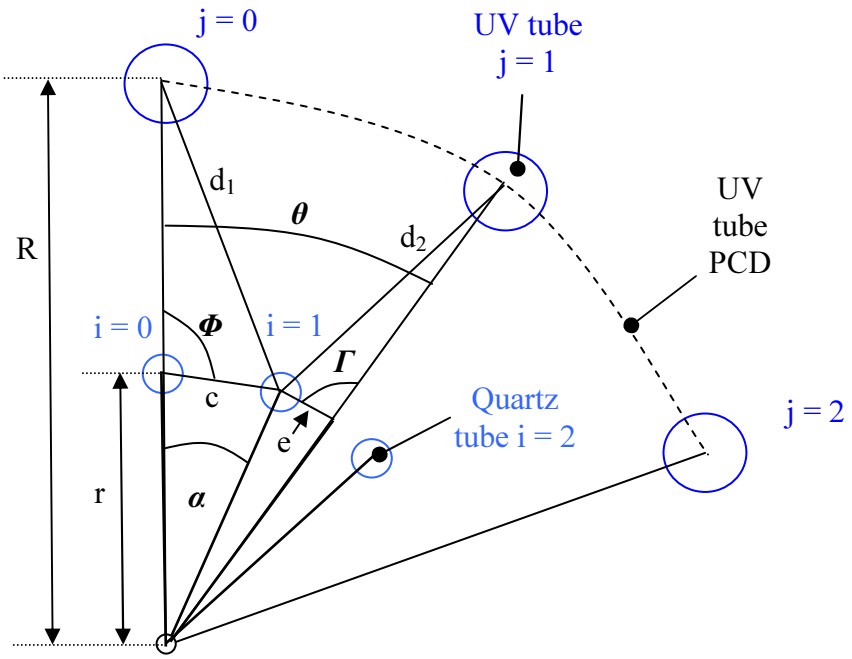

Figure A-1: Schematic representation of UV and quartz tube patterning for the derivation of the distance d_{ij}

For $d_{1,1}$

$$e = 2r\sin\frac{|\theta-\alpha|}{2} \qquad (1)$$

$$let\ \omega = |\theta-\alpha| \qquad (2)$$

$$\Gamma = \pi - \frac{\pi-\omega}{2}$$

$$\Gamma = \frac{\pi+\omega}{2} \qquad (3)$$

Substitute (2) into (1)

$$e = 2r\sin\frac{\omega}{2} \qquad (4)$$

Applying cos rule to solve for $d_{1,1}$

$$d_{1,1}{}^2 = e^2 + (R-r)^2 - 2e(R-r)\cos(\Gamma) \qquad (5)$$

Substitute (4) into (5)

$$d_{1,1} = \sqrt{e^2 + (R-r)^2 - 2e(R-r)\cos\left(\frac{\pi+\omega}{2}\right)} \qquad (6)$$

Substitute (4) into (6)

$$d_{1,1} = \sqrt{\left(2r\sin\frac{\omega}{2}\right)^2 + (R-r)^2 - 2\left(2r\sin\frac{\omega}{2}\right)(R-r)\cos\left(\frac{\pi+\omega}{2}\right)} \qquad (7)$$

Rearrangement yields equation (8) from (7)

$$d_{1,1} = \sqrt{\left(2r\sin\frac{\omega}{2}\right)^2 + (R-r)^2 - 4r(R-r)\left(\sin\frac{\omega}{2}\right)\cos\left(\frac{\pi+\omega}{2}\right)} \qquad (8)$$

The final form of the equation can be applied to any UV tube *j* and any quartz tube *i* as follows

$$\omega_{ij} = \left|\theta_j - \alpha_i\right| \qquad (9)$$

Equation (9) may be substituted in place of ω yielding Equation 3-3 from section 3.5.

$$d_{i,j} = \sqrt{\left(2r\sin\frac{\omega_{ij}}{2}\right)^2 + (R-r)^2 - 4r(R-r)\left(\sin\frac{\omega_{ij}}{2}\right)\cos\left(\frac{\pi+\omega_{ij}}{2}\right)}$$

A.2 Derivation of Equation 3-5 for the limits of angle ω

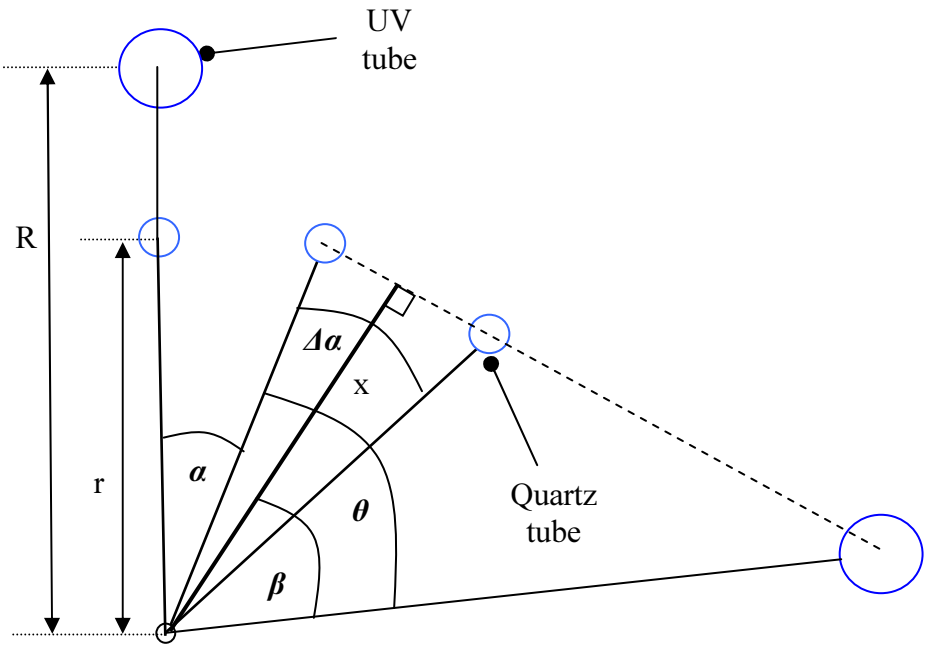

Figure A-2: Diagrammatic representation of quartz tube layout for detection of interference of UV light from UV tubes in close proximity

Defining variables:

$$\omega_{ij} = \left|\theta_j - \alpha_i\right| \qquad (1)$$

$$\theta_j = \alpha_i + 1/2\Delta\alpha + \beta \qquad (2)$$

$$\frac{x}{r} = \cos\frac{\alpha_i}{2}$$

$$x = r\cos\frac{\alpha_i}{2} \qquad (3)$$

$$\frac{x}{R} = \cos\beta \qquad (4)$$

Substitute (2) into (1) giving;

$$\omega_{ij} = \left|1/2\,\Delta\alpha_i + \beta\right| \qquad (5)$$

Substitute (3) into (4)

$$\frac{r\cos\frac{\alpha_i}{2}}{R} = \cos\beta$$

$$\beta = \cos^{-1}\left(\frac{r\cos\frac{\alpha_i}{2}}{R}\right) \tag{6}$$

Followed by substitution of (6) into (5)

$$\omega_{ij} = \left|\frac{\alpha_i}{2} + \cos^{-1}\left(\frac{r\cos\frac{\alpha_i}{2}}{R}\right)\right| \tag{7}$$

The value of ω must not exceed the value of equation (7) leading to the inequality;

$$\omega_{ij} < \left|\frac{\alpha_i}{2} + \cos^{-1}\left(\frac{r\cos\frac{\alpha_i}{2}}{R}\right)\right| \tag{8}$$

A second criteria also exists due to symmetry of the tube arrangement,

$$\omega_{ij} > 2\pi - \left(\left|\frac{\alpha_i}{2} + \cos^{-1}\left(\frac{r\cos\frac{\alpha_i}{2}}{R}\right)\right|\right) \tag{9}$$

Valid ω values must satisfy either of these criteria expressed in Section 3.5 by Equation 3-5.

A.3 Detailed emulsification reactor dimensions

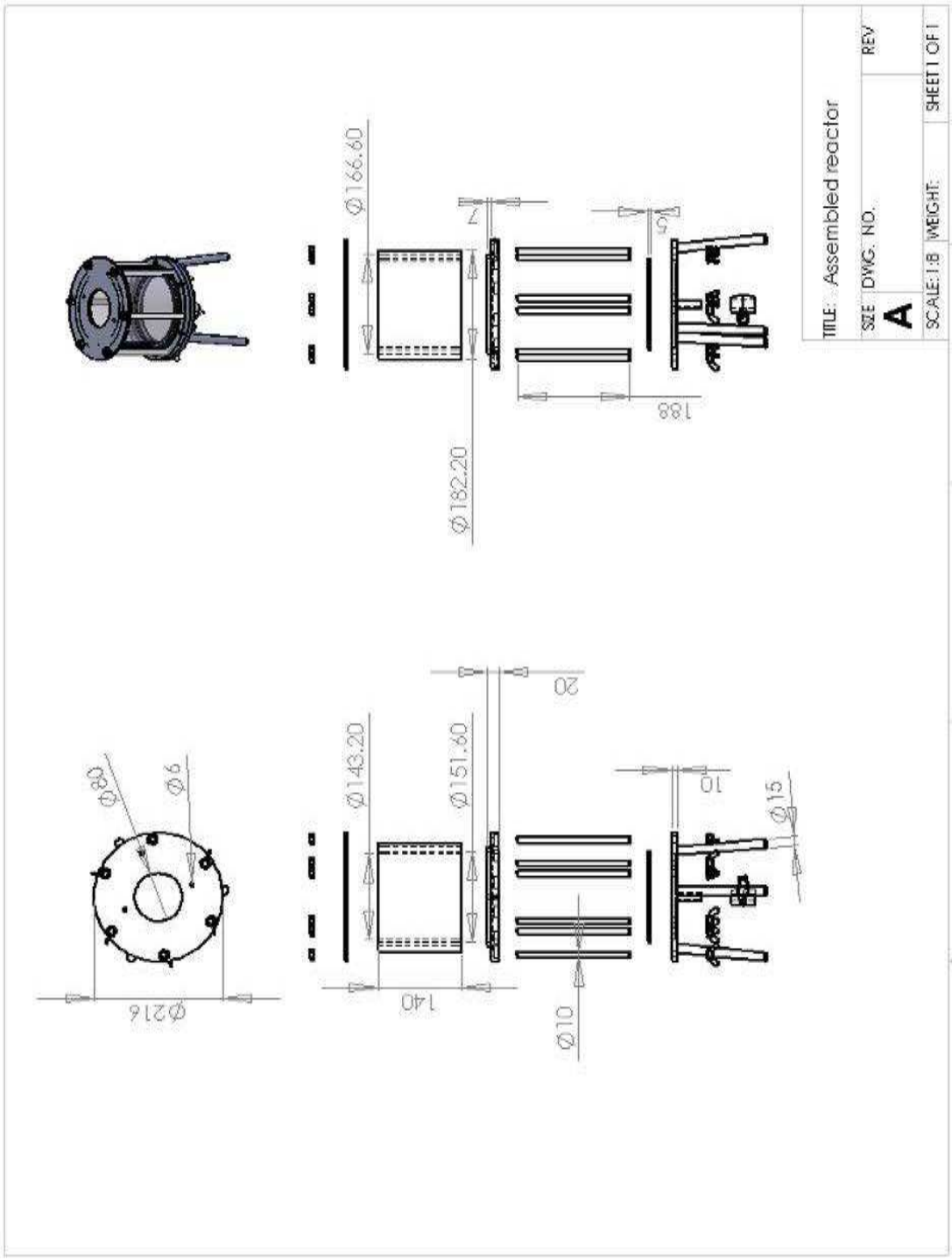

Figure A-3: Engineering drawing of emulsification reactor showing critical dimensions

A.4 Detailed UV grafting reactor dimensions

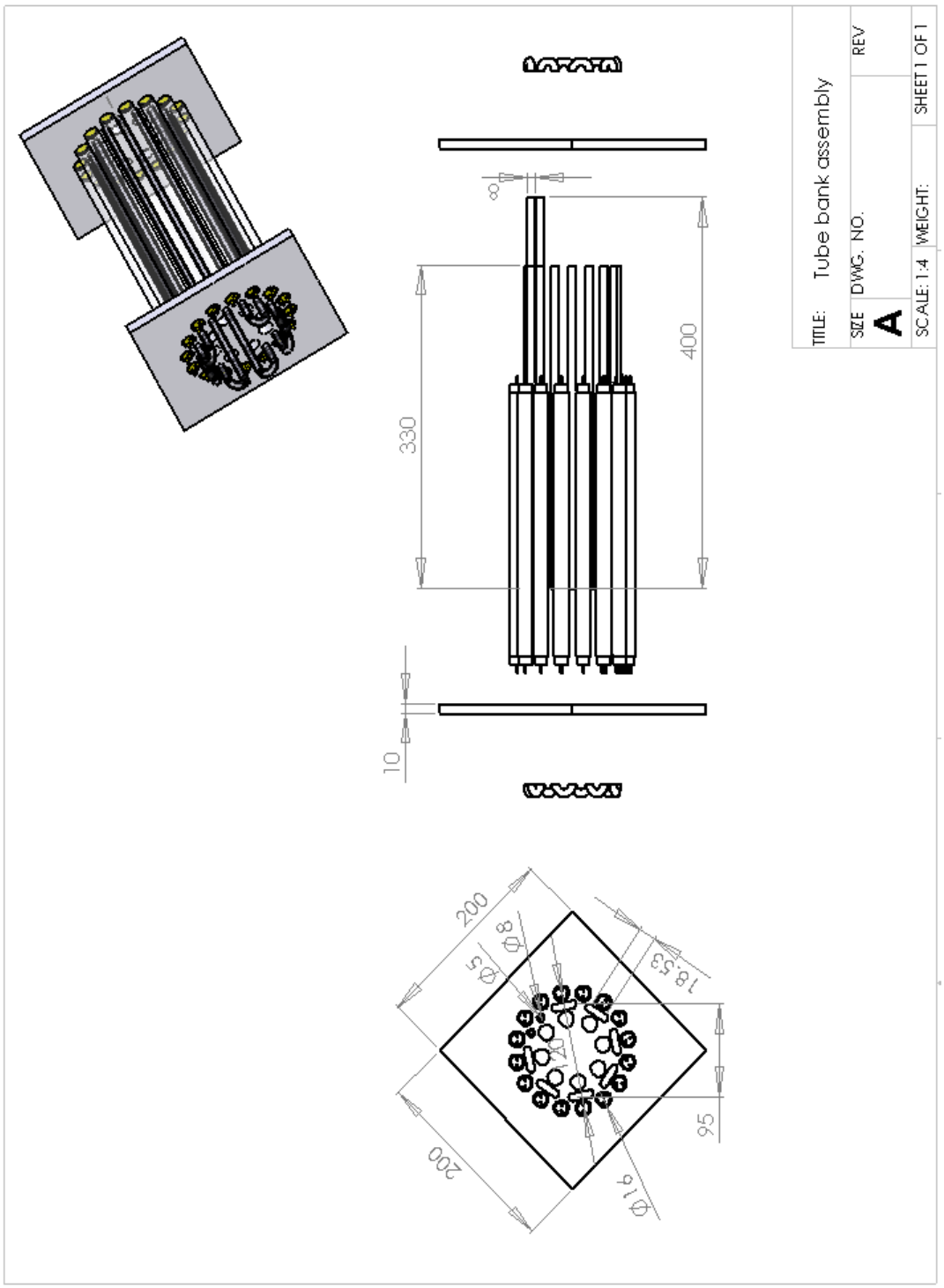

Figure A-4: Engineering drawing of UV grafting reactor showing critical dimensions

Appendix B. Sample calculations

B.1 UV tube arrangement calculation

UV tube arrangement
TUV 8W UV-C

Constants

UV tube radius from centre	*R*	60	mm
Number of UV tubes	*j*	10	
Lamp wattage rating	*P*	8	W
Actual UV produced	*P**	2.1	W
UV tube length	*L*	288.3	mm
UV tube outer diameter	UV_d	16	mm
Number of quartz tubes	*i*	16	
Quartz tube radius	*r*	48.5	mm
Quartz tube outer diameter	Q_d	7	mm

$$\omega_{ij} < \left| \frac{\alpha}{2} + \cos^{-1}\left(\frac{r\cos\frac{\alpha}{2}}{R} \right) \right|$$

$$\omega_{ij} > 2\pi - \left(\left| \frac{\alpha}{2} + \cos^{-1}\left(\frac{r\cos\frac{\alpha}{2}}{R} \right) \right| \right)$$

Calculated angles

Angle between UV tubes	θ	0.63	rad
Angle between quartz tubes	α	0.39	rad
Offset (quartz and UV tubes)	ξ	0.20	rad
Minimum ω	ω_{min}	0.85	rad
Maximum ω	ω_{max}	5.43	rad

$$d_{ij} = \sqrt{\left(2r\sin\frac{\omega_{ij}}{2}\right)^2 + (R-r)^2 - 4r(R-r)\left(\sin\frac{\omega_{ij}}{2}\right)\cos\left(\frac{\pi+\omega_{ij}}{2}\right)}$$

$$\omega_{ij} = \left|\theta_j - \alpha_i\right|$$

$$I_i = \sum_j \frac{\varepsilon}{4\pi d_{ij}^{\,2} + 2\pi L d_{ij}}$$

Distance calculation between UV and quartz tubes

Quartz tube no.	α_i	UV tube no.	θ_j	ω_{ij}	Distance	SA	Intensity	Total intensity	Min tube separation
	rad		rad	rad	mm	mm^2	$mW\ cm^{-2}$		mm
1	0.20	1	-0.20	6.09	15.6	313.7	6.69	12.5	4.12
	0.20	2	0.43	0.43	25.8	551.6	3.81		
	0.20	3	1.06	1.06					
	0.20	4	1.69	1.69					
	0.20	5	2.32	2.32					
	0.20	6	2.95	2.95					
	0.20	7	3.57	3.57					
	0.20	8	4.20	4.20					
	0.20	9	4.83	4.83					
	0.20	10	5.46	5.46	44.7	1062.0	1.98		
	0.20	11	6.09						
	0.20	12	6.72						
	0.20	13	7.34						
	0.20	14	7.97						
	0.20	15	8.60						
	0.20	16	9.23						
	0.20	17	9.86						
	0.20	18	10.49						
	0.20	19	11.11						
	0.20	20	11.74						
2	0.59	1	-0.59	5.69	33.4	744.2	2.82	14.5	0.19
	0.59	2	0.04	0.04	11.7	229.0	9.17		
	0.59	3	0.67	0.67	37.2	847.0	2.48		
	0.59	4	1.30	1.30					
	0.59	5	1.92	1.92					
	0.59	6	2.55	2.55					
	0.59	7	3.18	3.18					
	0.59	8	3.81	3.81					
	0.59	9	4.44	4.44					
	0.59	10	5.07	5.07					
	0.59	11	5.69						
	0.59	12	6.32						
	0.59	13	6.95						
	0.59	14	7.58						
	0.59	15	8.21						
	0.59	16	8.84						
	0.59	17	9.46						
	0.59	18	10.09						
	0.59	19	10.72						
	0.59	20	11.35						

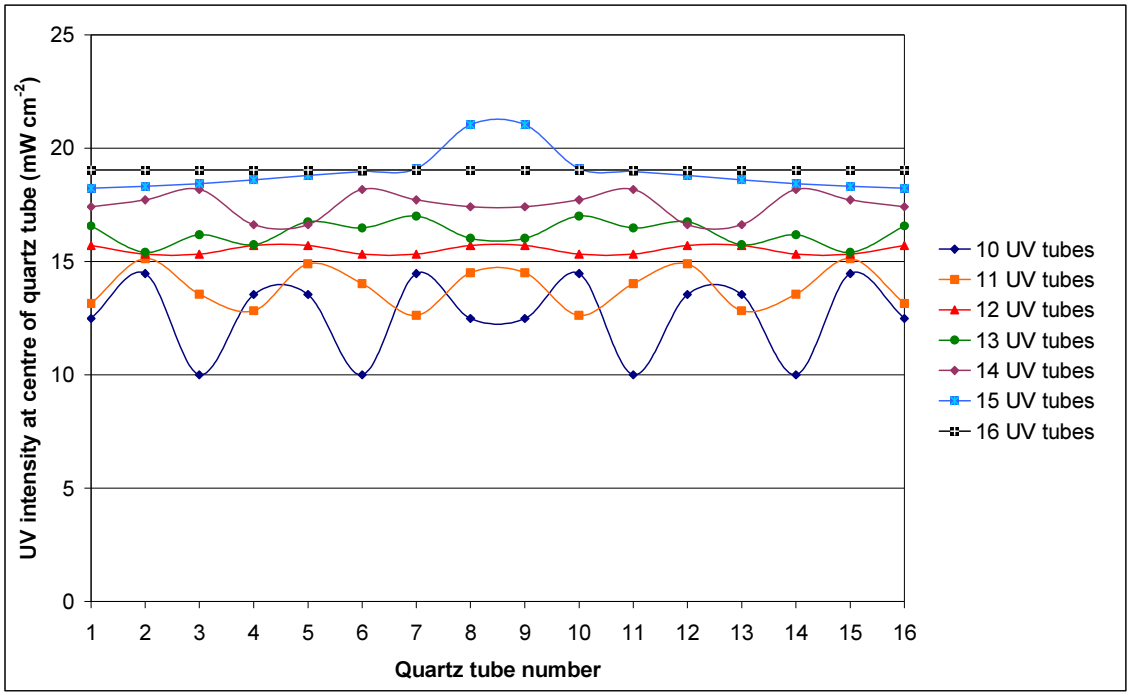

Figure B-1: UV intensity calculated for centre of quartz tubes for varied numbers of UV tubes at a 120 mm PCD

B.2 Microcapsule agglomeration Taguchi analysis

Recorded data

Test	Repeat 1		Repeat 2		
	R1	R1^2	R2	R2^2	Average
A	9.5	90.3	9	81.0	9.3
B	2	4.0	4	16.0	3.0
C	9	81.0	9	81.0	9.0
D	7	49.0	7	49.0	7.0
E	1	1.0	1	1.0	1.0
F	1	1.0	3	9.0	2.0
G	5	25.0	5	25.0	5.0
H	2	4.0	2	4.0	2.0
Total	36.5	255.3	40	266	

Main effects

Variable	Level 1	Level 2
Ethanol concentration	56.5	20
EtOH temperature	30.5	46
1 x 2 interaction	38.5	38
SDS concentration	48.5	28
Tween 80 concentration	44.5	32
Speed of amine addition	38.5	38
Degassing	46.5	30

Computation of interaction

Interaction	Average result
A1B1	6.1
A1B2	8
A2B1	1.5
A2B2	3.5

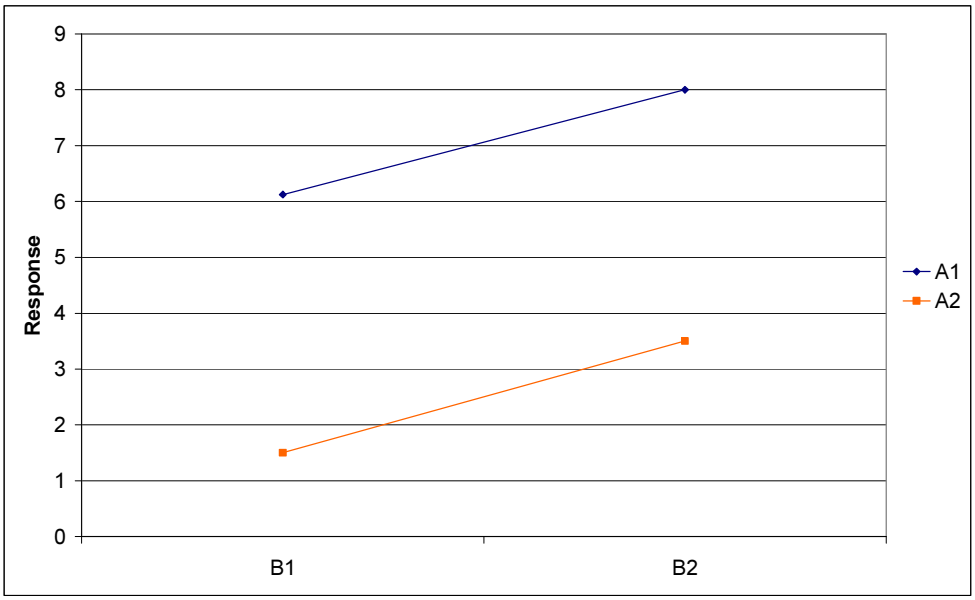

Figure B-2: Interaction factor response between ethanol concentration and temperature

The parallel lines in Figure B-2 indicate it is unlikely any interaction exists between ethanol concentration and temperature.

Analysis of variance

Total of results	76.5
Correction factor	365.8
Total Sum of Squares (SoS)	155.5
Pool if variance less than	0.1
Confidence limits	0.01

Variable	SoS	SoS pooled	DoF	V	S'oS	F	Fvalue	% Contribution
Ethanol concentration	83.3	83.3	1	83.3	82.7	160.3	11.3	53.2
EtOH temperature	15.0	15.0	1	15.0	14.5	28.9	11.3	9.3
1 x 2 interaction	0.0		0	pooled				
SDS concentration	26.3	26.3	1	26.3	25.7	50.6	11.3	16.6
Tween 80 concentration	9.8	9.8	1	9.8	9.2	18.8	11.3	5.9
Speed of amine addition	0.0		0	pooled				
Degassing	17.0	17.0	1	17.0	16.5	32.8	11.3	10.6
Error	4.1	4.16	8	0.52				4.34
Total	155.5		13					100

B.3 Taguchi analysis on variables affecting observed PAA graft yield

Recorded Data

Experiment number	Graft yield	Graft yield ^{2}
1	0.49	0.24
2	0.80	0.64
3	0.48	0.23
4	0.77	0.59
5	0.52	0.27
6	0.54	0.29
7	1.00	1.00
8	1.05	1.11
9	1.13	1.28
Total	6.78	5.65

Level totals

Variable	Level 1	Level 2	Level 3
Temperature	1.77	1.83	3.18
Concentration	2.26	2.37	2.15
Graft time	2.08	2.70	2.00
Reaction time	2.14	2.34	2.30

Main effects

Variable	Level 1	Level 2	L2 - L1	Level 3
Temperature	0.59	0.61	0.02	1.06
Concentration	0.75	0.79	0.04	0.72
Graft time	0.69	0.90	0.21	0.67
Reaction time	0.71	0.78	0.07	0.77

Analysis of variance

Total of results	76.5
Correction factor	365.8
Total Sum of Squares (SoS)	155.5
Pool if variance less than	0.1
Confidence limits	0.01

Variable	SoS	SoS pooled	DoF	V	S'oS	F	Fvalue	% Contribution
Ethanol concentration	83.3	83.3	1	83.3	82.7	160.3	11.3	53.2
EtOH temperature	15.0	15.0	1	15.0	14.5	28.9	11.3	9.3
1 x 2 interaction	0.0		0	pooled				
SDS concentration	26.3	26.3	1	26.3	25.7	50.6	11.3	16.6
Tween 80 concentration	9.8	9.8	1	9.8	9.2	18.8	11.3	5.9
Speed of amine addition	0.0		0	pooled				
Degassing	17.0	17.0	1	17.0	16.5	32.8	11.3	10.6
Error	4.1	4.16	8	0.52				4.34
Total	155.5		13					100